10-14-2011

Ground-Motion Prediction Equations for Central and Eastern North America (CENA)

Arash Zandieh

GROUND-MOTION PREDICTION EQUATIONS FOR CENTRAL AND EASTERN NORTH AMERICA (CENA)

By

Arash Zandieh

A Dissertation

Submitted in Partial Fulfillment of the

Requirements for the Degree of

Doctor of Philosophy

Major: Engineering

The University of Memphis

December 2011

To My Parents

&

My Wife Negin

ABSTRACT

Zandieh, Arash. Ph.D. The University of Memphis. December 2011. Ground-Motion Prediction Equations for Central and Eastern North America (CENA). Major Professor Shahram Pezeshk, Ph.D.

First, a new path model, including the geometrical spreading and the quality factor functions, is developed for the New Madrid seismic zone (NMSZ) using recorded small and moderate earthquakes. The database consists of 500 broadband seismograms from 63 events of magnitude *Mw* 2.5 to 5.2. All the broadband stations are located within the Mississippi embayment. The vertical components of the records are processed and used to define the path effect term in the frequency range of 0.2 to 30 Hz. At distances less than 70 km, the spectral amplitudes decay as R^{-1}; between 70 and 140 km, spectral amplitudes increase with distance and the geometric spreading is defined as $R^{+0.25}$; beyond 140 km, the attenuation is described by $R^{-0.5}$. The quality factor function is expressed as $Q = 614 f^{0.32}$ for frequencies greater than 1 Hz.

Second, the horizontal-to-vertical component (*H/V*) spectral ratio is used as an estimation of the site response in the NMSZ. The observed average *H/V* ratios suggest site amplification between 2 and 4 in the low-frequency range ($f \leq 5$ Hz) for stations located on the lower shear-wave velocity deposits (Lowlands). The higher shear-wave velocity deposits (Uplands) indicate low-frequency amplification between 1.5 and 3 Hz. Comparison of the observed *H/V* ratios with the theoretical amplification factors suggest that the *H/V* ratios can be a first estimate of the site amplifications. Afterward, the variability of the *H/V* ratios with distance is examined and no discernible trends are found; therefore, the path effect model developed for the vertical ground motions in

NMSZ using the database of this study is also applicable for the horizontal ground motions.

Finally, a hybrid empirical method is used to develop a new ground-motion prediction equation (GMPE), for eastern North America (ENA), using five new GMPEs developed for western North America (WNA). A new GMPE is derived for a magnitude range of 5 to 8 and closest distances to the fault rupture up to 1000 km for hard-rock sites in ENA. The new GMPE is compared with two GMPEs used in the 2008 national seismic hazard maps as well as with available observed data for ENA.

PREFACE

The manuscript of this dissertation includes three journal publications as chapters (Chapter 2,3, and 4). All three articles were submitted to the Bulletin of the Seismological Society of America (BSSA). Two of the three articles have already been published at the time of writing this document and the third one is accepted for publication and is in press. Following is a list of the articles used as chapters in this document:

1. Pezeshk, S., Zandieh, A., and B. Tavakoli (2011). Hybrid Empirical Ground-Motion Prediction Equations for Eastern North America Using NGA Models and Updated Seismological Parameters, *Bulletin of the Seismological Society of America* (in press).
2. Zandieh, A., and S. Pezeshk (2011). A Study of the Horizontal-to-Vertical Component Spectral Ratio in the New Madrid Seismic Zone, *Bulletin of the Seismological Society of America*, 101, 287–296.
3. Zandieh, A., and S. Pezeshk (2010). Investigation of Geometrical Spreading and Quality Factor Functions in the New Madrid Seismic Zone, *Bulletin of the Seismological Society of America*, 100, 2185–2195.

TABLE OF CONTENTS

LIST OF FIGURES

1 Introduction

In the field of earthquake engineering, ground-motion prediction models are frequently used to estimate the peak ground acceleration (PGA) and the pseudo spectral acceleration (PSA). In regions of the world where ground-motion recordings are plentiful such as western North America (WNA), the ground-motion prediction equations are obtained using empirical methods. In other regions such as eastern North America (ENA), with insufficient ground-motion data, alternative methods must be used to develop ground-motion prediction equations (GMPEs). One widely used model to estimate ground motion is the stochastic model. In this method earthquake source, propagation path, and near surface elements are modeled in the frequency domain. The accuracy of the stochastic procedure relies on models used to describe source, path, and near surface site condition.

In this research, I first focus on the propagation path effects. To develop proper regional ground-motion prediction equations which play a key role in the seismic hazard analysis, an accurate regional path term is essential. Path effect is modeled in the frequency domain by multiplying a geometrical attenuation function by an anelastic attenuation function which accounts for anelastic crustal path attenuation. In the first part of this research, Chapter 2, I estimate the path term including the geometrical spreading and quality factor functions for the New Madrid seismic zone (NMSZ) by examining recorded vertical-component seismograms in the region. The purpose is not to invalidate the use of the models already developed for ENA in NMSZ; rather, it is to provide an

alternative model for the path effect along with the other existing models. This will help in providing a better definition of epistemic uncertainties.

As mentioned previously, the efficiency of the stochastic method relies on the quality of the terms used in the method. After investigation of the path term in the NMSZ, I focus on the site term for the region in Chapter 3.

The amplification effect of local soil sediments on earthquake ground motion has been well established in earthquake engineering and engineering seismology. Site effects play an important role for site-specific ground-motion predictions and seismic hazard analysis. One of the standard empirical methods for evaluating site effects is to utilize earthquake recordings. Lermo and Chavez-Garcia (1993) presented a method based on Nakamura's (1989) technique to estimate the soil transfer function without a reference station. Nakamura (1989) used the horizontal-to-vertical component (*H/V*) spectral ratio to analyze Rayleigh waves and dynamic properties of subsurface using microtremor recordings; however, Lermo and Chavez-Garcia (1993) showed that the Nakamura technique can be applied to shear-wave part of earthquake records to evaluate the site effects. They found an agreement between the *H/V* ratios and the standard spectral ratio at their sites and showed that the *H/V* ratios are a robust estimate of the first resonant mode frequency and amplitude of the soil deposits.

I had two objectives for the study in Chapter 3. The first objective was to evaluate the *H/V* ratios as an estimation of the sediment amplification in the New Madrid seismic zone (NMSZ). The earthquake database used in Chapter 3 is the same as the one used in Chapter 2 (Zandieh and Pezeshk, 2010) to study the path effect for vertical-component

ground motions in the NMSZ. The observed average *H/V* ratios are also compared with the soil amplifications in the upper Mississippi embayment developed by Romero and Rix (2005) from the one-dimensional (equivalent-linear) method for generic regional profiles. The *H/V* ratios are also compared with the theoretical quarter-wavelength approximation.

The second objective was to examine the variability of *H/V* ratios with distance for small and moderate earthquakes in the NMSZ. Zandieh and Pezeshk (2010) studied the regional path effect in the NMSZ using the vertical-component of the broadband earthquake dataset. They determined the path effect as the geometrical spreading and quality factor functions for the NMSZ; therefore, by evaluating the *H/V* ratio variability with distance, one can demonstrate whether the path effect derived in Zandieh and Pezeshk (2010) is applicable for the horizontal-component ground motions as well.

The hybrid empirical method is another procedure to develop GMPEs in areas with sparse ground motions. This method uses the stochastic simulation method to adjust empirical GMPEs developed for the host region. The method is then used to estimate synthetic strong ground-motion parameters in the target region (where there are a limited number of strong-motion recordings). These adjustments take into account the differences in the earthquake source, wave propagation, and site-response characteristics between the two regions. The hybrid empirical method is used by several authors to develop GMPEs in ENA (Campbell, 2003, 2007, 2008; Tavakoli and Pezeshk, 2005).

Tavakoli and Pezeshk (2005) proposed a hybrid empirical model for ENA using a magnitude dependent stress parameter in the WNA stochastic simulations. They used a

generic source function as combination of single-corner and double-corner source models. Furthermore, they used the modified distance based on the Atkinson and Silva (2000) effective depth in the point-source stochastic simulations to mimic the finite-fault effects.

In Chapter 4, the goal is to update the Tavakoli and Pezeshk (2005) model to develop a new hybrid empirical GMPE for ENA using five new ground-motion prediction models developed by the PEER center for WNA (Abrahamson and Silva, 2008; Boore and Atkinson, 2008; Campbell and Bozorgnia, 2008; Chiou and Youngs, 2008; Idriss, 2008). Furthermore, recent new information on ENA seismological parameters such as stress parameter, geometric spreading, anelastic attenuation, and site response term are used to update the GMPE. In Chapter 4, the stochastic point-source model is used for both WNA and ENA regions to obtain ground motions at different magnitude-distance ranges of interest. A new functional form is defined for the GMPE, and a nonlinear regression analysis is performed to estimate period-dependent regression coefficients for a magnitude range of 5 to 8 and closest distances to the fault rupture up to 1000 km. GMPEs are developed for the response spectra (pseudo-acceleration, 5% damped) and the PGA, for hard-rock sites (near-surface shear-wave velocity $\beta_s \geq 2\,\mathrm{km/s}$, or NEHRP site class A), in ENA as a function of the moment magnitude and the closest distance to the fault rupture. The resulting ground-motion prediction model developed in this study is compared with other recent GMPEs as well as with the available observed data for ENA.

2 Investigation of Geometrical Spreading and Quality Factor Functions in the New Madrid Seismic Zone

2.1 Abstract

The accuracy and applicability of geometrical spreading and quality factor functions are investigated for the New Madrid seismic zone (NMSZ) using recorded small and moderate earthquakes. These functions represent the path effect in frequency domain.

The database used in this study consists of 500 broadband seismograms from 63 events of magnitude *Mw* 2.5 to 5.2, recorded by the Center for Earthquake Research and Information (CERI) at the University of Memphis. The hypocentral distances range from 10 to 400 km. All the broadband stations are located within the Mississippi embayment with different site conditions. The vertical components of the records are processed and used to define the path effect term in frequency range of 0.2 to 30 Hz. A hinged-trilinear geometrical spreading and a frequency-dependent quality factor functions are used to describe the path term. The regression analysis using a Genetic Algorithm indicates that at distances less than 70 km the spectral amplitudes decay as R^{-1}, between 70 and 140 km, spectral amplitudes increase with distance and the geometric spreading defined as $R^{+0.25}$, beyond 140 km, the attenuation is described by $R^{-0.5}$. The quality factor function is expressed as $Q = 614 f^{0.32}$ for frequencies greater than 1 Hz after the regression analysis. For the broader range of frequency used in this study (0.2 to 30 Hz) the *Q* function is described by a third-degree polynomial described as:

$\log Q(f) = 2.898 - 0.464 \log f + 1.238(\log f)^2 - 0.540(\log f)^3$. The results of this study are compared to those of Atkinson (2004) and Samiezade-Yazd *et al.* (1997). The path term obtained in this study can be used in the stochastic method to predict ground motions in NMSZ and eastern North America (ENA).

2.2 Introduction

In seismic areas of the world such as eastern North America (ENA), where strong ground-motion data are sparse, developing models to predict ground-motion is of great significance. These models estimate the ground motion corresponding to seismological characteristic of the region such as magnitude, distance, and local site conditions. One widely used model to estimate ground motion is the stochastic model. In this method earthquake source, propagation path, and near surface elements are modeled in the frequency domain (Boore, 2003). Atkinson and Boore (1995, 1998, 2006), Frankel *et al.* (1996), and Toro *et al.* (1996) are examples of using the stochastic method to develop ground-motion prediction equations in ENA. The accuracy of the stochastic procedure relies on models used to describe source, path, and near surface site condition. In this study, we only focus on the propagation path effects. Path effect is modeled in the frequency domain by multiplying a geometrical attenuation function by an anelastic attenuation function (Boore, 2003)

$$P(R, f) = Z(R) \exp\left[-\pi f R / Q(f) \beta_s\right] \qquad (2\text{-}1)$$

where $Z(R)$ is the geometrical spreading function, $Q(f)$ is the quality factor function which accounts for anelastic crustal path attenuation, β_s is the shear wave velocity of the crust, f is the frequency, and R is the hypocentral distance. In practice, there is a trade-off between the anelastic attenuation and the geometrical spreading, i.e. the empirical data does not have the ability to distinguish between the two and only the overall path effect attenuation can be described by the analysis of the ground-motion amplitudes (Atkinson and Mereu, 1992). According to equation (2-1), at near-source distances, the path effect is mostly dominated by the geometrical spreading and the anelastic attenuation affects the path term considerably at larger regional distances. Atkinson and Mereu (1992) used a regression analysis on a dataset of 1200 vertical component seismograms, from 100 small and moderate earthquakes to study the attenuation of the Fourier amplitude of acceleration in southeastern Canada. They found that the geometrical spreading is described by $R^{-1.1}$ at distances less than 70 km which is slightly faster than the theoretical attenuation of the direct waves in an ideal whole-space (R^{-1}). Between 70 and 130 km the spectral amplitudes are approximately constant (R^{0}) because the direct waves are joined by postcritical reflections from Moho discontinuity. Beyond 130 km amplitudes decay as $R^{-0.5}$ consistent with theoretical attenuation of the *Lg* surface waves in a half-space (Atkinson and Mereu, 1992). The corresponding quality factor function is given by $Q = 670 f^{0.33}$. Atkinson and Boore (1995) modified the geometrical spreading at distances less than 70 km to R^{-1} and refitted the *Q* model to $Q = 680 f^{0.36}$. Atkinson (2004) studied 1700 seismograms from 186 earthquakes of magnitude m_N 2.5-5.6 recorded on hard rock sites of southeastern Canada and northeastern United States.

Atkinson (2004) determined the amplitude decay as $R^{-1.3}$ within 70 km of the source which is faster than previous studies. From 70 km to 140 km Moho bounced waves cause a decrease in attenuation to $R^{+0.2}$. In the transition zone, spectral amplitudes increase with distance for low frequencies (Atkinson, 2004). Beyond 140 km, the attenuation is described by $R^{-0.5}$. For frequency above 1 Hz, Atkinson (2004) represented the Q model as $Q = 893 f^{0.32}$ and over all frequency range she described the Q function by a third-degree polynomial. Sonley and Atkinson (2006) studied the path attenuation at distances less than 100 km from the source in the Charlevoix seismic zone of eastern Canada. They analyzed three-component seismograms from 350 earthquakes and found the geometrical attenuation of $R^{-1.36}$ for distances less than 70 km. Allen *et al.* (2007) studied 1200 vertical-component records from 84 earthquakes in southeastern Australia which is also considered a stable continental region (SCR) much like ENA. They found that the low-frequency amplitudes decay can be described as $R^{-1.3}$ within 90 km of the source. From 90 to 160 km, because of the postcritical reflections the geometrical spreading is approximated by $R^{+0.1}$ and beyond 160 km low-frequency amplitudes decay as $R^{-1.6}$. Allen and Atkinson (2007) compared the source spectra and attenuation in ENA and southeastern Australia and concluded that the properties of these two regions are very similar at short distances ($R < 70$ km). At larger distances observed attenuation differences may be due to differences in crustal structure. Samiezade-Yazd *et al.* (1997) examined nearly 2200 vertical-component waveforms from 237 earthquakes in the NMSZ and defined the distance scaling for earthquakes in the NMSZ including a multi-hinged geometrical spreading function, a multi-hinged duration function, and an

exponential quality factor function. They determined the geometrical spreading function as $R^{-1.0}$ for distances less than 50 km, $R^{-0.25}$ for distances from 50 to 120 km, $R^{0.0}$ for distances from 120 to 200 km, $R^{-0.5}$ for distances from 200 to 220 km, and $R^{-1.0}$ for distances from 220 to 500 km. The quality factor function coherent with this geometrical spreading function is described as $Q = 900 f^{0.3}$ (Samiezade-Yazd *et al.*, 1997). This latter study may suggest there is a regional variability in path attenuation term in between central United States, specifically the NMSZ, and the other regions of ENA such as southeastern Canada.

To develop proper regional ground-motion prediction equations which play a key role in the seismic hazard analysis, an accurate regional path term is essential. An appropriate path term is also necessary to derive a proper source spectrum of the recorded earthquakes. In this study, we estimate the path term including the geometrical spreading and quality factor functions for NMSZ by examining recorded seismograms in the region. The purpose of this study is not to invalidate the use of the models already developed for ENA in NMSZ; rather, it is to provide an alternative model for the path effect along with the other existing models. This will help in providing a better definition of epistemic uncertainties.

The procedure used in this study is similar to the method used by Atkinson and Mereu (1992) to model the functional form of attenuation curves in southeastern Canada. A Monte Carlo simulation is used to test the statistical significance of the evaluated functional forms for the geometrical spreading and the quality factor functions. The resulting path effect model is compared with Atkinson (2004) model.

2.3 Database

In this project the seismograms recorded by the Center for Earthquake Research and Information (CERI) broadband stations are used. CERI's broadband stations consist of eleven stations. These stations and their identifications are listed in Table 2-1. The locations of broadband stations are shown in Figure 2-1. All the broadband stations are located in the Mississippi embayment with different site conditions. The database consists of 500 broadband seismograms from 63 local events of magnitude M_w 2.5 to 5.2 which occurred from 2000 to 2009. The hypocentral distances range from 10 to 400 km. The distribution of earthquakes in magnitude and distance is shown in Figure 2-2. The most notable event in the database is the M_w 5.2 earthquake struck near Mt. Carmel in southern Illinois on Friday morning, 18 April 2008 at 09:36:59 UTC (04:37 CDT). Map of CERI's broadband stations as well as the location of earthquakes used in this study are shown in Figure 2-1.

The sensor type of all broadband stations is the Guralp CMG40T. This instrument has a velocity response which is flat between 30 sec and 50 Hz. We used the high gain channel with a sampling rate of 100 samples per second.

It should be noted that only the vertical component ground motions are used in this study. One of the techniques used to estimate the site response is the observed horizontal-to-vertical component (*H/V*) ratio (Nakamura, 1989; Lermo and Chavez-Garcia, 1993; Atkinson and Cassidy, 2000). In this approach the site amplification assumed to be negligible for the vertical component and hence the vertical component may mostly reflect the effects of the source and path attenuation. Therefore, the spectral

Table 2-1
CERI broadband station list

Station Name	Latitude	Longitude	Elevation (m)	Sensor	Location
GLAT	36.26937	-89.28756	120.0	CMG40T	Glass, TN
GNAR	35.9652	-90.0178	71.0	CMG40T	Gosnell, AR
HALT	35.91060	-89.33953	85.0	CMG40T	Halls, TN
HBAR	35.5550	-90.6572	74.0	CMG40T	Harrisburg, AR
HICK	36.5409	-89.2288	141.0	CMG40T	Hickman, KY
HENM	36.7160	-89.4717	88.0	CMG40T	Henderson Mound, MO
LNXT	36.10138	-89.49127	144.0	CMG40T	Lenox, TN
LPAR	35.6019	-90.3002	66.5	CMG40T	Lepanto, AR
PARM	36.6635	-89.7522	85.0	CMG40T	Stahl Farm, MO
PEBM	36.11312	-89.86229	76.0	CMG40T	Pemiscott Bayou, MO
PENM	36.4502	-89.6280	85.0	CMG40T	Penman, Portageville, MO

ratio of the horizontal to vertical component can be used to estimate the site amplification of the horizontal component. Lermo and Chavez-Garcia (1993) showed that the *H/V* ratio technique works well in estimating the frequency and amplitude of the first resonant response mode in sedimentary deposits. Atkinson and Cassidy (2000) examined the applicability of the *H/V* ratio to determine the soil amplification of the Fraser River Delta, British Columbia, and concluded that the *H/V* ratio is a reasonable first approximation to amplification and is useful for sites with unknown soil profiles. Atkinson (2004)

developed the attenuation model for the vertical component, due to the paucity of the horizontal data, and applied it to the horizontal-component database. After examining the residuals, no trends were found with distance; and she concluded that an independent model for horizontal component is not necessary. The *H/V* ratio, as an approximation of the site amplification is applied to the vertical-component model to predict the horizontal-component (Atkinson, 2004). In this study we only used vertical-component ground motions to estimate the path term. We assumed that the site effects are negligible for the vertical component. The study of the *H/V* ratio and its ability to estimate the site effects in the NMSZ is the subject of our future studies. In fact, by checking the variability of *H/V* ratio with distance, a conclusion can be made if the path effect derived in this study is applicable for the horizontal-component ground motions as well.

2.4 Data Processing

Each waveform contains direct, reflected, and refracted phases of both *S* and *P* waves. Atkinson and Mereu (1992) and Atkinson (2004) used the shear window, a part of the signal containing shear-wave phases, to model the attenuation caused by the path. The shear-window starts when the first direct shear-wave arrives and ends when all significant shear phases arrive. In this study, we examined the difference between using shear window and the whole waveform length. This is done for several waveforms with different hypocentral distances while the waveforms are dominated by different phases at different distances. As distance increases the direct waves will be joined by reflected and refracted waves. It should be noted that the earthquakes used in this study are all local

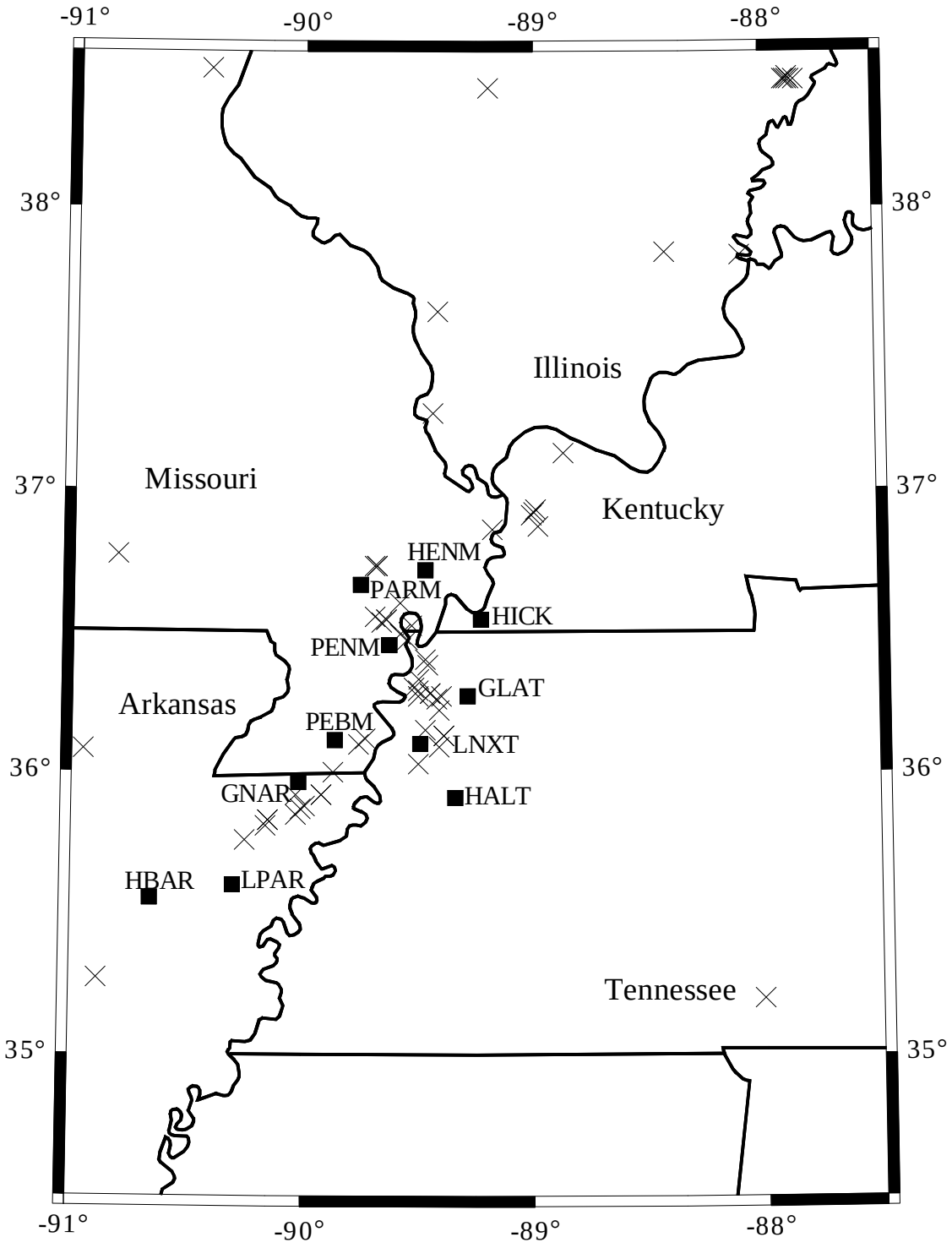

Figure 2-1. Map of CERI's broadband stations (squares) and earthquakes used in this study (crosses).

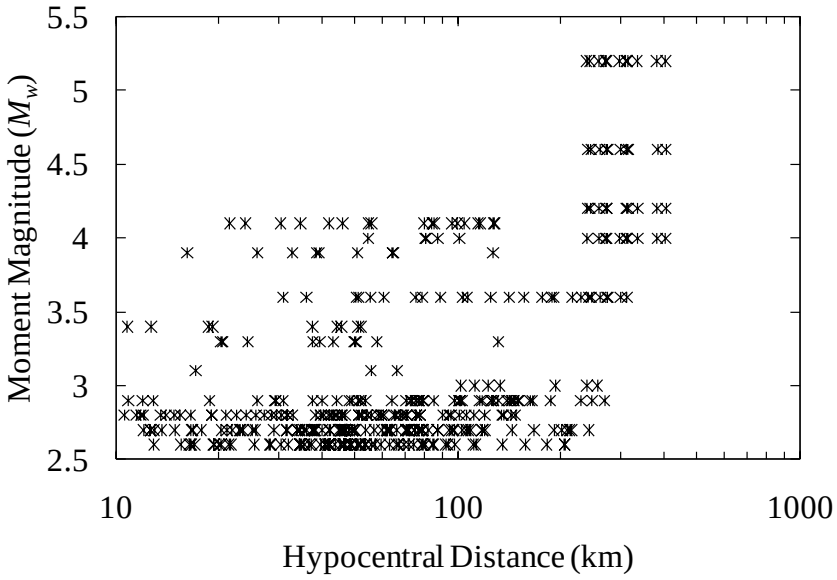

Figure 2-2. Magnitude and distance distribution of earthquakes used in this study.

earthquakes with hypocentral distances less than 400 km with maximum focal depth of 30 km. Therefore, the observed phases in waveforms are limited. We concluded that the Fourier amplitudes are very close when using shear window or the whole record. Figure 2-3 shows this comparison for three records with different hypocentral distances. As it can be observed from Figure 2-3, the acceleration power spectral density spectrums (power spectra) of the records are very close for shear window and whole length of the signal. The details on calculating the power spectra are discussed later in this section.

To obtain Fourier spectrum of the signal while excluding the pre-event noise, we used Welch's method of Power Spectral Density (PSD) estimation (Welch, 1967). Welch's method consists of dividing the time series data into overlapping segments, computing periodogram (squared amplitude of discrete-time Fourier transform) of each windowed segment, and then averaging the PSD estimates. In this study, we used 256-

sample segments with 50% overlap. Each segment is windowed using the Hamming window to minimize the spectral leakage between frequencies. For the sampling rate of 100 samples per second the duration of each segment is 2.5 seconds, 1024 Fourier transform points are used while evaluating the Fast Fourier Transform (FFT) of the windowed segment; therefore, the frequency bins from FFT are 0.0977 Hz wide.

The recorded waveforms are first corrected for the instrument response using the instrument transfer function. Then the velocity is converted to acceleration and the PSD of acceleration, Pa, is calculated using Welch's Method. The obtained power spectra should be corrected for pre-event noise. The noise window for each waveform is the segment of the record ahead of the P arrival. The noise window is processed in the same way as the signal and the noise PSD, PN, is calculated. The PSD of the noise-corrected acceleration signal, Ps, is given by:

$$P_s = P_a - P_N \tag{2-2}$$

The Fourier amplitude of the noise-corrected acceleration is the square root of power spectra calculated in equation (2-2). At this stage the signal-to-noise ratio was evaluated for each record for different frequencies. Data were selected for further analysis only at frequencies for which the signal-to-noise ratio exceeded 2.

The Fourier spectrum of ground acceleration for each waveform in the database are obtained using the discussed method and tabulated for frequencies of 0.2 to 30 Hz. It should be noted that data are most abundant in the frequency range of 1 to 10 Hz.

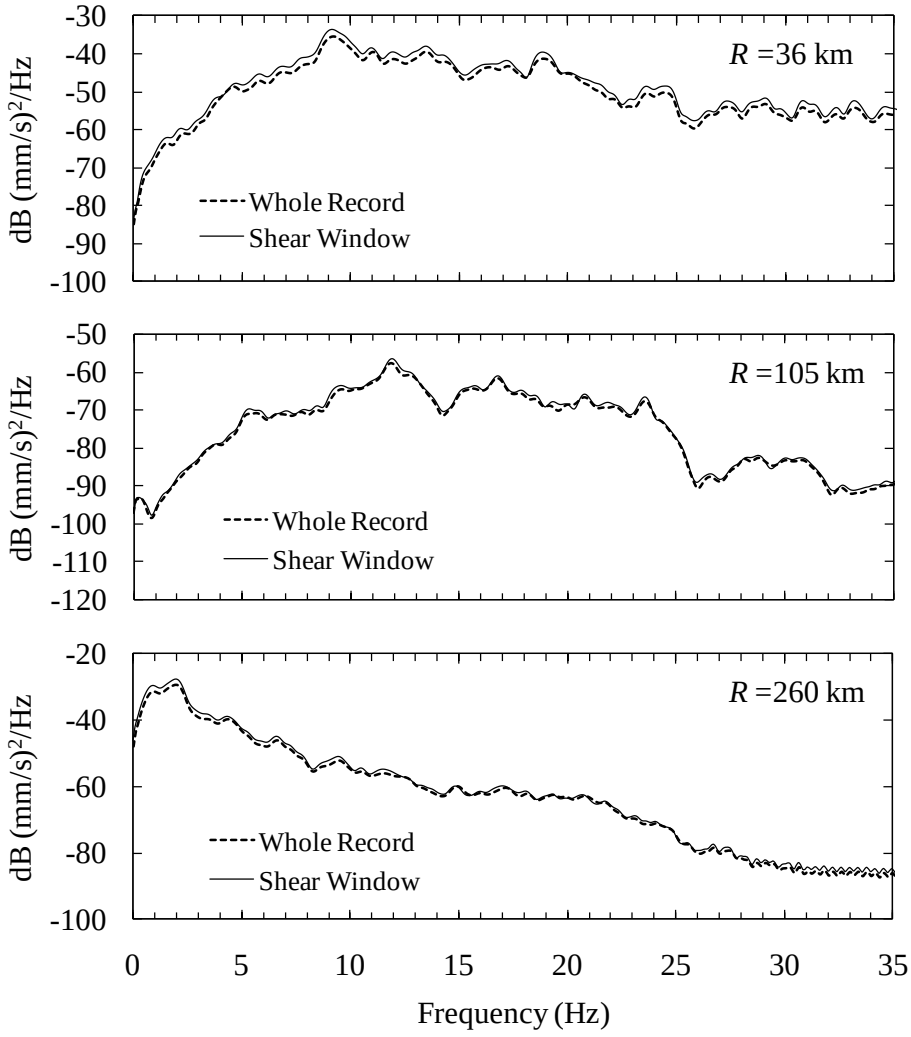

Figure 2-3. Comparison of the shear window and the whole length record power spectra for three records with different hypocentral distances.

2.5 Analysis of Path Effect

In this study a procedure similar to that introduced by Atkinson and Mereu (1992) is used to analyze the path effect. The geometrical spreading function and quality factor function is estimated using regression of data to an equation which models the observed spectral amplitudes. This equation is given by (Atkinson and Mereu, 1992)

$$\log A_{ij}(f) = \log A_i^s(f) - B(f)\log R_{ij} - C(f)R_{ij} + \log S_j(f) \qquad (2\text{-}3)$$

where $A_{ij}(f)$ is the observed spectral amplitude of earthquake i at station j at frequency f, $A_i^s(f)$ is the source spectral amplitude of earthquake i, R is the hypocentral distance, $B(f)$ is the geometrical spreading coefficient, $C(f)$ is the coefficient of anelastic attenuation, and $S_j(f)$ is the site response term for station j (Atkinson and Mereu, 1992). The relation between coefficient $C(f)$ and quality factor is defined by Atkinson and Mereu (1992) as follows:

$$Q(f) = \left[\log(e)\pi f\right] / \left[C(f)\beta_s\right] \qquad (2\text{-}4)$$

where β_s is the shear-wave velocity. Some studies of attenuation in ENA used a frequency dependent quality function of the form $Q(f) = Q_0 f^n$ $(n \geq 0)$ where $Q(f)$ increases with frequency (Atkinson and Mereu, 1992; Atkinson and Boore, 1995; Samiezade-Yazd *et al.*, 1997).

Atkinson and Mereu (1992) described the geometrical spreading function, by a hinged-trilinear functional form, in which the slope is different in three distance segments of less than 70 km, 70 to 130 km, and beyond 130 km. Atkinson (2004) used the same functional form while studying attenuation of ground-motion in Southeastern Canada and the Northeastern United States. The hinged-trilinear form of the geometrical spreading is given by:

$$B(f)\log R_{ij} = \begin{cases} b_1(f)\log R_{ij} & R_{ij} \leq R_1 \\ b_1(f)\log R_1 + b_2(f)\log(R_{ij}/R_1) & R_1 < R_{ij} \leq R_2 \\ b_1(f)\log R_1 + b_2(f)\log(R_2/R_1) + b_3(f)\log(R_{ij}/R_2) & R_{ij} > R_2 \end{cases} \qquad (2\text{-}5)$$

At close distances the direct waves are dominant and based on theoretical studies of the geometrical spreading in a homogeneous elastic whole-space $b_1 = 1.0$ (Atkinson and Mereu, 1992). Atkinson (2004) found the attenuation steeper than R^{-1} at distances less than 70 km. At distances beyond 70 km the postcritical reflections from Moho discontinuity join the direct waves and cause an energy enhancement and decrease the attenuation rate (Burger *et al*., 1987; Atkinson and Mereu, 1992). At large and regional distances multiple refractions and reflections of the shear waves trapped in crustal guides, *Lg* waves, dominate the records (Atkinson and Mereu, 1992). Atkinson (2004) and Atkinson and Mereu (1992) assumed the value of 0.5 for the geometric spreading coefficient b_3 for *Lg* waves, based on several studies. In this study we also fixed the value of b_3 to 0.5.

Several studies used the hinged- trilinear geometrical spreading form of equation (2-5) in their ground-motion modeling studies (Atkinson and Mereu, 1992; Atkinson and Boore, 1995; Atkinson, 2004). Atkinson and Mereu (1992) found that there is no significant dependence of $b_1(f)$, $b_2(f)$, and $b_3(f)$ on frequency and their resulting coefficient were: $b_1 = 1.1 \pm 0.1$; $b_2 = 0.0 \pm 0.2$; $b_3 = 0.5$; $R_1 = 70 \pm 5\,\text{km}$; and $R_2 = 130 \pm 10\,\text{km}$. They also described the quality function as $Q(f) = 670 f^{0.33}$. Atkinson (2004) confirmed the independence of coefficient to frequency and found the best result when $b_1 = 1.3$; $b_2 = -0.2$; $b_3 = 0.5$; $R_1 = 70\,\text{km}$; and $R_2 = 140\,\text{km}$. Atkinson (2004) expressed the quality factor for frequencies greater than 1 Hz as $Q(f) = 893 f^{0.32}$. For a wider range of frequencies (0.2 to 20 Hz) *Q* is modeled by a third-degree

polynomial of $\log Q(f) = 3.052 - 0.393\log f + 0.945(\log f)^2 - 0.327(\log f)^3$. Allen *et al.* (2007) also described the *Q* for southeastern Australia as a third-degree polynomial given by $\log Q(f) = 3.66 - 1.44\log f + 0.768(\log f)^2 + 0.058(\log f)^3$. Samiezade-Yazd *et al.* (1997) determined a multi-hinge geometrical spreading function similar to equation (2-5), but with four hinge points instead of two, to descried the distance scaling in the NMSZ up to 500 km. In their model, the *b* coefficients and hinge points are: $b_1 = 1.0$; $b_2 = 0.25$; $b_3 = 0.0$; $b_4 = 0.5$; $b_5 = 1.0$; $R_1 = 50\,\text{km}$; $R_2 = 120\,\text{km}$; $R_3 = 200\,\text{km}$; and $R_4 = 220\,\text{km}$. The Quality factor function in their study is described by $Q = 900 f^{0.3}$.

For modeling the attenuation caused by path, the method proposed by Atkinson and Mereu (1992) is used. In equation (2-3) the source term is the only term which depends on the event exclusively and not on the station location. We take advantage of this dependency and normalize all the observed amplitudes to the source level. In the algorithm used in this study to find the path effect, and explained later, the source term is evaluated for each event at each station then, the path term is found by minimizing the differences between source terms, $\log A_{ij}^s(f)$, evaluated for all j stations recorded event i. By rearranging equation (2-3) and replacing $\log A_i^s(f)$ with $\log A_{ij}^s(f)$

$$\log A_{ij}^s(f) = \log A_{ij}(f) + B(f)\log R_{ij} + C(f)R_{ij} - \log S_j(f) \qquad (2\text{-}6)$$

where $\log A_{ij}^s(f)$ is the source parameter evaluated for event i at station j. It should be noted that the site term is assumed to be constant at each station and is event invariant while the ground motion intensities of the events in the database are low enough to prevent any nonlinear soil behavior.

Our goal is to find the best model for path the attenuation, consisting of the geometrical spreading and the quality factor, using the available NMSZ database. Therefore, the objective is to find the variables $b_1(f)$, $b_2(f)$, $b_3(f)$, R_1, R_2, $C(f)$, and $S_j(f)$ using equations (3) through (6). Applying different combinations of the mentioned parameters in equation (2-6), results in an estimation of the source amplitude corresponding to station j, $A_{ij}^s(f)$. The best combination is the one which minimizes the mean absolute value of residuals defined as:

$$res_i = \frac{1}{N}\sum_{j=1}^{N}\left|\log A_{ij}^s(f) - \overline{\log A_i^s(f)}\right| \qquad (2\text{-}7)$$

where $\overline{\log A_i^s(f)}$ is the average of $\log A_{ij}^s(f)$ over all N stations subscribed by j

$$\overline{\log A_i^s(f)} = \frac{1}{N}\sum_{j=1}^{N}\log A_{ij}^s(f) \qquad (2\text{-}8)$$

In other words, the best solution is the one which results in almost the same source terms for stations that recorded the same events.

In this study a Genetic Algorithm (GA) is used to find the best combination of variables $b_1(f)$, $b_2(f)$, $b_3(f)$, R_1, R_2, $C(f)$, and $S_j(f)$ (Holland, 1975; Goldberg, 1989). The GA focuses on a population of variables, which are created randomly in the range defined by the constraints. Variables are grouped in sets; each of which is called a string and composed of a series of characters that defines a possible solution for the problem. The performance of the variables, as described by the objective function and the constraints is represented by the fitness of each string. A mathematical expression, called a fitness function, calculates a value for a solution of the objective function. The fitter

solution gets the higher value and the ones that violate the objective function and constraints are penalized. Therefore, like what happens in nature, the fittest and best solutions will survive and get the chance to be a parent of the next generation. In a crossover procedure, two selected parents reproduce the next generation. The procedure first divides the selected parent strings into segments and then some of the segments of a parent string are exchanged with corresponding segments of another parent string. The mutation operation guarantees diversity in the generated populations. This is done by flipping (0 to 1 or vice versa) a randomly selected bit in the selected binary string to create a muted string. Mutation prevents a fixed model of solutions from being transferred to the next generation (Holland, 1975; Goldberg, 1989).

GA tries different combination of the variables and finds the best solution which minimizes the mean value of the errors defined in equations (7) over all events. Therefore, the objective function which has to be minimized by GA is defined as

$$Objective\,Function = \frac{1}{M}\sum_{i=1}^{M} res_i \qquad (2\text{-}9)$$

where M is the number of events.

We used the hinged-trilinear functional form of equation (2-5) for geometrical spreading function. In GA, the constraints imposed on the coefficient *b* of the hinged-trilinear geometrical spreading function of equation (2-5) are:

$1.0 \le b_1 \le 2.0;\ -0.5 \le b_2 \le 0.5;$ and $b_3 = 0.5$. Parameters R_1 and R_2 in equation (2-5) were not treated as the regression variables in GA. Instead, the GA process was repeated for all combinations of $R_1 = 50, 60, 70, \ldots 120$ and $R_2 = 70, 80, 90, \ldots 160$. The

combination which yields the minimum residuals is selected. The overlapped values of the parameters R_1 and R_2 were included to examine the possibility of a bilinear shape of the equation (2-5). As mentioned before, we assumed that the soil amplification for the vertical-component is negligible. To fulfill this assumption in the regression analysis, the average site term $\log S_j(f)$ over all stations should be set to zero. To impose this constraint on the regression analysis, we added the term $\frac{1}{N}\sum_{j=1}^{N}\left|\log S_j(f)\right|$ to the right hand side of equation (2-7) to minimize it along with the $\frac{1}{N}\sum_{j=1}^{N}\left|\log A_{ij}^{s}(f)-\overline{\log A_i^{s}(f)}\right|$ term during the GA analysis.

2.6 Results

The proposed GA procedure is applied to the database considering a frequency range of 0.2 to 30 Hz using a 0.1 log increments. Analyses show that there is no significant dependence of coefficients b_1, b_2 and b_3 on frequency. The resulting parameters for the geometrical spreading function are: $b_1 = 1.0$; $b_2 = -0.25$; $b_3 = 0.5$; $R_1 = 70\,\text{km}$; and $R_2 = 140\,\text{km}$. The result for the $Q(f)$ function is shown in Figure 2-4. The *Q* function has larger amplitudes at low-frequencies ($f < 1\text{Hz}$). We fitted a third-degree polynomial to the estimated *Q* values as

$$\log Q(f) = 2.898 - 0.464\log f + 1.238(\log f)^2 - 0.540(\log f)^3 \qquad (2\text{-}10)$$

For the frequencies higher than 1 Hz, the *Q* function can be described by the exponential form as $Q(f) = 614 f^{0.32}$.

As the site term was constrained in the regression analysis (average site term was set to zero over all stations) the evaluated site terms are very small. At all frequencies and for all stations the site terms are less than 0.03 log units.

For each event in the database, the averaged source spectrum over all the recording stations, defined by equation (2-8), is estimated after GA regression analysis. Any azimuthal bias engendered in source spectrum determined by an individual station would be diminished by averaging the estimates from multiple stations (Atkinson and Cassidy, 2000). The estimated source spectra of the events used in this study for magnitudes Mw 3.0- 4.1 are shown in Figure 2-5 as well as the Brune (1970, 1971) source model.

The overall shape of the evaluated source spectra is consistent with the Brune spectrum. In Figure 2-5, the Brune spectra are plotted for a stress drop of 50 bars which matches the evaluated high-frequency spectral levels for magnitudes *Mw* 3.0- 4.1. In fact, the stress drop of 50 bars is not recommended for use with the stochastic point- or finite-source ground-motion simulations for moderate and large events in the NMSZ. Atkinson (2004) also found the stress drops of significantly less than 150 bars for events with $Mw < 4.0$ in southeastern Canada and northeastern United States. She determined that, the stress drop increases with moment magnitude for events with $Mw < 4.3$ and it reaches an approximately constant level of 100 to 200 bars for larger events. In this study, we did not evaluate the stress drop for event with $Mw > 4.1$ due to paucity of data in this magnitude range. The comparison shown in Figure 2-5 is only made to illustrate the consistency between overall shapes of the evaluated source spectrum in this study with

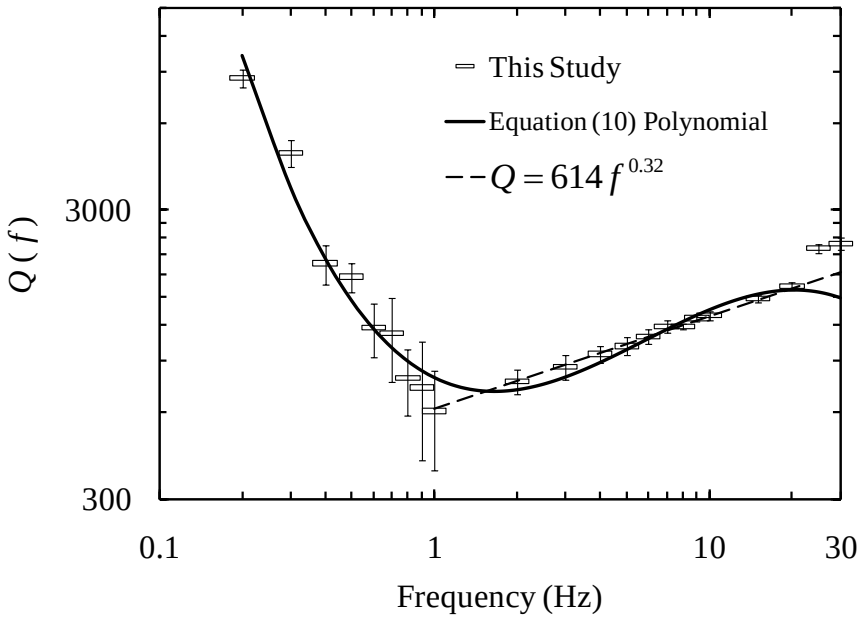

Figure 2-4. *Q* values obtained by regression analysis in this study (rectangles) with their standard errors bars; third-degree polynomial fitted to *Q* values (solid line); and linear Q model for $f > 1\text{Hz}$ (dashed line).

the Brune spectrum.

To have a visual comparison of the observed data with the model obtained for the path effect, the source and site terms are removed from recorded amplitudes. The remaining spectral amplitudes represent the path effect. The site and source corrected amplitudes are referred as "normalized amplitudes" (Atkinson and Mereu, 1992) and are given by

$$\log A_{ij}^{norm}(f) = \log A_{ij}^{s}(f) - \log A_{ij}(f) + \log S_j(f) \qquad (2\text{-}11)$$

where $\log A_{ij}^{norm}(f)$ is the normalized amplitude. The averaged source, equation (2-8), is used as the source term, $\log A_{ij}^{s}(f)$, for each event. The normalized amplitudes

for several frequencies are shown in Figure 2-6 along the path term of $B(f)\log R + C(f)R$ computed using the coefficients derived in this study. The scatter

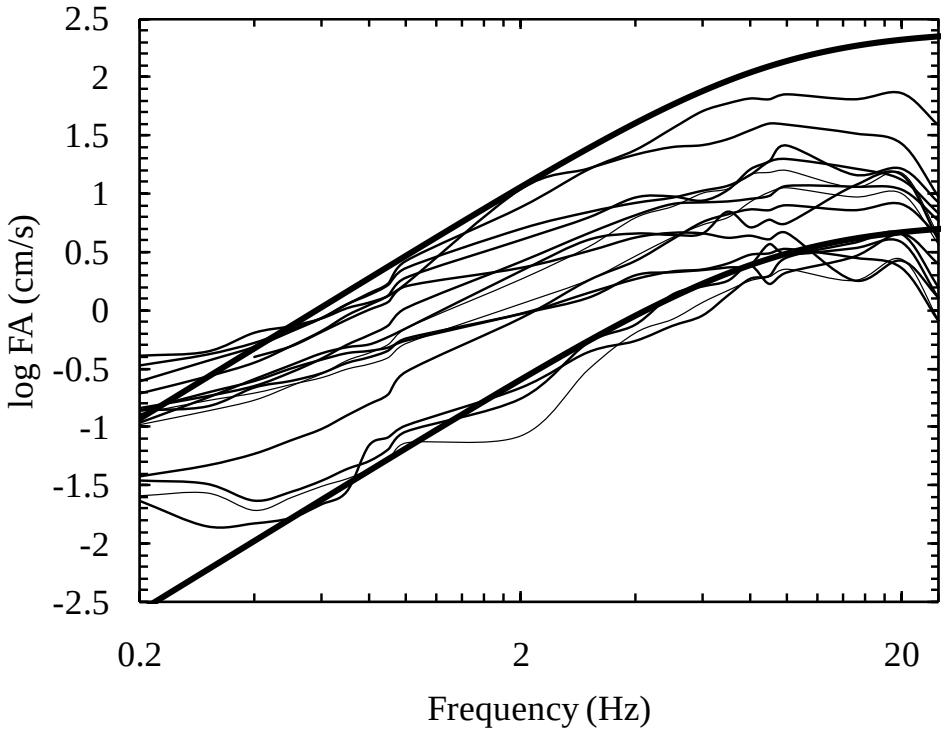

Figure 2-5. Estimated source spectra for events of $3.0 \le M_w \le 4.1$ (light lines) and the Brune source spectra (heavy lines). The Brune source model is plotted for stress drop of 50 Bars.

observed in Figure 2-6 shows the uncertainty involved with the data. To study the statistical significance of this scatter, we subtract the estimated path term from normalized amplitudes and define them as residuals given by:

$$\text{res}^{norm} = \log A_{ij}^{norm}(f) - B(f)\log R_{ij} + C(f)R_{ij} \qquad (2\text{-}12)$$

By substituting equation (2-11) into equation (2-12) and comparing it to equation (2-3), the residuals defined in equation (2-12) are also the residuals of the regression defined as the logarithm of the observed Fourier amplitudes minus the logarithm of the predicted

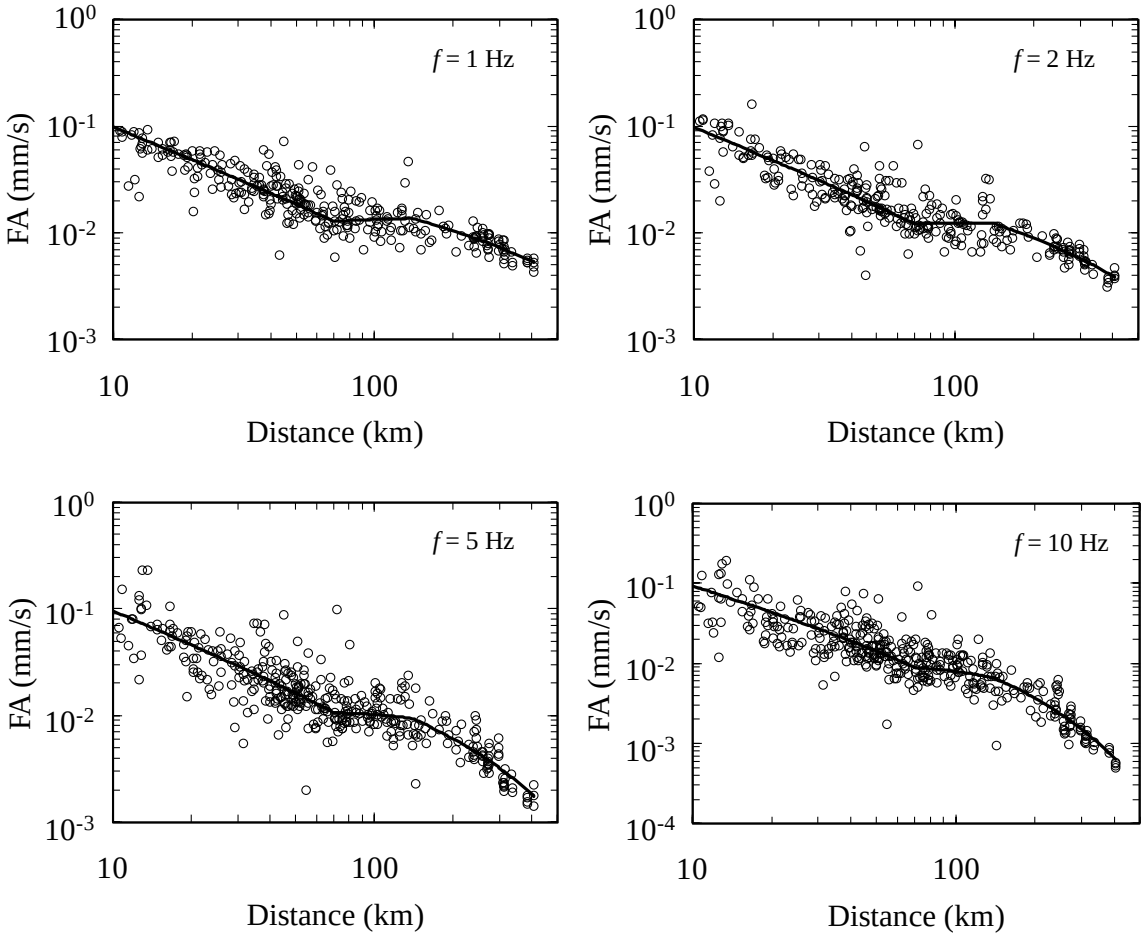

Figure 2-6. Observed normalized amplitudes (circles) and the predicted path effect (solid lines) for frequencies 1, 2, 5, and 10 Hz.

Fourier amplitudes defined by equation (2-3). Figure 2-7 shows the residuals defined by equation (12) versus distance for two frequencies of 1 and 5 Hz. As it can be observed, there is no apparent trend in residuals versus the distance. Statistical analysis of the residuals in equation (2-12) shows that these residuals are normally distributed with a

zero mean. It should be noted that the residuals defined in equation (2-12) have the logarithmic units; therefore, the residuals in non-logarithmic scale have the lognormal distribution. The residuals defined in equation (2-12) are used to evaluate the statistical properties, including standard errors and confidence interval, of the estimated path effect parameters.

The averaged residuals and their standard deviation at each station are plotted in Figure 2-8 for frequencies 1 and 5 Hz. While the site response term is neglected (the evaluated site terms, $\log S_j(f)$, are very small for all stations), the averaged residuals by station would be a measure of the significance of the site response at the stations. It should be noted that the variability observed in Figure 2-8, shows uncertainty exists in the Fourier amplitudes of ground motions at each stations. The uncertainty existing in the site term and the way it is treated in the study consists of only one part of the total uncertainty. By averaging the residuals by stations we were investigating if there is an unusual deviation at a station. While, the residuals are averaged by stations, an observed deviation might be caused by an unpredicted site term at that specific site station. In other words, if a significant deviation in one station with respect to the others is observed, one can conclude relatively, that the site effect has a larger impact on the observed amplitudes at that site. In Figure 2-8, we can see deviations for all the sites. This is more sensible when looking at the standard deviations of the residuals as well as the mean. However, the variability seen by standard deviations in Figure 2-8 suggests there may be some site responses, especially at high frequencies, for few stations. To test the precision of the estimated parameters, their standard errors and confidence intervals are evaluated using

the Monte Carlo simulation technique (Press *et al*., 2007). For this purpose, 1000 datasets of the normalized amplitudes, equation (2-11), where simulated for the given estimated parameters $b_1(f)$, $b_2(f)$, $b_3(f)$, and $C(f)$. The datasets are simulated by bootstrapping

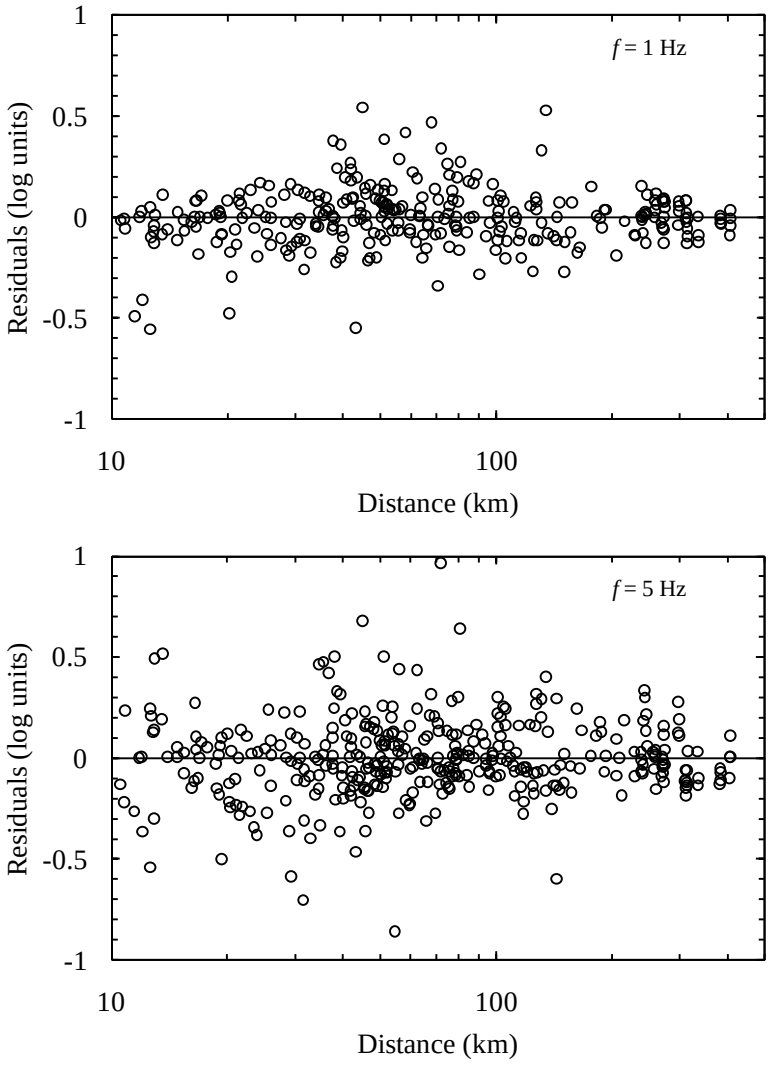

Figure 2-7. Residuals (log units) of the regression versus distance (equation (2-12)), for frequencies of 1 and 5 Hz.

the residuals (Efron and Tibshirani, 1993). The simulations were performed for frequency ranges of 1 to 10 Hz, in 0.1 log frequency increments, where the data are most plentiful.

Thus, we used the form of $Q(f) = 614 f^{0.32}$ to define $C(f)$. At each frequency the normalized amplitudes, equation (2-11), are generated by adding randomly generated residuals to the given $B(f)\log R + C(f)R$ term which is evaluated for the same

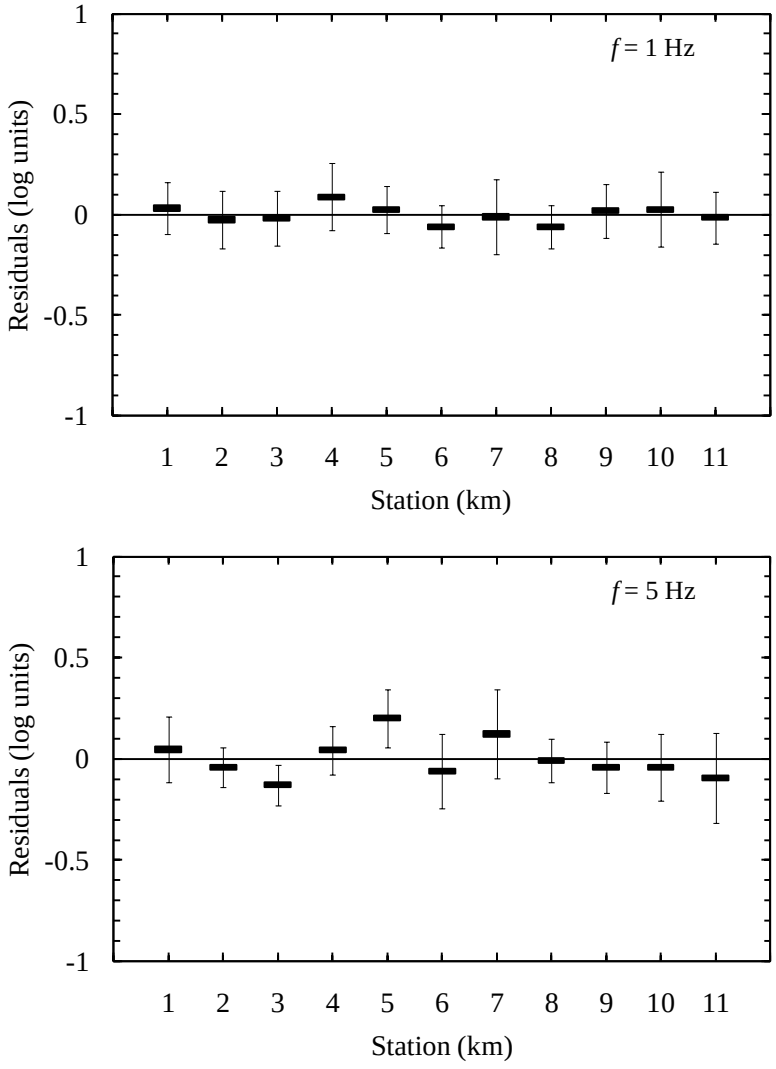

Figure 2-8. Averaged residuals (log units) and their standard deviation at each station, for frequencies of 1 and 5 Hz. Station numbers are based on the station names provided in Table 2-1.

distances, *R*, as the original database. The random residuals are drawn from a normal distribution with zero mean and standard deviation equal to the standard deviation of the original database residuals defined by equation (2-12). For each simulated normalized amplitude dataset a regression analysis is used to find the path attenuation coefficients $b_1(f)$, $b_2(f)$, $b_3(f)$, and $C(f)$. The standard errors of the estimated parameters (the bootstrap estimated of the standard error) are the standard deviation of the estimated parameters of the simulated datasets (Efron and Tibshirani, 1993). In regression analysis of the simulated datasets the *Q* function is constrained to $Q(f) = Q_0 f^{0.32}$ to evaluate the standard error of the Q_0. Also, the parameter b_3 is fixed to value of 0.5 in the regression. It should be noted that the mean of the estimated parameters attained from the simulated datasets are the same as the original database ($b_1 = 1.0$, $b_2 = -0.25$, and $Q_0 = 614$). The calculated standard errors $(\hat{\text{se}})$ are: $\hat{\text{se}}(b_1) = 0.09$, $\hat{\text{se}}(b_2) = 0.25$, and $\hat{\text{se}}(Q_0) = 25$.

There are several methods to evaluate the bootstrap confidence interval. The simplest one is the standard bootstrap confidence interval which works when the estimator is normally distributed. The $100(1-\alpha)\%$ standard bootstrap confidence interval on the estimator parameter is defined as (Efron and Tibshirani, 1993):

$$\text{Estimate} = \pm z_{\alpha/2}.\hat{\text{se}} \tag{2-13}$$

where $z_{\alpha/2}$ is the upper $100_{\alpha/2}$ percentage point of the standard normal distribution and $\hat{\text{se}}$ is the bootstrap estimate of the standard error. In this study the distribution of the regression estimator parameters of the simulations, b_1, b_2, and Q_0, are close to normal

distribution. Therefore, equation (2-13) is used to estimate the confidence intervals. For example, the 90% confidence interval on the path attenuation parameters are: $b_1 = 1.0 \pm 0.15$, $b_2 = -0.25 \pm 0.41$, $b_3 = 0.5$, and $Q = (614 \pm 41.12) f^{0.32}$. It should be noted that the hypocentral distance ranges in the database used in this study is from 10 to 400 km. Therefore, the result of this study is applicable for distances greater than 10 km, and any use of this model for distances less than 10 km should be done with caution.

The path term, $P(R, f)$, derived in this study is compared to those obtained in Atkinson (2004) and Samiezade-Yazd *et al.* (1997) (see Figure 2-9) for frequencies of 1 and 5 Hz. To make a consistent comparison of two path attenuation models according to the available data, the attenuation models of Atkinson (2004) and Samiezade-Yazd *et al.* (1997) are scaled to a level that provides the minimum sum of the squared residuals for the data on the plot. There are some differences between Atkinson (2004) model and the result of this study especially at close distances caused by a lower value for coefficient $b_1 = 1.0$ compared to that of Atkinson (2004) ($b_1 = 1.3$) . The attenuation predicted by Atkinson (2004) study is on average 20% higher than the result of this study for distances less than 40 km. However, based on the error analysis on the coefficient b_1, the 90% confidence interval of this coefficient is $b_1 = 1.0 \pm 0.15$. Therefore, the value of $b_1 = 1.3$ of the Atkinson (2004) model lies close to the upper limit of the 90% confidence interval on coefficient b_1 in this study. In general, the difference between the two models is not very significant for distances greater than 40 km. The Samiezade-Yazd *et al.* (1997) path model is very close to the developed model in this paper for distances less than 50 km

since the b_1 coefficient are the same for the two models. The greatest differences between the two models are for distances from 60 to 100 km and also greater than 180 km. The attenuation predicted by Samiezade-Yazd *et al.* (1997) model is about 12% and 22% higher than that predicted in our model, respectively, for the distance ranges of 60-100 km and greater than 180 km.

It should be noted that source, site, and path term are correlated, and there is always a trade-off between these terms. Therefore, the reader is cautioned against using the path model derived in this study along with the source or site parameters deduced from other studies assuming different types of the path models.

2.7 Conclusions

In this study, 500 seismograms recorded by CERI's broadband stations for events of magnitude M_w 2.5 to 5.2 are used to determine the path term in the New Madrid seismic zone in the frequency domain. The vertical components of the records are corrected for the pre-event noise and their Fourier amplitudes of acceleration are computed over a broad frequency range of 0.2-30 Hz. A regression procedure using GA is used to determine the best values for parameters defining the shape of attenuation caused by path. This attenuation is described by geometrical spreading and quality factor functions. A hinged-trilinear functional form is assumed for geometrical spreading, and the regression indicated that the spectral amplitudes decay as $1/R$ at distances less than 70 km, between 70 and 140 km, spectral amplitudes increase with distance and the geometrical spreading is defined as $R^{+0.25}$, beyond 140 km, the geometrical spreading is

described as $R^{-0.5}$. The increased attenuation in the transition zone is caused by postcritical reflections from Moho discontinuity (Burger *et al.,* 1987; Atkinson and Mereu, 1992). The quality factor function is expressed as $Q = 614 f^{0.32}$ for frequencies greater than 1 Hz after the regression analysis. For the broader range of frequency used in this study (0.2 to 30 Hz) the *Q* function is described by a third-degree polynomial described as $\log Q(f) = 2.898 - 0.464 \log f + 1.238(\log f)^2 - 0.540(\log f)^3$.

The confidence intervals and standard errors of the estimated path attenuation parameters are evaluated using the Monte Carlo simulation technique. The result for path attenuation effect is compared to the results of Atkinson (2004) and Samiezade-Yazd *et al.* (1997) model. This comparison is shown in Figure 2-9 and discussed throughout the paper.

The result of this study can be used within the stochastic method to predict ground motions in NMSZ and ENA. It also can be used along with other path models that already exist in ENA regions to help provide a better representation of epistemic uncertainties caused by the regional variability of path effects in ENA.

2.8 Data and Resources

Seismograms used in this study were collected as part of the ANSS Central and Eastern United States. Data can be obtained from the Advanced National Seismic System from http://earthquake.usgs.gov/monitoring/anss/regions/mid/ (last accessed April 2010).

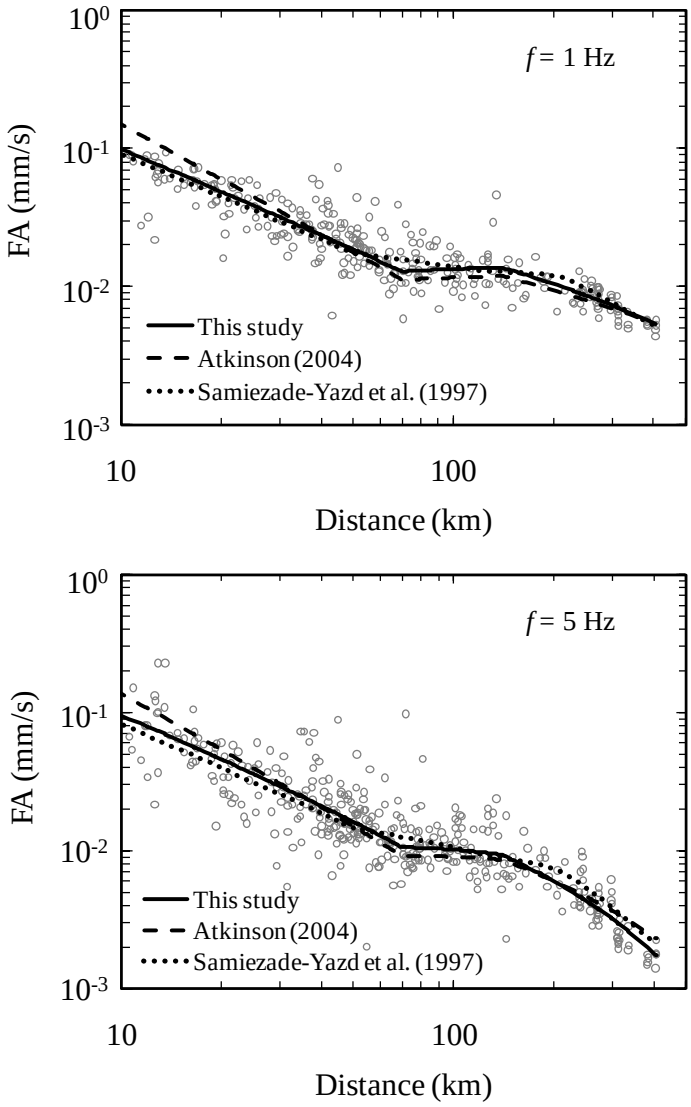

Figure 2-9. Comparison of the path term obtained in this study (solid line) with those of Atkinson (2004) (dashed line) and Samiezade-Yazd *et al.* (1997) (dotted line). Attenuation models of Atkinson (2004) and Samiezade-Yazd *et al.* (1997) are scaled to a level that provides the minimum sum of the squared residuals for the data on the plot (circles).

2.9 Acknowledgments

We wish to thank many people who contributed data, information, or criticisms. In particular, we wish to thank Mitch Withers for providing broadband seismograms and Heather DeShon and Christy Chiu for helping in data processing. We thank Gail Atkinson for her insightful and constructive guidance. We also thank Gail Atkinson and anonymous reviewers for their thorough comments and suggestions, which greatly helped improve the article.

2.10 References

Allen, T. I., and G. M. Atkinson (2007). Comparison of Earthquake Source Spectra and Attenuation in Eastern North America and Southeastern Australia, *Bull. Seism. Soc. Am*. **97**, 1350–1354.

Allen, T. I., P. R. Cummins, T. Dhu, and J. F. Schneider (2007). Attenuation of ground-motion spectral amplitudes in southeastern Australia, *Bull. Seism. Soc. Am*. **97**, 1279–1292.

Atkinson, G. M. (2004). Empirical attenuation of ground motion spectral amplitudes in southeastern Canada and the northeastern United States, *Bull. Seismol. Soc. Am*. **94**, 1079–1095.

Atkinson, G. M., and D. M. Boore (1995). New ground motion relations for eastern North America, *Bull. Seism. Soc. Am.* **85**, 17–30.

Atkinson, G. M., and D. M. Boore (1998). Evaluation of models for earthquake source spectra in eastern North America, *Bull. Seism. Soc. Am*. **88**, 917–934.

Atkinson, G., and D. Boore (2006). Ground motion prediction equations for earthquakes in eastern North America, *Bull. Seism. Soc. Am*. **96**, 2181–2205.

Atkinson, G., and J. Cassidy (2000). Integrated use of seismograph and strong motion data to determine soil amplification in the Fraser Delta: results from the Duvall and Georgia Strait earthquakes, *Bull. Seism. Soc. Am*. **90**, 1028–1040.

Atkinson, G., and R. Mereu (1992). The shape of ground motion attenuation curves in southeastern Canada, *Bull. Seism. Soc. Am.* **82**, 2014–2031.

Boore, D. M (2003). Prediction of ground motion using the stochastic method, *Pure Appl. Geophys.* **160**, 635–676.

Brune, J. (1970). Tectonic stress and the spectra of seismic shear waves, *J. Geophys. Res*. **75**, 4997–5009.

Brune, J. (1971). Correction: Tectonic stress and the spectra of seismic shear waves, *J. Geophys. Res.* **76**, 5002.

Burger, R., P. Somerville, J. Barker, R. Herrmann, and D. Helmberger (1987). The effect of crustal structure on strong ground motion attenuation relations in eastern North America, *Bull. Seism. Soc. Am*. **77**, 420–439.

Efron, B., and R. Tibshirani, (1993). *An Introduction to the Bootstrap*, Chapman & Hall, New York.

Frankel, A., C. Mueller, T. Barnhard, D. Perkins, E. Leyendecker, N. Dickman, S. Hanson, and M. Hopper (1996). National seismic hazard maps: Documentation June 1996, *U.S. Geological Survey Open–File Rept.* 96–532.

Goldberg, D. E. (1989). *Genetic Algorithms in Search, Optimization, and Machine Learning*, Addison Wesley.

Holland, J. H. (1975). *Adaptation in Natural and Artificial Systems*, Ann Arbor: The University of Michigan Press.

Lermo, J., and F. Chavez-Garcia (1993). Site effect evaluation using spectral ratios with only one station, *Bull. Seism. Soc. Am.* **83**, 1574–1594.

Nakamura, Y. (1989). A method for dynamic characteristics estimation of subsurface using microtremor on the ground surface, ***QR RTRI 30***, 25–33.

Press, W. H., S. A. Teukolsky, W. T. Vetterling, and B. P. Flannery (2007). *Numerical Recipes*, Cambridge University Press, Cambridge.

Samiezade-Yazd, M., R. B. Herrmann, L. Malagnini, and W. Liu (1997). A regional comparison of vertical ground motion in North America, 1434-94-G-2403, Saint Louis University, St. Louis, Missouri, www.eas.slu.edu/People/RBHerrmann/GroundMotion.

Sonley, E., and G. M. Atkinson (2006). Path-Specific Attenuation in Eastern Canada, *Bull. Seism. Soc. Am.* **96**, 1375–1382.

Toro, G. R., N. A. Abrahamson, and J. F. Schneider (1997). Model of strong ground motions from earthquakes in central and eastern North America: best estimated and uncertainties, *Seis. Res. Lett.* **68**, 41–57.

Welch, P. D. (1967). The Use of Fast Fourier Transform for the Estimation of Power Spectra: A Method Based on Time Averaging Over Short,

Modified Periodograms, *IEEE Transactions Audio Electroacoustics*, Volume **AU-15**, 70-73.

3 A Study of Horizontal-to-Vertical Component Spectral Ratio in the New Madrid Seismic Zone

3.1 Abstract

The horizontal-to-vertical component (*H/V*) spectral ratio of the small and moderate earthquake ground motions for the shear-wave window is used as an estimation of the site response in the New Madrid seismic zone (NMSZ). The database used in this study consists of 500 broadband seismograms from 63 events of magnitude *Mw* 2.5 to 5.2, recorded on eleven stations operated by the University of Memphis Center for Earthquake Research and Information (CERI) at the University of Memphis. All the broadband stations are located within the Mississippi embayment. Soil deposits overlying the rock basement of the embayment strongly affect the amplitudes of the ground motions. The horizontal to vertical component ratios are evaluated for the frequency range of 0.2 to 20 Hz. The observed average *H/V* ratios suggest site amplification between 2 and 4 in the low-frequency range ($f \leq 5\,\mathrm{Hz}$) for stations located on the lower shear-wave velocity deposits (Lowlands). The higher shear-wave velocity deposits (Uplands) indicate low-frequency amplification between 1.5 and 3 Hz. The observed average *H/V* ratios are also compared with the soil amplifications in the upper Mississippi embayment developed by Romero and Rix (2005) from the one-dimensional (equivalent-linear) method for generic regional profiles. The *H/V* ratios are also compared with the theoretical quarter-wavelength approximation. These comparisons suggest that the *H/V* ratios can be a first estimate of the site amplifications.

Finally, the variability of the *H/V* ratios with distance is examined and no discernible trends are found; therefore, the path effect model developed by Zandieh and Pezeshk (2010) for the vertical ground motions in NMSZ using the database of this study is also applicable for the horizontal ground motions.

3.2 Introduction

The amplification effect of local soil sediments on earthquake ground motion has been well established in earthquake engineering and engineering seismology. Site effects play an important role for site-specific ground-motion predictions and seismic hazard analysis. One of the standard empirical methods for evaluating site effects is to utilize earthquake recordings. In this method, site effects are evaluated as the spectral ratios of the recorded earthquake ground motions at free-field stations located on soil with those recorded on a reference rock station (Borcherdt, 1970). This method is optimized when both the reference station and free-field (soil) stations record the same events. Furthermore, the location of the reference station with respect to others should be such that the path effect does not affect the incidence ground motion. Other factors such as basin shape (i.e., Mississippi embayment, etc.) can focus or defocus the ray paths within a basin, but not at the rock site outside the basin. Lermo and Chavez-Garcia (1993) presented an alternative empirical method based on Nakamura's (1989) technique to estimate the soil transfer function without a reference station. Nakamura (1989) used the horizontal-to-vertical component (*H/V*) spectral ratio to analyze Rayleigh waves and dynamic properties of subsurface using microtremor recordings; however, Lermo and

Chavez-Garcia (1993) showed that the Nakamura technique can be applied to shear-wave part of earthquake records to evaluate the site effects. They found an agreement between the *H/V* ratios and the standard spectral ratio at their sites and showed that the *H/V* ratios are a robust estimate of the first resonant mode frequency and amplitude of the soil deposits. Bour *et al*. (1998) used the Nakamura's technique on microtremor recordings to establish the seismic microzonation in term of a predominant frequency map of a plain near the Rhone Delta (South of France). Bour *et al*. (1998) found agreement of the fundamental frequencies between the *H/V* ratios and the numerical transfer functions of soil columns in the regions. Atkinson and Cassidy (2000) studied the amplification effects of deep sediments of the Fraser River Delta, British Colombia using earthquake ground motions. They found that weak motions are amplified between three and six times in the Fraser River Delta over a broad frequency range (i.e., 0.2 to 4 Hz) with the high-frequency motions more attenuated. They compared the estimated amplifications with the observed *H/V* ratios and concluded that the *H/V* ratio appears to be a reasonable first approximation of site effects (Atkinson and Cassidy, 2000). They found good agreement between *H/V* ratios and theoretical amplifications although *H/V* ratios underestimate the amplification at low-frequencies. They also showed that the *H/V* ratio for rock sites in western British Columbia matches the amplification calculated using the quarter-wavelength approximation based on the regional shear-wave velocity profile. Siddiqqi and Atkinson (2002) used the *H/V* ratio to determine the amplification of rock sites across Canada. Their database consisted of 424 earthquakes, recorded on rock sites by the Canadian National Seismograph Network, with a magnitude 2 or larger. The average *H/V*

ratios were consistent with the expected amplification due to shear-wave velocity gradient for rock sites. The average *H/V* ratios increased from unity for low-frequencies to a factor of 1.2 to 1.6 at high-frequencies (10 Hz). They also found a correlation for *H/V* ratios with local geological conditions (Siddiqqi and Atkinson, 2002). Woolery *et al*. (2009) studied the suitability of the evaluated horizontal-to-vertical ratio of ambient noise and also the time-averaged shear-wave velocity of the upper 30 m of soils and rock at a site (V_{s30}) from the shallow seismic refraction/reflection profiles for estimating site effects in the lower Wabash River Valley area of southern Indiana and Illinois. They also used the *H/V* ratios of the shear-wave for the southwestern Indiana earthquake of 18 June 2002 for estimating site effects. These methods were compared with linear one-dimensional site amplification approximations. There was only a weak correlation between the linear 1-D amplification curves and the site effects predicted by the two horizontal-to-vertical ratios or the V_{s30} classification of the site. Woolery *et al*. (2009) found that earthquake *H/V* ratios along with the site-specific 1-D modeling did a better job predicting observed ground motions than ambient noise *H/V* ratios. However, they emphasized the need for additional observation from sufficient events to evaluate the effectiveness of the technique.

We had two objectives for this study. The first objective was to evaluate the *H/V* ratios as an estimation of the sediment amplification in the New Madrid seismic zone (NMSZ). Our database consisted of 500 broadband seismograms from 63 events recorded by the University of Memphis Center for Earthquake Research and Information (CERI)

with magnitudes between *Mw* 2.5 and 5.2. Zandieh and Pezeshk (2010) used the same database to study the path effect for vertical-component ground motions in the NMSZ.

The second objective was to examine the variability of *H/V* ratios with distance for small and moderate earthquakes in the NMSZ. Zandieh and Pezeshk (2010) studied the regional path effect in the NMSZ using the vertical-component of the broadband earthquake dataset. They determined the path effect as the geometrical spreading and quality factor functions for the NMSZ; therefore, by evaluating the *H/V* ratio variability with distance, one can demonstrate whether the path effect derived in Zandieh and Pezeshk (2010) is applicable for the horizontal-component ground motions as well. Atkinson (2004) developed the attenuation model for the vertical component, due to the paucity of the horizontal data, and applied it to the horizontal-component database. After she examined the residuals, no trends were found with distance; therefore, an independent model for horizontal component was not necessary. The *H/V* ratio, as an approximation of the site amplification is then applied to the vertical-component model to predict the horizontal-component (Atkinson, 2004).

3.3 Database

Our project used three-component broadband seismograms from eleven CERI seismic network stations. These stations and their identification are listed in Table 3-1. All the broadband stations are located in the Mississippi embayment with different site conditions based on their different depths to basin and potential regional differences in soil properties. The database consists of 500 broadband seismograms from 63 events of

magnitude *Mw* 2.5 to 5.2. All the earthquakes occurred between 2000 and 2009. We used the high gain channel with sampling rate of 100 samples per second. The hypocentral distances ranged between 10 and 400 km. A map of CERI's broadband stations along with the location of earthquakes used in this study is shown in Figure 3-1.

Table 3-1
CERI broadband station list

Station Name	Latitude	Longitude	Elevation (m)	Sensor	Location
GLAT	36.26937	-89.28756	120.0	CMG40T	Glass, TN
GNAR	35.9652	-90.0178	71.0	CMG40T	Gosnell, AR
HALT	35.91060	-89.33953	85.0	CMG40T	Halls, TN
HBAR	35.5550	-90.6572	74.0	CMG40T	Harrisburg, AR
HICK	36.5409	-89.2288	141.0	CMG40T	Hickman, KY
HENM	36.7160	-89.4717	88.0	CMG40T	Henderson Mound, MO
LNXT	36.10138	-89.49127	144.0	CMG40T	Lenox, TN
LPAR	35.6019	-90.3002	66.5	CMG40T	Lepanto, AR
PARM	36.6635	-89.7522	85.0	CMG40T	Stahl Farm, MO
PEBM	36.11312	-89.86229	76.0	CMG40T	Pemiscott Bayou, MO
PENM	36.4502	-89.6280	85.0	CMG40T	Penman, Portageville, MO

In this study, the spectral ratios of the horizontal to vertical components for the shear-wave window of the waveforms are evaluated. Each waveform contains direct, reflected, and refracted phases of both S and P waves. Atkinson and Mereu (1992) and Atkinson

(2004) used the shear window, a part of the signal containing shear-wave phases, to model the attenuation caused by the path and propagation of the shear-wave energy that may cause damage to structures. We used the same definition and processing procedure for the shear-wave window as used by Atkinson and Mereu (1992). The shear-window starts when the first direct shear-wave arrives and contains shear-wave phases (i.e., *S*, *SmS*, *Lg*, *Sn*, etc.). At near distances (i.e., less than 70 to 100 km) the shear window contains the direct shear-wave. As distance increases, the direct shear-wave is joined by reflections from crustal interfaces and the Moho discontinuity. At regional distances of several hundred km (200 to 1000 km), the shear window includes the *Sn* and *Lg* phases. For each waveform used in our study, including the two horizontal and the vertical component of each record, the Fourier amplitude of the shear-wave window is evaluated and corrected for the noise. To obtain the Fourier spectrum of the signal while excluding the noise, we used the Welch's method of Power Spectral Density (PSD) estimation (Welch, 1967). Welch's method consists of dividing the time series data into overlapping segments, computing periodogram (squared amplitude of discrete-time Fourier transform) of each windowed segment, and then averaging the PSD estimates. In this study, we used 256-sample segments with 50% overlap. Each segment is windowed using the Hamming window to minimize the spectral leakage between frequencies. For the sampling rate of 100 samples per second the duration of each segment is 2.5 seconds, 1024 Fourier transform points are used while evaluating the Fast Fourier Transform (FFT) of the windowed segment; therefore, the frequency bins from FFT are 0.0977 Hz wide.

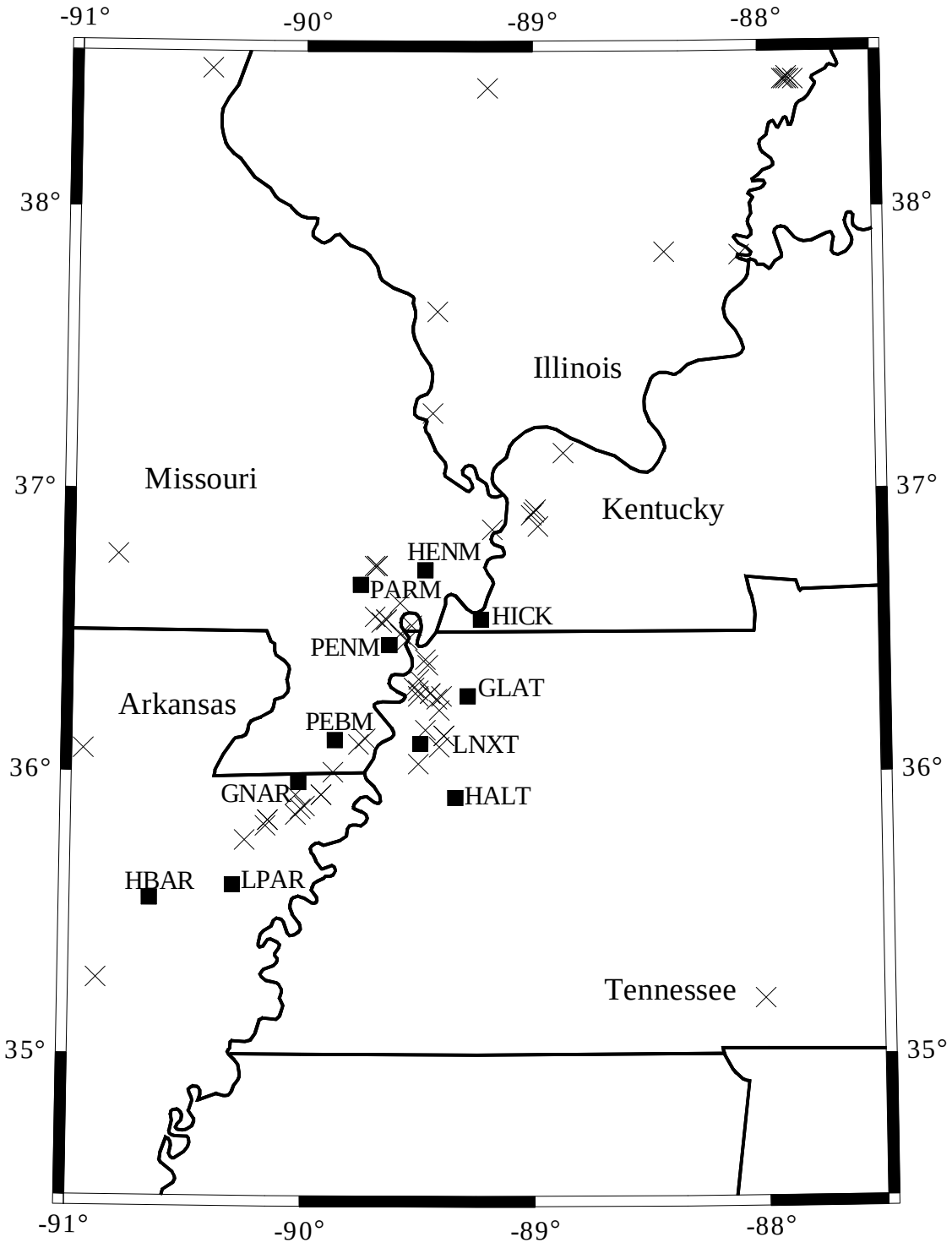

Figure 3-1. Map of CERI's broadband stations (triangles) and earthquakes used in this study (crosses).

The recorded waveforms are first corrected for the instrument response using the instrument transfer function. Then the velocity is converted to acceleration and the PSD of acceleration is calculated using the Welch's Method. The obtained power spectra should be corrected for the noise. The noise window for each waveform is one segment of the record ahead of the shear-wave window arrival. For the case where the noise segment contains the P wave, a segment preceding the P wave is selected as the noise window. In other words, the pre-event noise is removed from the signal. The noise window is processed in the same way as the signal and the noise PSD is calculated. The PSD of the noise-corrected acceleration signal is evaluated by subtracting the noise PSD from the signal (i.e., the shear-wave window) PSD. The Fourier amplitude of the noise-corrected acceleration is the square root of the calculated power spectra. The signal-to-noise ratio was evaluated for each record for different frequencies and data were selected for further analysis only at frequencies for which the signal-to-noise ratio exceeded 2.

The Fourier spectrum of ground acceleration for each waveform in the database is obtained using the discussed method for the N-S, E-W, and vertical components and the *H/V* ratios for E-W and N-S components were evaluated and tabulated for frequencies between 0.2 and 20 Hz.

3.4 The New Madrid Seismic Zone Geology

The NMSZ is located in the Central United States in the Mid-Mississippi River Valley. It is the source for the 1811-1812 large $(M_W \geq 7.0)$ earthquake sequence. A detailed summary of geological and seismological studies of the NMSZ along with

interpretations on historical seismicity can be found in Johnston and Schweig (1996). The Mississippi embayment is a large wedge-shaped synclinal structure that dips south along its primary axis from southern Illinois to the Gulf of Mexico, and is filled with post-Paleozoic-aged sediments. Van Arsdale and TenBrink (2000) document the stratigraphic characteristics for these deposits in the Upper Mississippi embayment. In general, these sediments consist of sand, silt, and clay with thickness from 477 m at New Madrid, Missouri, to 1 km near Memphis, Tennessee (Van Arsdale and TenBrink, 2000). The ground motions in the region will be affected by the thickness and dynamic properties of these deep soil deposits, as well as the basin effects which trap the seismic energy within the embayment. A contour map for thickness of the sediments on top of the Paleozoic basement in the Upper Mississippi embayment from Van Arsdale and TenBrink (2000) is shown in Figure 3-2.

Toro *et al.* (1992) classified the embayment into two regions based on the age of near-surface geologic deposits. These two regions consist of the recent Holocene-age alluvial deposits in floodplains, called Lowlands, and the older Pleistocene-age terrace deposits, called Uplands. Romero and Rix (2005) studied the effect of the deep soil deposits in the Upper Mississippi embayment. They developed generic shear-wave velocity profiles for the Lowlands and Uplands deposits up to 70 meters by aggregating the characteristic profiles (profiles represent the typical profile for a particular area based on compiled profiles with an uncertainty defined from the site-specific analysis) obtained for the Memphis Metropolitan Area (MMA) and measured profiles outside the MMA based on their geologic location within the Mississippi embayment. The Lowlands

deposits have lower shear-wave velocities in the upper 70 meters compared with the Uplands deposits. Romero and Rix (2005) then used the shear wave velocity of geologic deposits that had previously been estimated to the Paleozoic basement for several sites in the Upper Mississippi embayment and generated a V_s profile for deep soils extending from 70 meters to the maximum depth of the Upper Mississippi embayment at an approximate depth of 1000 meters. This deep soil profile was combined with both the Lowlands and Uplands profiles to create a V_s profile for the entire soil column. Finally, they used the Catchings (1999) crustal model developed for Memphis, constrained by both seismic refraction and gravity modeling, as the crustal velocity structure for geologic deposits below 1000 meters and developed final generic profiles. The effect of varying embayment depths to determine the site effects was considered by truncating the embayment model at depths of 1000, 600, and 100 meters and extending the crustal model to maintain a constant crustal thickness.

The physiographic features of Lowlands and Uplands deposits are shown in Figure 3-3. Based on the Romero and Rix (2005) classification of the embayment, stations GLAT, HALT, HICK, and LNXT lie on the Lowlands deposits and stations GNAR, HBAR, HENM, LPAR, PARM, PENM, and PEBM lie on the Uplands deposits.

3.5 Results

The calculated *H/V* ratios for each station at each direction show event-to-event variability. We used the mean *H/V* ratio of all events as the indicative *H/V* ratios for each station. The event-to-event variability is described as the standard deviation and 90%

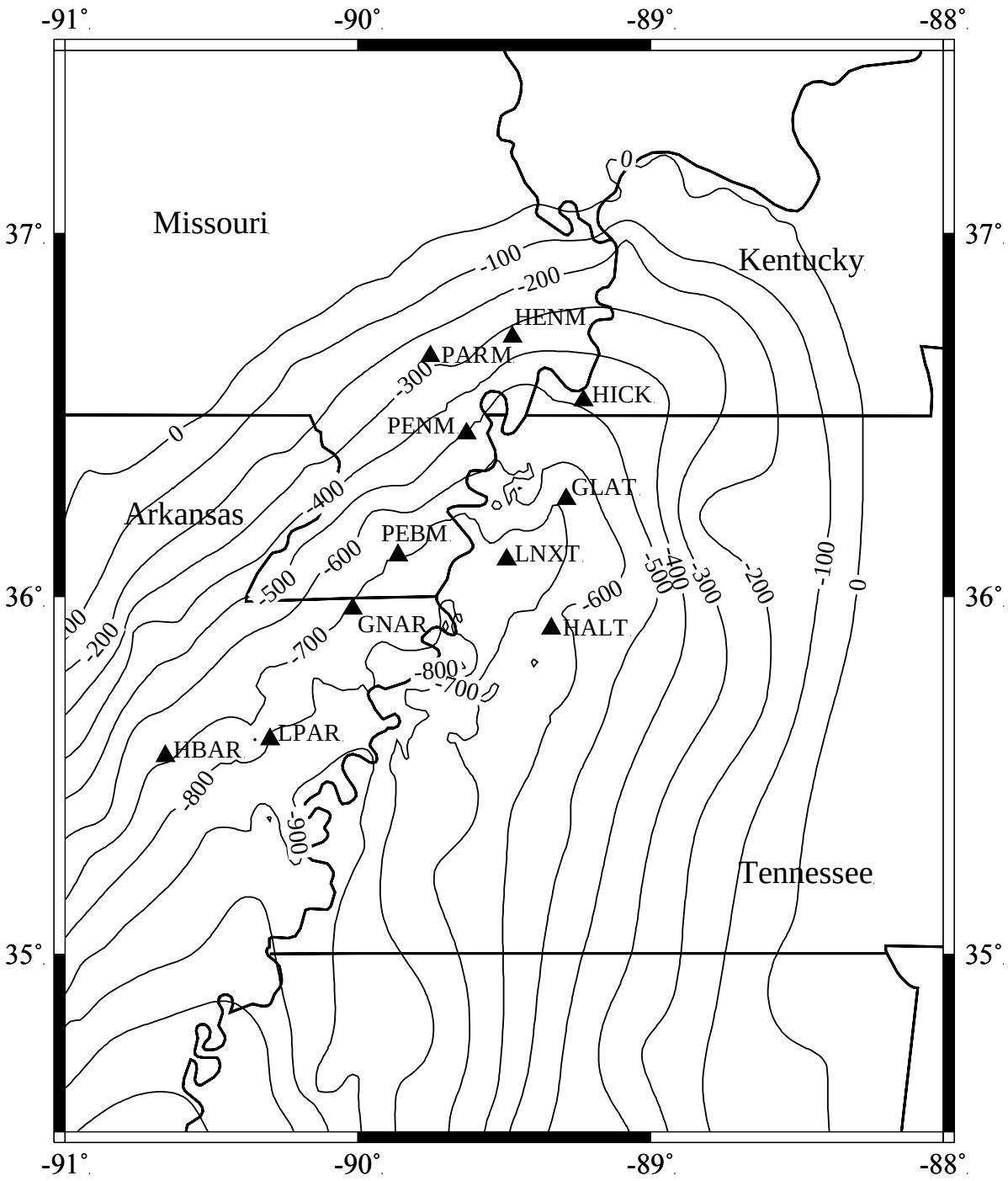

Figure 3-2. Contour map of the top of the Paleozoic strata of the Mississippi embayment after Van Arsdale and TenBrink (2000). Solid triangles denote the CERI's broadband stations.

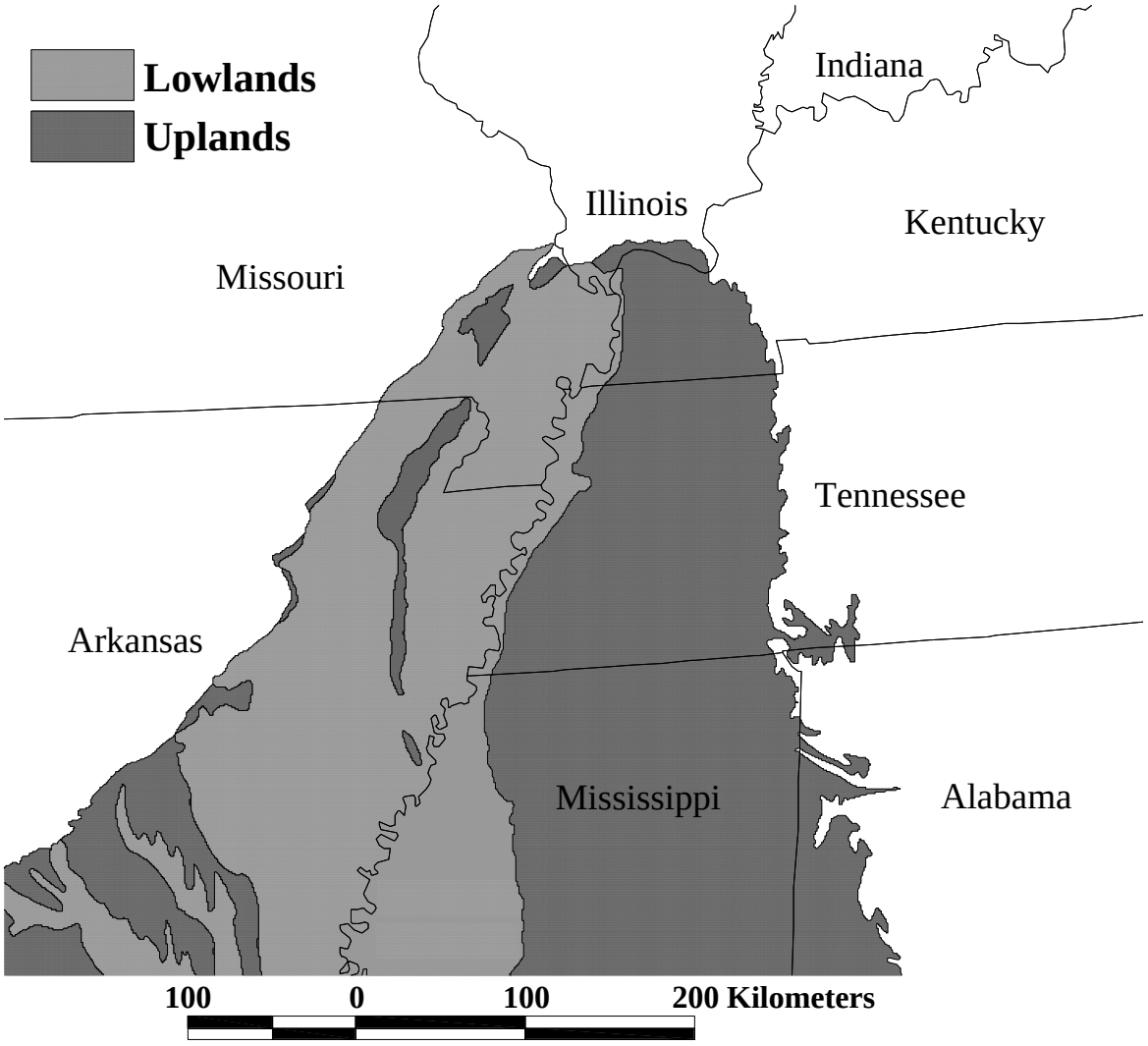

Figure 3-3. The geologic features of Lowlands and Uplands deposits (source of Figure: Romero and Rix, 2005).

confidence interval for the mean. For example, the *H/V* ratios, their mean, standard deviation, and 90% confidence intervals of the mean for stations HICK and LPAR are shown in Figure 3-4 for the N-S direction. Another important consideration is the variability of the *H/V* ratios for each of the horizontal components. The results show

consistency between the mean of *H/V* ratios for each direction. As an example, the mean *H/V* ratios for each of the E-W and N-S directions are compared for stations GLAT and GNAR in Figure 3-5. The mean *H/V* ratios for both directions are similar; therefore, for the remaining results we will only show the E-W direction for brevity. The mean and the standard deviation for the *H/V* ratios from all eleven broadband stations are shown in Figure 3-6a. The *H/V* ratios for stations lying on the Lowlands and Uplands deposits are separated in Figure 3-6b. All the stations located on Lowlands show amplifications between 2 and 4 in the low-frequency range (i.e., $f \leq 5\,\mathrm{Hz}$). For higher frequencies, the *H/V* ratio decreases with exception of some individual peaks. Among all the stations on Lowlands, the amplifications at station PEBM have an anomalous shape with a peculiar large amplification factor of about five at the frequency near 5.3 Hz. This behavior is not observed in the station GNAR, which is the closest station to PEBM (40 km spaced out) with the same depth to Paleozoic based on the Van Arsdale and TenBrink (2000) map shown in Figure 3-2. This may be caused by a local geologic structure. This is also a limitation with all the ground-motion response predictions and observations. Woolery *et al*. (2009) found in their study on Wabash River Valley that deeper geologic rock structure, as well as lateral geologic variation on the scale of a few 10's to 100's of meters can have significant effects on the ground-motion response predictions and observations. Although their study was outside the embayment where 3-D effects are less problematic with observational data, it is still germane globally. Stations lying on Uplands amplify the weak motions by a factor of 1.5 to 3 for the frequency range of

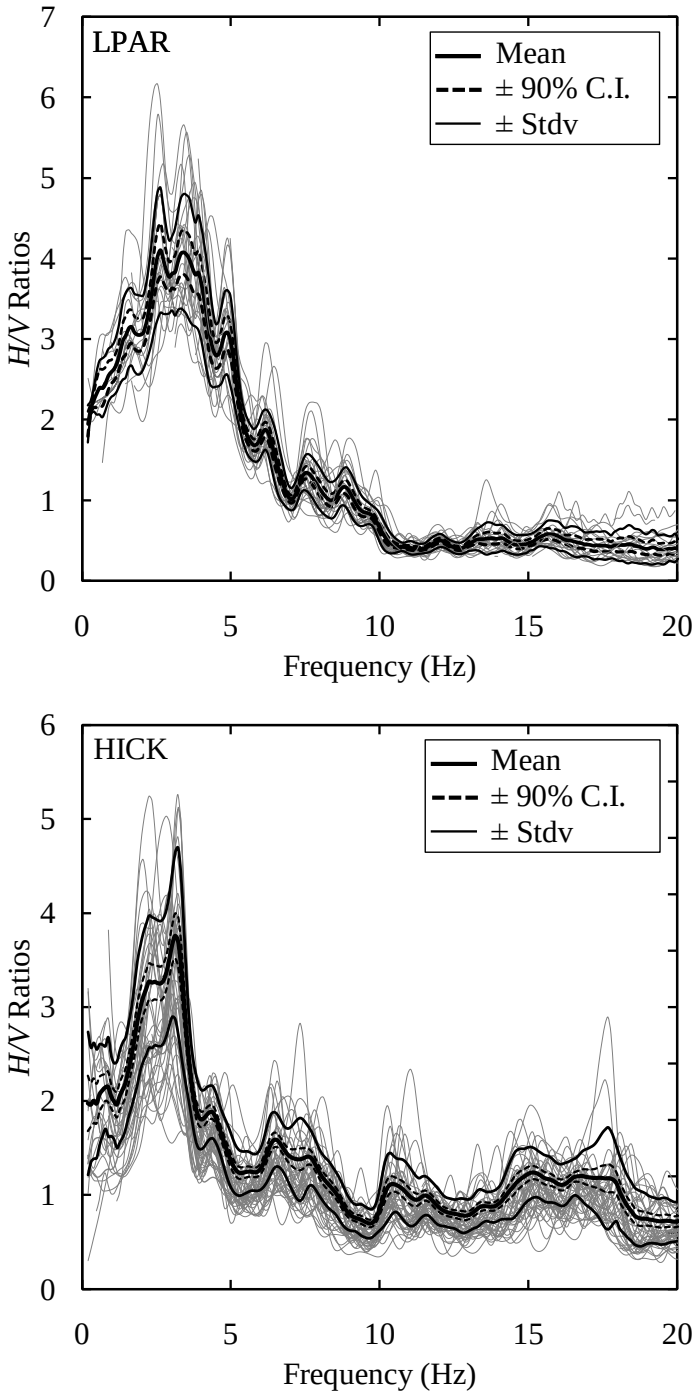

Figure 3-4. Observed *H/V* ratios at stations LPAR and HICK (gray lines).Heavy solid lines show the mean *H/V* ratios, thin solid lines show the standard deviation of the observations, and dotted lines show the 90% confidence limit on the mean.

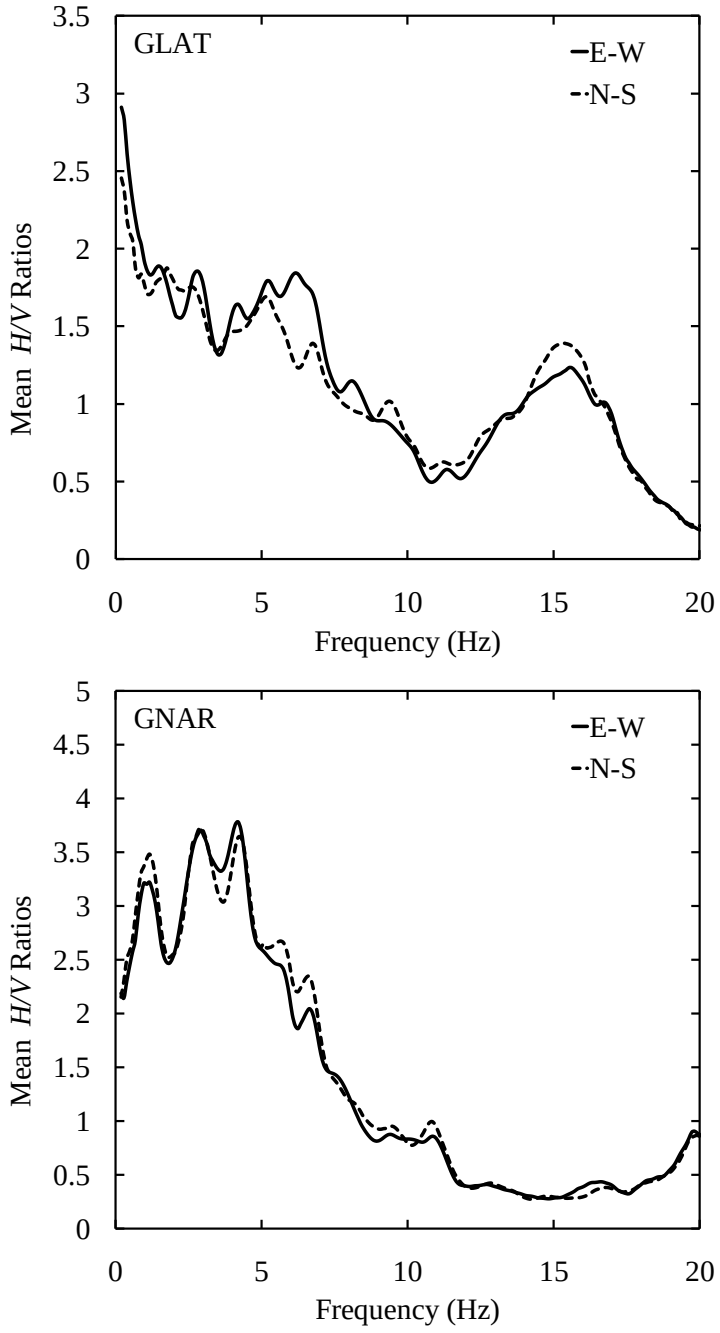

Figure 3-5. Mean *H/V* ratios for stations GLAT and GNAR. The solid lines show the Mean *H/V* ratios in E-W direction and dotted lines show the mean *H/V* ratios for the N-S direction.

$f \leq 5\,\text{Hz}$ with the exception of station LNXT which has a peak *H/V* ratio of about 3.8 near 3 Hz. Station LNXT is located on the Lowlands-Uplands boundary, and has a similar site amplification as Lowlands observations. It should be noted that the reported amplification factors are based on mean *H/V* ratios and individual *H/V* ratios are as large as a factor of 7 in some cases; therefore, the standard deviation in *H/V* ratios should be considered for the estimated amplifications As a general observation, in Lowlands region, the stations located on thinner deposits (see Figure 3-2) shows higher amplifications at frequency range of between 5 and 15 Hz compare to stations which have higher depth to the Paleozoic basement.

The site amplifications presented in this study are compared with those developed by Romero and Rix (2005) for the Upper Mississippi embayment. The site amplifications in Romero and Rix (2005) are evaluated for the generic shear-wave velocity profiles which were developed for Central United States and Mississippi embayment. They used the stochastic method to simulate the rock motions at the base of soil columns; and a one-dimensional equivalent-linear site response analysis is employed to calculate the site rock ground motion. The detailed geotechnical and seismological factors used to evaluate the site amplification are not discussed here. For further information on the geotechnical and seismological factors and their effects on the calculated site factors readers are referred to Romero and Rix (2005).

In Romero and Rix (2005) study, soil parameters including the shear-wave velocity profiles and dynamic material properties were randomized to account for uncertainty; and 30 simulations were performed for each scenario earthquakes. The

(a)

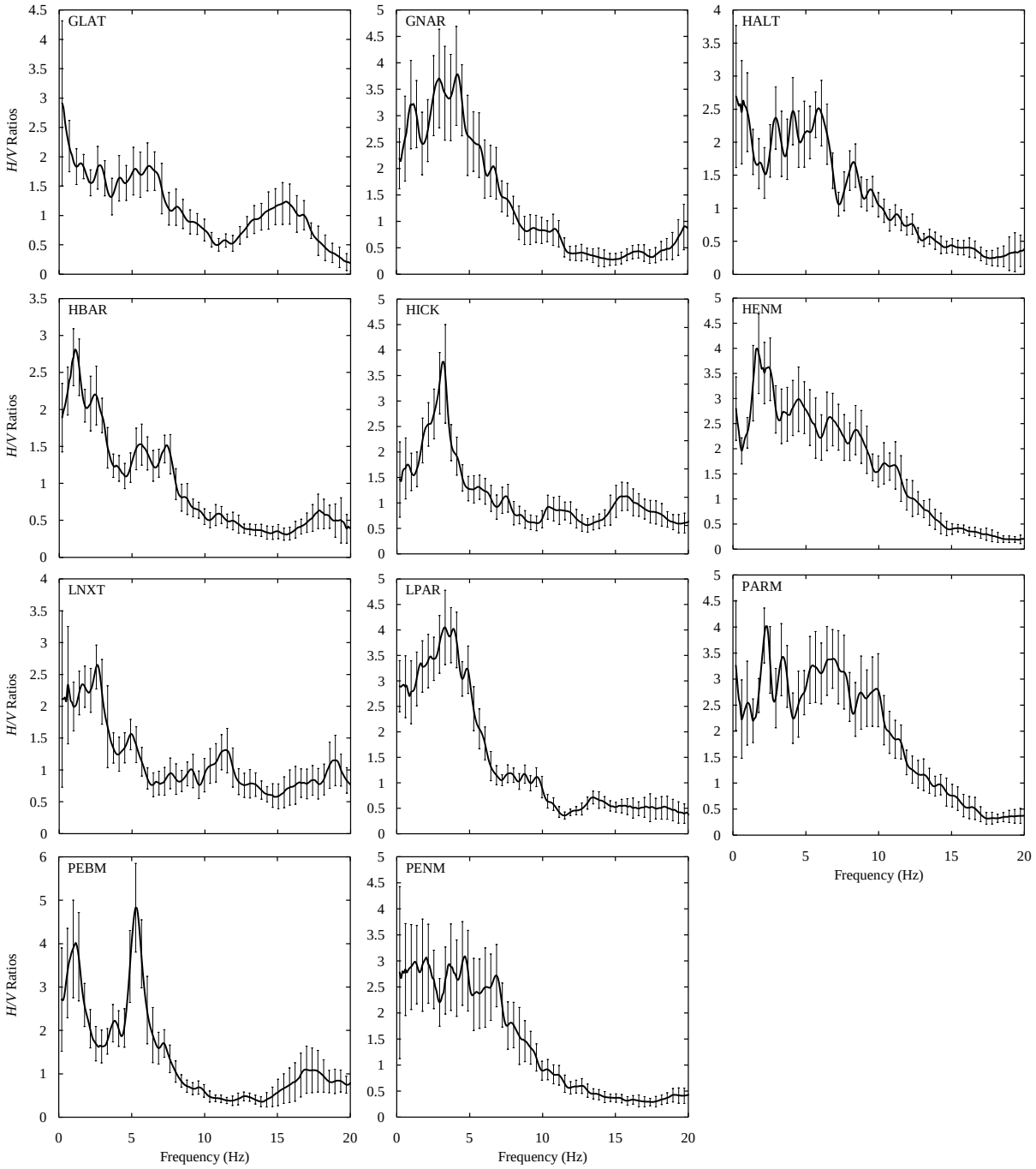

Figure 3-6. Observed mean *H/V* ratios for all the stations for E-W direction: (a) The mean *H/V* ratios for each stations. The error bars show the standard deviation. (b) The mean *H/V* ratios for stations classified by their location on Uplands or Lowlands profiles.

(b)

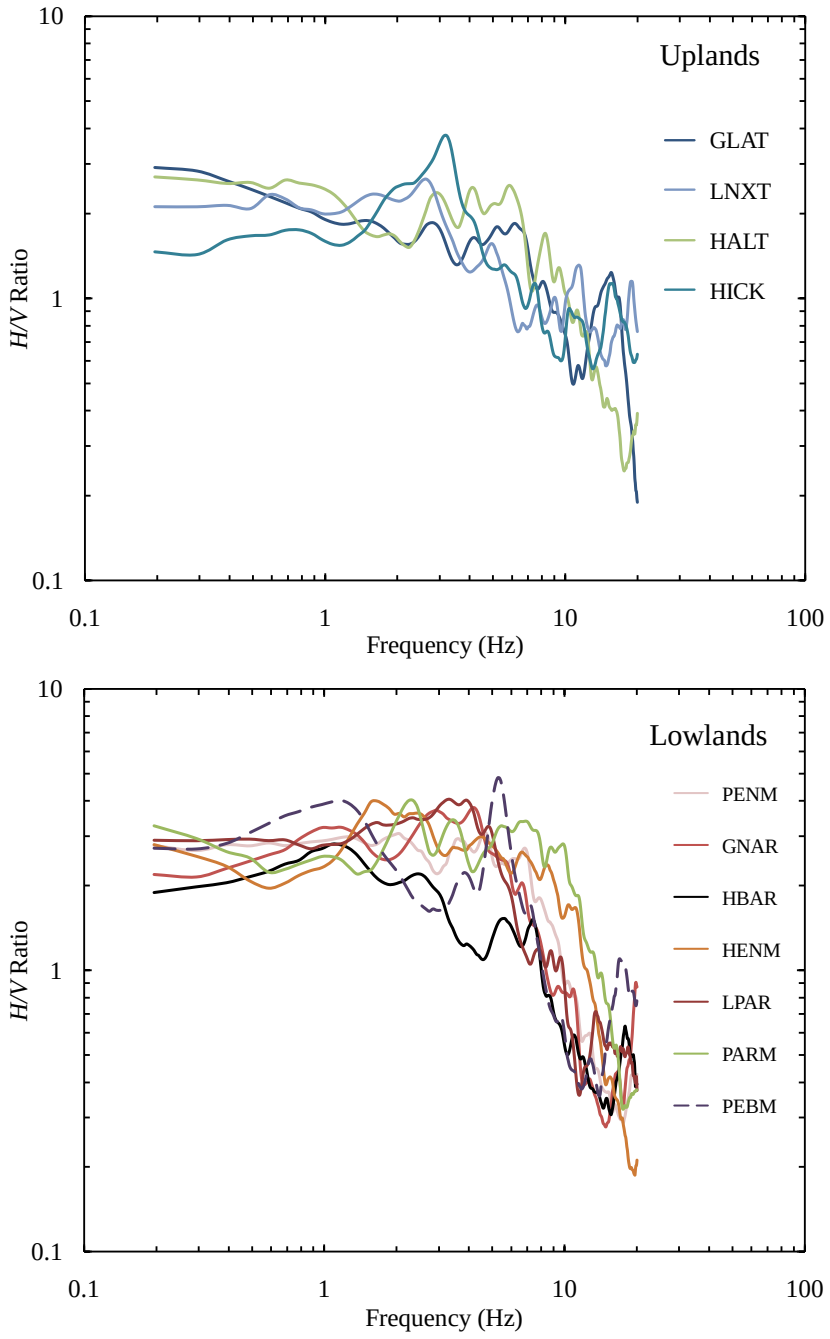

Figure 3-6. (*Continued*)

amplifications. The site response in the scheme of Fourier amplification is the ratio of Fourier amplitudes of the estimated ground-motion at the ground surface to that of the

amplifications reported in their study are the median of the simulations for a reference earthquake scenario with a moment magnitude of 6.5 and an epicentral distance of 50 km on the NEHRP site class A $(V_s = 2040\,\text{m/s})$ hard rock base. The median PGA for this scenario earthquake is 0.076 (g) for the rock motion. The two profiles considered are the Uplands and Lowlands profiles with three embayment depths for each of these soil profiles: (1) 100 meters, (2) 600 meters, and (3) 1000-meters (Romero and Rix, 2005). It should be noted that the ground motion intensities of the events in the database are low enough to prevent any nonlinear soil behavior; therefore, we used linear site amplifications reported by Romero and Rix (2005) for a consistent comparison. In Figure 3-7, the site amplifications for their Uplands soil profile with the depths of 100, 600, and 1000 meter are compared with the *H/V* ratios for stations GLAT, HALT, HICK, and LNXT. Also, the same comparison is made for the Lowlands soil profile and the *H/V* ratios for stations GNAR, HENM, PENM, PARM, and LPAR. In Figure 3-7, the Romero and Rix (2005) amplifications are given only for soil column depth of 100, 600, and 1000 meters and the basin effect is not included in the site response analysis while the stations are located on different thicknesses of soil (Figure 3-2) within the embayment. This fact makes it difficult to carry out a fair comparison. Based on the fundamental differences between the two methods a quantitative comparison may not be appropriate. Romero and Rix (2005) predict lower amplification for frequencies greater than 1.5 Hz in Lowlands and higher amplification for frequencies greater than 3 Hz in Uplands. However, the *H/V* ratios are relatively consistent with the Romero and Rix (2005) amplifications for low

frequencies of $f \leq 2\,\mathrm{Hz}$ for both Lowlands and Highlands. It seems that the Romero and Rix (2005) amplifications drop off more rapidly than *H/V* ratios for high frequencies.

Our *H/V* ratios are also compared to the theoretical amplification estimated by the quarter-wavelength method (Joyner *et al*., 1981). The linear characteristic of the method is compatible with the weak ground motions used in this study. The frequency-dependent amplification factors calculated using quarter-wavelength approximation are smooth; moreover, the method does not account for resonance effects. In this study, we used the result of the quarter-wavelength approximation applied to the Upper Mississippi embayment by Romero and Rix (2005). They used the quarter-wavelength method on the Uplands and Lowlands generic profiles and used the kappa value of 0.048 sec for deposits in the embayment reported by Herrmann and Akinci (2000). The parameter kappa (κ) defines a low-pass filter of the form $\exp(-\pi\kappa f)$ which attenuates high-frequency energy (Anderson and Hough, 1984). Our *H/V* ratios are compared with the site amplifications calculated using quarter-wavelength method by Romero and Rix (2005) for the Uplands and Lowlands profiles (Figure 3-8). The quarter-wavelength approximation for the Uplands profile is compared to the *H/V* ratios for stations GLAT, HALT, HICK, and LNXT. Also, the same comparison is made for the Lowlands soil profile and the *H/V* ratios for stations GNAR, HENM, PENM, PARM and LPAR. The *H/V* ratios correlate with the theoretical quarter-wavelength estimates for the Uplands profile for frequencies less than 10 Hz. The *H/V* ratios on average show higher estimations than the quarter-wavelength method for Uplands. The Lowlands profile also

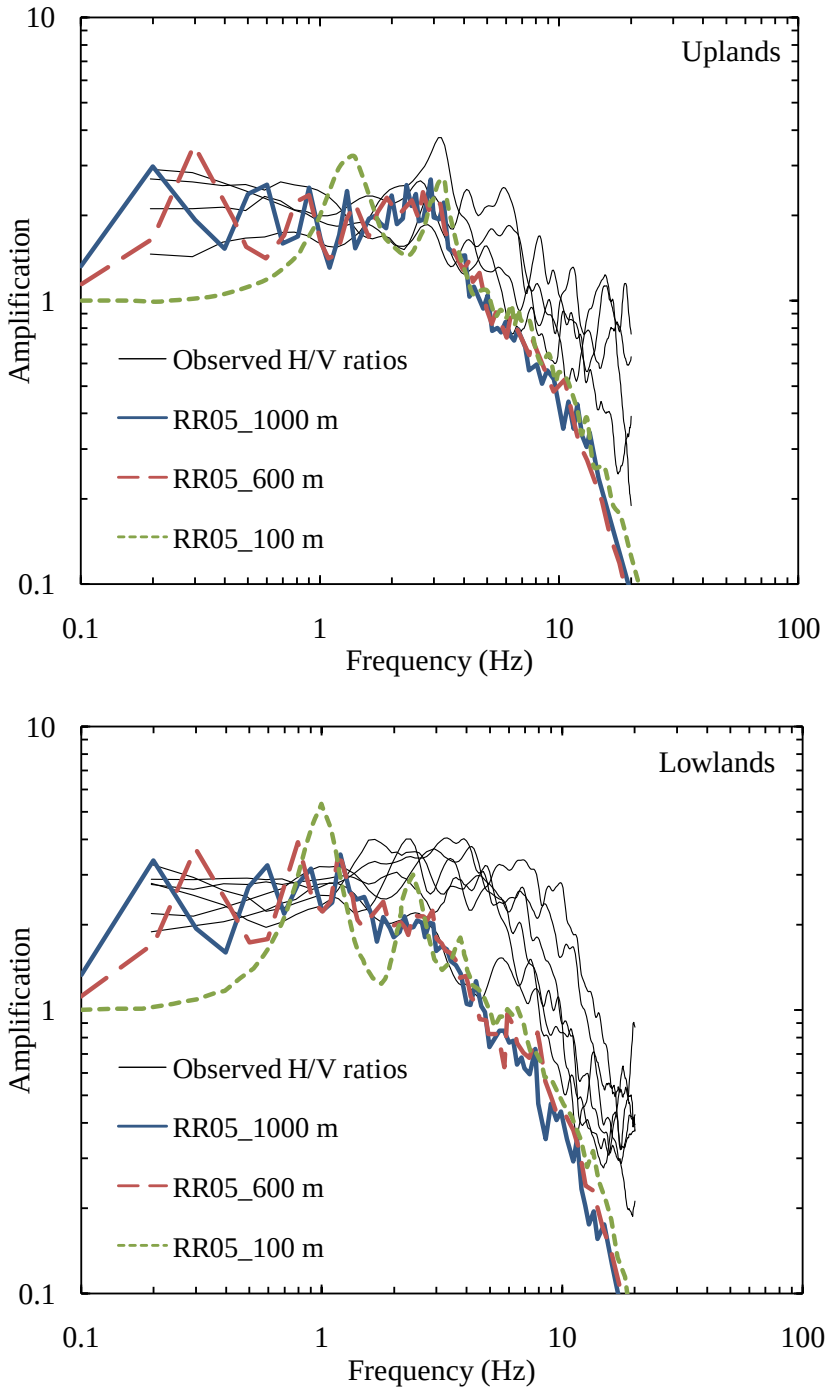

Figure 3-7. Comparison of the amplifications obtained in this study for E-W direction (thin lines) with those of Romero and Rix (2005) (thick lines), for the Uplands profiles (upper) and the Lowlands profiles (lower). The Romero and Rix (2005) amplification factors are denoted by RR05 for the three soil column depths of 100, 600, and 1000 meters.

correlates with the quarter-wavelength method except in the frequency range between 2 and 8 Hz where the *H/V* ratios have higher values than the quarter-wavelength approximations. Larger peaks observed at specific frequencies, are likely the result of resonant effects which are not accounted for in the quarter-wavelength method (Atkinson and Cassidy, 2000).

The agreement between *H/V* ratios and quarter-wavelength estimates suggests that the *H/V* ratios could be a first approximation of the site effects. Obviously, the two methods are not correlated in all bandwidths based on the fundamental differences between them. The smooth prediction of the quarter-wavelength method is because it does not account for the resonant effects in the soil column (Atkinson and Cassidy, 2000) while multiple peaks are observed in the *H/V* ratios in specific frequencies.

Another aspect of this study is to examine the variability of *H/V* ratios with distance. Zandieh and Pezeshk (2010) analyzed the vertical-component ground motions using the same database as in this study and determined that the path effect considering the geometrical spreading and quality factor functions for the NMSZ. By characterizing the variability of *H/V* ratios with distance, one can determine if the path effect derived in Zandieh and Pezeshk (2010) for the vertical-component is applicable for the horizontal-component ground-motions as well. At each frequency, we plotted the individual *H/V* ratios for all stations against distance and examined the trend by fitting a straight line. The frequency steps for the Fourier amplitudes are approximately 0.0977 Hz (~0.1 Hz) based on our signal processing. We also, evaluated the standard error for the slope of the fitted line (Montgomery and Runger, 2002). As a typical example, the plots of *H/V* ratios

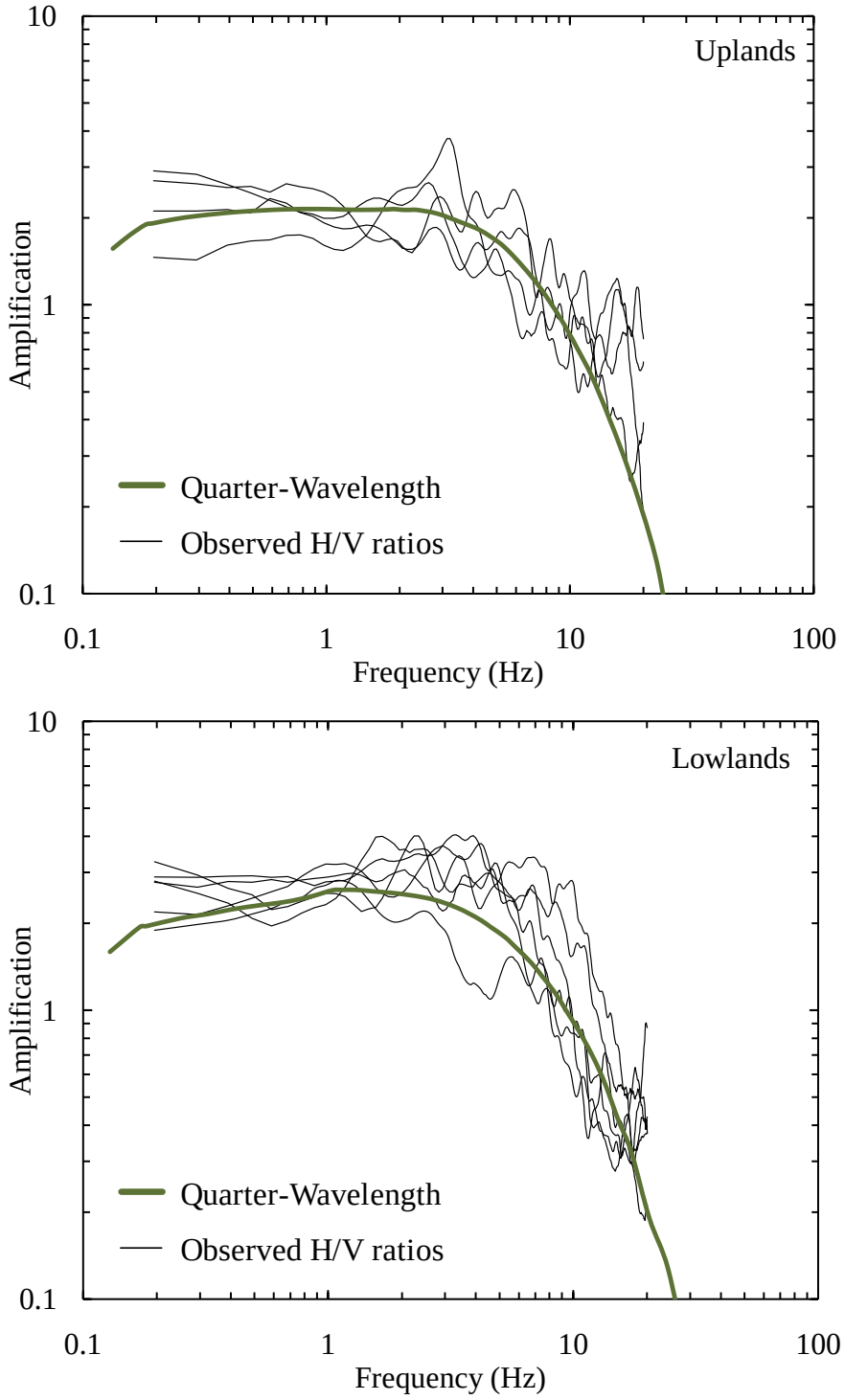

Figure 3-8. Comparison of the amplifications obtained in this study for E-W direction (thin lines) with the quarter-wavelength approximations (thick lines), for the Uplands profiles (upper) and the Lowlands profiles (lower).

versus distance at frequencies of 1 and 5 Hz are shown in Figure 3-9 along with the fitted straight line to the data points and the standard error of the slope. The slope is 0.0009 and its standard error is 0.0005 for 1 Hz. At 5 Hz the slope is 0.0006 and its standard error is 0.0008. For all the frequencies, the slope of the fitted line in close to zero and its standard error is between 0.0005 and 0.0009. We evaluated the confidence intervals of the slope using the *t*-distribution (Montgomery and Runger, 2002). Considering a slope of 0.0009 with the standard error of 0.0009, the 95% confidence interval on the slope of the regression line is [-0.0009, 0.0027]. We interpret that there is no significant trends apparent in *H/V* ratios versus distance. This leads us to conclude that the path model developed for the vertical-component ground-motion for the NMSZ region in Zandieh and Pezeshk (2010) can be used to describe the path effect for horizontal components as well. The path term developed in Zandieh and Pezeshk (2010) consists of a hinged-trilinear geometrical spreading function and a frequency-dependent quality factor function. Their analysis of the geometrical spreading indicates that at distances less than 70 km the spectral amplitudes decay as R^{-1}, between 70 and 140 km the spectral amplitudes increase with distance and the geometrical spreading is defined as $R^{+0.25}$. Beyond 140 km, the attenuation is described by $R^{-0.5}$. The quality factor function is expressed as $Q = 614 f^{0.32}$ for frequencies greater than 1 Hz (Zandieh and Pezeshk, 2010).

3.6 Conclusions

Lermo and Chavez-Garcia (1993) showed that the Nakamura (1989) *H/V* ratio technique

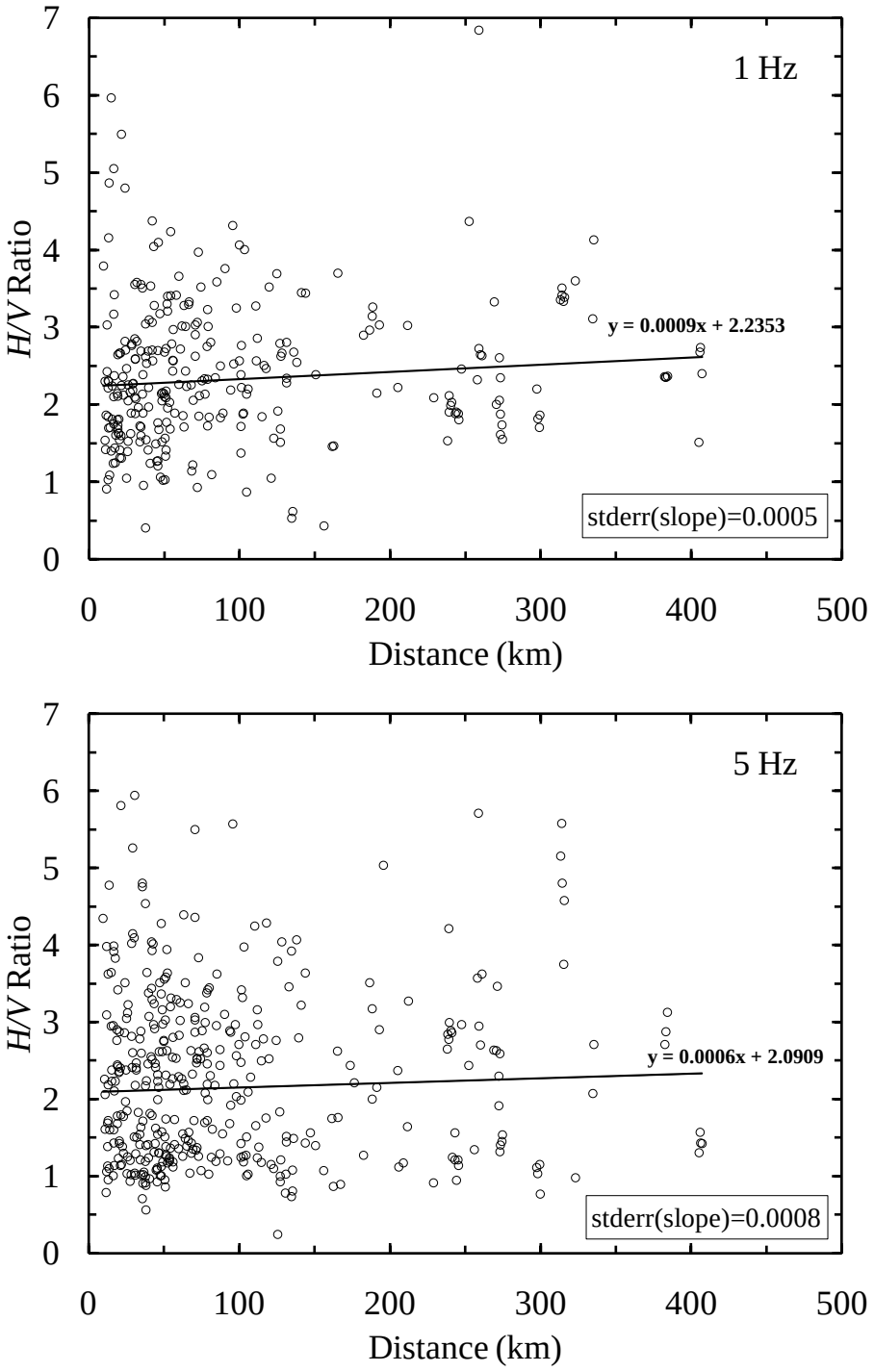

Figure 3-9. Observed *H/V* ratios versus distance for frequencies of 1 and 5 Hz (circles). The solid lines are the fitted straight lines to data points. The equation of the fitted lines along with the standard error of the slope, stderr(slope), are also shown.

can be applied to shear-wave part of the recorded ground motions, and the *H/V* ratios provide a reasonable estimate of the first resonant mode frequency and amplitude of the soil deposits. We applied the *H/V* ratios of the shear-wave window for the recorded ground motions to sites in the NMSZ for site effect evaluation. The database consisted of 500 seismograms from 63 events between magnitude M_w 2.5 and 5.2 that were recorded by eleven CERI broadband stations. The calculated *H/V* ratios at each station, show considerable event-to-event variability; therefore, the mean *H/V* ratios for all events is used as an indicator of the site amplification for the sites. Stations located on Lowlands deposits amplify the weak motions by factors of 2 to 4 at low frequencies range and stations located on Uplands deposits show amplification factors between 1.5 and 3 at low-frequencies ($f \leq 5\,\mathrm{Hz}$). The mean *H/V* ratios are compared with the soil amplifications derived by Romero and Rix (2005) for Lowlands and Uplands generic profiles using the one-dimensional equivalent-linear. The *H/V* ratios are relatively consistent with the Romero and Rix (2005) amplifications for the low frequencies of $f \leq 2\,\mathrm{Hz}$ while for high frequencies the Romero and Rix (2005) amplifications drop off more rapidly than *H/V* ratios. Romero and Rix (2005) predict a lower amplification for frequencies greater than 1.5 Hz in Lowlands and a higher amplification for frequencies greater than 3 Hz in Uplands.

The observed *H/V* ratios are also compared with the quarter-wavelength method. The *H/V* ratios are in good agreement with the theoretical quarter-wavelength estimates for the Uplands and Lowlands profiles within certain bandwidths (less than 10 Hz for Uplands and outside the range between 2 and 8 Hz for Lowlands) suggesting that the *H/V*

ratios could be a first approximation of the site effects. The smooth prediction of the quarter-wavelength method is because it does not account for the resonant effects in the soil column (Atkinson and Cassidy, 2000) while multiple peaks are observed in the *H/V* ratios in specific frequencies.

The variability of the *H/V* ratios with distance is also examined and no discernible trends were found; therefore, the path effect model developed by Zandieh and Pezeshk (2010) for the vertical ground motions in NMSZ is applicable for the horizontal ground motions as well. The path term includes a hinged-trilinear geometrical spreading function and a frequency-dependent quality factor function.

3.7 Data and Resources

Seismograms used in this study were collected as part of the ANSS Central and Eastern United States. Data can be obtained from the Advanced National Seismic System from http://earthquake.usgs.gov/monitoring/anss/regions/mid/ (last accessed April 2010).

3.8 Acknowledgments

We wish to thank many people who contributed data, information, or criticisms. In particular, we wish to thank Mitch Withers for providing broadband seismograms and Heather DeShon and Christy Chiu for helping in data processing. We thank Gail Atkinson for her insightful and constructive guidance. We also thank anonymous

reviewers for their thorough comments and suggestions, which greatly helped improve the article.

3.9 References

Atkinson, G. M. (2004). Empirical attenuation of ground motion spectral amplitudes in southeastern Canada and the northeastern United States, *Bull. Seism. Soc. Am*. **94**, 1079–1095.

Atkinson, G., and J. Cassidy (2000). Integrated use of seismograph and strong motion data to determine soil amplification in the Fraser Delta: results from the Duvall and Georgia Strait earthquakes, *Bull. Seism. Soc. Am*. **90**, 1028–1040.

Atkinson, G., and R. Mereu (1992). The shape of ground motion attenuation curves in southeastern Canada, *Bull. Seism. Soc. Am.* **82**, 2014–2031.

Catchings, R.D. (1999). Regional Vp, Vs, Vp/Vs, and Poisson's Ratios across Earthquake Source Zones from Memphis, Tennessee, to St. Louis, Missouri, *Bull. Seism. Soc. Am*. 89, 1591–1605.

Borcherdt, R. D. (1970). Effects of local geology on ground motion near San Francisco Bay, *Bull. Seism. Soc. Am*. **60**, 29–61.

Bour, M., D. Fouissac, P. Dominique, and C. Martin (1998). On the use of micro-tremor recordings in seismic microzonation, *Soil Dyn. Earthquake Eng*. **17**, 465–474.

Johnston, A.C., and E.S. Schweig (1996). The enigma of the New Madrid earthquakes of 1811- 1812, Annual Review of Earth and Planetary Sciences. **24**, 339–384.

Lermo, J., and F. Chavez-Garcia (1993). Site effect evaluation using spectral ratios with only one station, *Bull. Seism. Soc. Am*. **83**, 1574–1594.

Montgomery, D. C., and G. C. Runger (2002). *Applied Statistics and Probability for Engineers*, John Wiley and Sons Inc., New York.

Nakamura, Y. (1989). A method for dynamic characteristics estimation of subsurface using microtremor on the ground surface, *Quarterly Report of Railway Technical Institute (RTRI)*, **30**, 25–33.

Romero, S. M., and G. J. Rix (2005). Ground motion amplification in the Upper Mississippi embayment, GIT-CEE/GEO-01-1, School of Civil and Environmental Engineering, Georgia Institute of Technology, Atlanta, Georgia.

Siddiqqi, J., and G. Atkinson (2002). Ground motion amplification at rock sites across Canada, as determined from the horizontal-to-vertical component ratio, *Bull. Seism. Soc. Am*. **92**, 877–884.

Toro G.R., W.J. Silva, R.K. McGuire, and R.B. Herrmann (1992). Probabilistic seismic hazards mapping of the Mississippi embayment, *Seism. Res. Lett.* **63**, 449–475.

Van Arsdale, R.B., and R.K. TenBrink (2000). Late Cretaceous and Cenozoic Geology of the New Madrid Seismic Zone, *Bull. Seism. Soc. Am*. **90**, 345–356.

Welch, P. D. (1967). The Use of Fast Fourier Transform for the Estimation of Power Spectra: A Method Based on Time Averaging Over Short, Modified Periodograms, *IEEE Transactions Audio Electroacoustics*, Volume **AU-15**, 70-73.

Zandieh, A., and S. Pezeshk (2010). Investigation of Geometrical Spreading and Quality Factor Functions in the New Madrid Seismic Zone, *Bull. Seism. Soc. Am.* **100**, 2185–2195.

4 Hybrid Empirical Ground-Motion Prediction Equations for Eastern North America Using NGA Models and Updated Seismological Parameters

4.1 Abstract

In the field of earthquake engineering, ground-motion prediction models are frequently used to estimate the peak ground acceleration (PGA) and the pseudospectral acceleration (PSA). In regions of the world where ground-motion recordings are plentiful such as western North America (WNA), the ground-motion prediction equations are obtained using empirical methods. In other regions such as eastern North America (ENA), with insufficient ground-motion data, alternative methods must be used to develop ground-motion prediction equations (GMPEs). The hybrid empirical method is one such method used to develop ground-motion prediction equations in areas with sparse ground motions. This method employs the stochastic simulation method to adjust empirical GMPEs developed for a region with abundant strong motion recordings in order to estimate strong-motion parameters in a region with a sparse database. The adjustments take into account differences in the earthquake source, wave propagation, and site-response characteristics between the two regions.

In this study, a hybrid empirical method is used to develop a new GMPE for ENA, using five new ground-motion prediction models developed by the Pacific Earthquake Engineering Research Center (PEER) for WNA. A new ENA GMPE is derived for a magnitude range of 5 to 8 and closest distances to the fault rupture up to 1000 km. GMPEs are developed for the response spectra (pseudo-acceleration, 5%

damped) and the PGA for hard-rock sites in ENA. The resulting ground-motion prediction model developed in this study is compared with two ENA ground-motion models used in the 2008 national seismic hazard maps as well as with available observed data for ENA.

4.2 Introduction

The near-source amplitudes and attenuation of ground-motion amplitudes in engineering applications is of great significance. For seismic hazard applications, ground motions are often estimated using mathematical equations, which are called ground-motion prediction equations (GMPEs). These equations relate the ground-motion parameters (the most commonly used are the peak ground acceleration, PGA, and the pseudospectral acceleration, PSA) to seismological parameters of a specific region such as earthquake magnitude, source-to-site distance, local site conditions, and style of faulting. In areas of the world such as western North America (WNA), where ground-motion recordings are plentiful due to highly active seismicity and a dense instrumental recording network, the GMPEs are obtained using empirical methods. An example is the Next Generation Attenuation (NGA) project by the Pacific Earthquake Engineering Research Center (PEER) (Power *et al.*, 2008). In the NGA project, five different ground-motion models are developed for WNA (Abrahamson and Silva, 2008; Boore and Atkinson, 2008; Campbell and Bozorgnia, 2008; Chiou and Youngs, 2008; Idriss, 2008).

For regions with historical or observed seismicity but insufficient strong ground-motion data, GMPEs cannot be developed using empirical methods. An example of such

a region is eastern North America (ENA), which is considered a stable continental region with abundant ground-motion data of moderate and small events but sparse data in the magnitude-distance range of most engineering interest. In areas like ENA, stochastic simulation methods can be used to estimate strong ground motions for the distance and magnitude range of interest. These estimations can then be used to develop a GMPE using in the same approach that is used for actual ground-motion data. In this approach, a stochastic representation of the ground motion is developed using seismological models of the source spectrum and the propagation path (McGuire and Hanks, 1980; Hanks and McGuire, 1981; Boore 1983, 2003). Examples of using the stochastic method to develop GMPEs in ENA are Atkinson and Boore (1995, 1998, 2006), Frankel *et al.* (1996), and Toro *et al.* (1997).

GMPEs developed based on actual data are often well constrained, depending on the richness of the database, and represent the inherent characteristics of ground motions especially in the near-source regions. On the other hand, GMPEs obtained from stochastic models may lack realistic near-source characteristics, especially the magnitude saturation. This happens because the stochastic point-source model is not constrained to represent near-source characteristics of actual ground motions. This issue in the stochastic point-source model is improved through the stochastic double-corner model (Atkinson and Boore, 1995, 1998; Atkinson and Silva, 1997) and the more complicated finite-fault models (Beresnev and Atkinson, 1999, 2002; Motazedian and Atkinson, 2005; Atkinson and Boore, 2006).

The hybrid empirical method (Campbell, 2000, 2003) is another procedure to develop GMPEs in areas with sparse ground motions. This method uses the stochastic simulation method to adjust empirical GMPEs developed for the host region, which in this study is WNA. The method is then used to estimate synthetic strong ground-motion parameters in the target region, which in this study is ENA (where there are a limited number of strong-motion recordings). These adjustments take into account the differences in the earthquake source, wave propagation, and site-response characteristics between the two regions. The hybrid empirical method is used by several authors to develop GMPEs in ENA (Campbell, 2003, 2007, 2008; Tavakoli and Pezeshk, 2005). The hybrid empirical method has also been used for Central Europe (Scherbaum *et al.*, 2005), southern Spain, and southern Norway (Douglas *et al.*, 2006).

Campbell (2003) proposed a hybrid empirical method based on a point-source stochastic model using four empirical GMPEs for WNA. Campbell (2007) updated this hybrid empirical ground-motion model using the new WNA empirical ground-motion prediction model by Campbell and Bozorgnia (2008) in the NGA project. He used a stress drop of 140 bars for ENA point-source stochastic simulations and developed GMPEs for sites with the NEHRP B/C site condition $(V_{s30} = 760\,\mathrm{m/s})$. Campbell (2008) used a stress drop of 280 bars in stochastic simulations of ENA ground motions to obtain a better agreement with the Atkinson and Boore (2006) finite-source simulations, and derived revised hybrid empirical ground-motion estimations in ENA. The Campbell (2008) ground motions are determined for a NEHRP A site condition $\left(V_{s30} \geq 2000\,\mathrm{m/s}\right)$ in ENA using the empirical amplification factors used in Atkinson and Boore (2006).

Tavakoli and Pezeshk (2005) proposed a hybrid empirical model for ENA using a magnitude dependent stress parameter in the WNA stochastic simulations. They used a generic source function as combination of single-corner and double-corner source models. Furthermore, they used the modified distance based on the Atkinson and Silva (2000) effective depth in the point-source stochastic simulations to mimic the finite-fault effects.

The purpose of this article is to update the Tavakoli and Pezeshk (2005) model to develop a new hybrid empirical GMPE for ENA using five new ground-motion prediction models developed by the PEER center (Power *et al.*, 2008) for WNA (Abrahamson and Silva, 2008; Boore and Atkinson, 2008; Campbell and Bozorgnia, 2008; Chiou and Youngs, 2008; Idriss, 2008). Furthermore, recent new information on ENA seismological parameters such as stress parameter, geometric spreading, anelastic attenuation, and site response term are used to update the GMPE. In this study, the stochastic point-source model is used for both WNA and ENA regions to obtain ground motions at different magnitude-distance ranges of interest. A new functional form is defined for the GMPE, and a nonlinear regression analysis is performed to estimate period-dependent regression coefficients for a magnitude range of 5 to 8 and closest distances to the fault rupture up to 1000 km. GMPEs are developed for the response spectra (pseudo-acceleration, 5% damped) and the PGA, for hard-rock sites (near-surface shear-wave velocity $\beta_s \geq 2\,\mathrm{km/s}$, or NEHRP site class A), in ENA as a function of the moment magnitude and the closest distance to the fault rupture. The resulting ground-

motion prediction model developed in this study is compared with other recent GMPEs as well as with the available observed data for ENA.

4.3 Hybrid Empirical Method

In the hybrid empirical method, the target region (ENA in this study) ground motions are predicted from the host (WNA in this study) empirical GMPEs using modification factors between two regions (Campbell, 1987, 2000, 2003). These theoretical modification factors are calculated as the ratio of stochastic simulations of ground motions for two regions. Using regional seismological parameters in simulations, the adjustment factors reflect the regional differences in source, path, and site. In the hybrid empirical method, the empirically derived ground-motion models for the host region are mapped onto the target region considering the seismological regional disparities. The key assumption in the hybrid empirical method is that the near-source distance and magnitude saturation effects for the target region (ENA) is considered to be the same as those observed in the host region (WNA). Another interpretation of the method is that the differences between the empirical and stochastic estimations for the host region are applied to the stochastic ground-motion predictions in the target region as corrections to derive a hybrid empirical model.

In this study, the computer program gm_td_drvr, one of the SMSIM programs (Boore, 2005) is used to perform the stochastic simulation of ground-motion amplitudes for both WNA and ENA, using the seismological parameters given in Table 4-1. The

output of the program is the PGA or the PSA at given periods. The adjustment factors are the ratio of the simulated spectral values for ENA with respect to those for WNA.

Table 4-1
Median Parameter Values Used with the Stochastic Method in WNA and ENA

Parameter	WNA	ENA
Source spectrum model	Single-corner-frequency ω^{-2}	Single-corner-frequency ω^{-2}
Stress parameter, $\Delta\sigma$ (bars)	80	250
Shear-wave velocity at source depth, β_s (km/s)	3.5	3.7
Density at source depth, ρ_s (gm/cc)	2.8	2.8
Geometric spreading, $Z(R)$	$\begin{cases} R^{-1.0}; R < 40\,km \\ R^{-0.5}; R \geq 40\,km \end{cases}$	$\begin{cases} R^{-1.3}; R < 70\,km \\ R^{+0.2}; 70 \leq R < 140\,km \\ R^{-0.5}; R \geq 140\,km \end{cases}$
Quality factor, Q	$180 f^{0.45}$	$\max(1000, 893 f^{0.32})$
Source duration, T_s (sec)	$1/f_a$	$1/f_a$
Path duration, T_p (sec)	$0.05R$	$\begin{cases} 0; & R \leq 10\,km \\ +0.16R; & 10 < R < 70\,km \\ -0.03R; & 70 < R \leq 130\,km \\ +0.04R; & R > 130\,km \end{cases}$
Site amplification, $A(f)$	Boore and Joyner (1997)	Atkinson and Boore (2006)
Kappa, κ_0 (sec)	0.04	0.005

4.4 Stochastic Ground-Motion Simulation

In stochastic simulation methods, the ground-motion acceleration is modeled as a filtered Gaussian white noise modulated by a deterministic envelope function defined by seismological parameters. The filter parameters are determined by either matching the

empirical properties of the spectrum of the strong ground-motion theoretical spectral shapes, or are determined on the basis of reliable physical characteristics of the earthquake source and propagation media (Hanks and McGuire, 1981; Boore, 1983, 2003). Recent investigations into the stochastic point source model and its relationship to stochastic finite fault models are given in Atkinson *et al.* (2009) and Boore (2009).

A point-source model is used in this study for stochastic simulations. In this model the total Fourier amplitude spectrum of displacement, $Y(M_0, R, f)$, for horizontal ground motions due to shear-wave propagation may be modeled as (Boore, 2003):

$$Y(M_0, R, f) = E(M_0, f)P(R, f)G(f)I(f) \tag{4-1}$$

where M_0 is the seismic moment (dyne-cm), R is the distance (km), and f is the frequency (Hz). $E(M_0, f)$ is the point-source spectrum term, $P(R, f)$ is the path effect function, $G(f)$ is the site response term, and $I(f)$ is the type of motion function.

In the stochastic point-source model, the earthquake source is assumed to be focused at a point, which is a reasonable assumption for small earthquakes and when the distance from source to site is considerably larger than source dimensions. For large earthquakes the finite-fault effects influence the ground motions especially at close distances. Atkinson and Silva (2000) defined an effective distance, R'_{rup}, to be used in point-source stochastic simulations to mimic the finite-fault effects. They defined a magnitude-dependent equivalent point-source depth, h, to modify the closest distance to fault rupture, R_{rup}, and to account for the fact that most of the surface of a finite fault will be at a distance greater than R_{rup}:

$$R'_{rup} = \sqrt{R_{rup}^2 + h^2} \tag{4-2}$$

where from Atkinson and Silva (2000):

$$\log h = -0.05 + 0.15M \tag{4-3}$$

In this study, the effective distance, R'_{rup}, is used in the stochastic simulations to evaluate the adjustment factors. The NGA models are first evaluated for a set of R_{rup} distances, and then corresponding R'_{rup} distances from equation (4-3) are used in the stochastic simulations to determine the adjustment factors for R_{rup} distances. Finally, the hybrid empirical model for ENA is derived as a function of R_{rup}.

We employed the seismological model parameters used in Atkinson and Boore (2006), Atkinson *et al.* (2009), and Boore (2009) for ENA, and parameters used in Atkinson and Silva (2000) for WNA to simulate ground motions. The seismological model parameters for both ENA and WNA regions are summarized in Table 4-1, and are discussed in more detail in the following sections. We did not model the uncertainty associated with the stochastic model parameters, that is, only one scalar value is used as the median parameter values.

4.4.1 Earthquake Source Model

We used the Brune (1970, 1971) point-source spectrum for the source modeling in stochastic simulations. The Brune model is a single-corner frequency point source spectrum in which stress parameter, $\Delta\sigma$, controls the high-frequency level of the

spectrum. The choice of stress parameter for stochastic ground-motion simulations in ENA has been the subject of several studies such as Atkinson and Boore (2006), Atkinson et al. (2009), Boore (2009), and Boore et al. (2010). The preference of the stress parameters used for both ENA and WNA regions is discussed in the following sections.

4.4.1.1 Choice of Stress Parameter in ENA

Atkinson and Boore (2006) used a median stress parameter of 140 bars for ENA in their finite-fault simulations using the computer code EXSIM (Motazedian and Atkinson, 2005). Campbell (2008) found that a higher stress parameter (e.g., 280 bars) has to be used with SMSIM to predict ground motions similar to those of Atkinson and Boore (2006). Atkinson *et al.* (2009) and Boore (2009) found that the stress parameter of 250 bars should be used in SMSIM simulations in order to attain agreement with the Atkinson and Boore (2006) finite-fault predictions, due to differences in normalization conventions between the two programs. They also pointed out that using the effective distance measure proposed by Boore (2009) in the SMSIM calculations results in a much better match between SMSIM and EXSIM results at close distances.

Boore *et al.* (2010) determined the stress parameter for eight well-recorded earthquakes in ENA with data that are largely at distances of 100-800 km. They showed that estimates of $\Delta\sigma$ are correlated to the rate of geometrical spreading at close distances using SMSIM point-source simulations, they evaluated a geometric-mean $\Delta\sigma$ of 250 bars for the Atkinson (2004) attenuation model (including geometrical spreading and quality factor function) for the case in which the 1988 Saguenay earthquake is included.

Atkinson and Assatourians (2010) found a stress parameter of 250 bars for the magnitude 5.0 Val-des-Bois Quebec earthquake.

Based on the previous discussion, a stress parameter of 250 bars is used in the ENA point-source stochastic simulations, together with the attenuation model of Atkinson (2004), to be consistent with the study of Boore *et al.* (2010) and the findings of Atkinson *et al.* (2009) and Atkinson and Assatourians (2010).

4.4.1.2 Choice of Stress Parameter in WNA

Atkinson and Silva (2000) examined ground motions for California using a stochastic finite-fault model, and introduced an equivalent two-corner-frequency point-source spectrum which mimics the conspicuous finite-fault effects. They showed that the double-corner-frequency source model and the Brune single-corner frequency spectrum with the stress parameter of 80 bars are close for moment magnitudes (M_w) less than 6.0, and the goodness-of-fit to the data are equivalent. However, at large magnitudes and low frequencies, where finite-fault effects become significant, the two models become different due to the spectral sag in the double-corner model.

In this study, a stress parameter of 80 bars is used for the point-source stochastic simulations for WNA using the Brune single-corner frequency model. In Figure 4-1, the stochastic simulations using a stress parameter of 80 bars for WNA are compared to NGA model predictions for an M_w 6.0 earthquake at distance R_{rup} =10 km. The comparison is made at M_w 6.0 to avoid small-magnitude bias in NGA models for small magnitudes (Atkinson and Morrison, 2009; Chiou *et al.*, 2010; Atkinson and Boore, 2011), and to avoid the large magnitude issue associated with finite-fault effects in the

stochastic modeling. In other words, we anchor the WNA stress drop at moderate magnitudes, where this parameter is most robust and most comparable to the ENA stress value. This comparison shows reasonable agreement between the NGA models and the WNA stochastic ground-motion simulations developed in this study. It should be noted that the seismological parameters of Table 4-1 and the effective distance from Atkinson and Silva (2000) are used in the simulations.

4.4.2 Filter Function of the Transfer Media

The path effect, $P(R, f)$ in equation (4-1), consists of a geometrical spreading function and an anelastic attenuation term described by the quality factor function (Boore, 2003).

4.4.2.1 Choice of Path Model for ENA

Atkinson and Boore (2006) used the trilinear geometrical spreading along with the quality factor of Atkinson (2004) in their simulations. Boore *et al.* (2010) found that stress parameter is strongly tied to the choice of geometrical spreading. They consider four geometrical spreading functions, ranging from a simple $1/R$ model at all distances to more complicated bi-and trilinear functions and determined the stress parameter for eight ENA earthquakes for each path model. As mentioned previously, for the Atkinson (2004) path model the median stress parameter of 250 bars were estimated for ENA events including Saguenay. They showed that the simple $1/R$ model fits the data, most of it being in the distance range of 100 – 800 km, as well as more complex models. However, the presence of a flat or increasing geometrical spreading at intermediate

distances affects the ground motions at the distances of most engineering concern(within 100 km) significantly (Boore *et al.*, 2010).

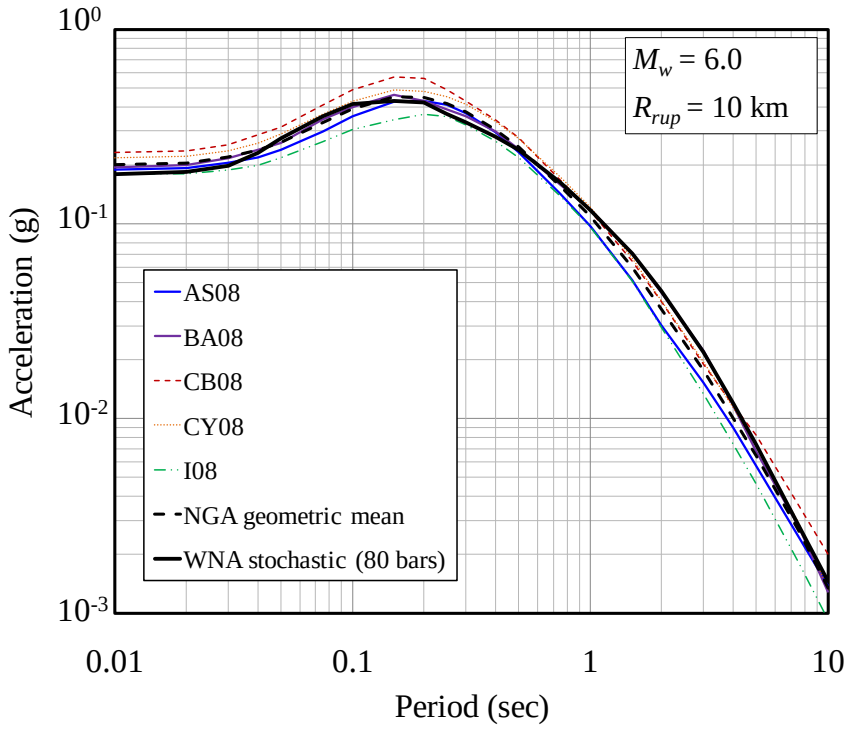

Figure 4-1. Comparison of 5%-damped acceleration response spectra predicted by NGA models with the spectrum predicted from point-source stochastic simulations of this study for M_w 6.0 at $R_{rup} = 10\,\text{km}$ using stress parameter of 80 bars. AS08: Abrahamson and Silva (2008); BA08: Boore and Atkinson (2008); CB08: Campbell and Bozorgnia (2008); CY08: Chiou and Youngs (2008); I08: Idriss (2008).

Atkinson and Assatourians (2010) studied five ENA earthquakes and found that the data fit better if the geometrical spreading of Atkinson (2004) is assumed for hypocentral distances beyond 10 km and a 1/*R* model is used from 1 to 10 km.

The path model of Atkinson (2004) is used in this study for the stochastic simulations. This model is derived from a large database dominated by small earthquakes (i.e., point sources) and has not been confirmed for large events where finite-fault effects

are evident. We assume that using the effective distance in point-source simulations (equation 4-2) captures the finite-fault effects, and therefore the Atkinson (2004) model will apply to the attenuation of R'_{rup}. The alternative treatment of near-source attenuation suggested in Atkinson and Assatourians (2010) (i.e., switching to 1/*R* from 1 to 10 km) is not employed here since the effective distance of Atkinson and Silva (2000) is being used and further saturation is not required (G. Atkinson, personal commun., 2010). The geometrical spreading function and the quality factor function of Atkinson (2004) are provided in Table 4-1.

4.4.2.2 Choice of Path Model for WNA

Raoof *et al.* (1999) derived an attenuation model for Southern California from studying 820 three-component broadband recordings from 140 moderate-to-large earthquakes over distances of hundreds of km. The model consists of a bilinear geometrical spreading function with a 40-km crossover distance ($1/R$ for $R \le 40\,\text{km}$ and $R^{-0.5}$ for larger distances), coupled to an quality factor function of the form $Q = 180 f^{0.45}$. The model is determined for data within the 0.25 and 5 Hz range. Atkinson and Silva (2000) used the Raoof *et al.* (1999) path model in their finite-fault simulations. Malagnini *et al*. (2007) studied a dataset of 5,769 waveforms from 281 small-to-moderate events located within 200 km of the San Francisco Bay Area to derive a regional attenuation model for frequencies ranging between 0.25 and 20 Hz. Their study supports the path model developed by Raoof *et al.* (1999) since it includes a geometrical spreading coefficient of –1.0 for $R \le 30\,\text{km}$ and –0.6 for larger distances, and an anelastic

attenuation of $Q = 180 f^{0.42}$. Therefore, the path model of Raoof *et al.* (1999) is used in this study for the simulation of ground motions in WNA.

4.4.3 Site Effects

The site effect, $G(f)$ in equation (4-1), can be separated into site amplification factors, and a near-surface attenuation term, which models the near surface damping effects and is independent of path. We employed the model of Anderson and Hough (1984) for near-source attenuation, which is described as a low-pass filter and is defined by the decay slope of the spectrum at high frequencies, kappa (κ_0) (at near-source distances).

4.4.3.1 Choice of Site Effects for ENA

Campbell (2003) and Tavakoli and Pezeshk (2005) developed hybrid empirical models for the ENA hard-rock shear-wave velocity profile and the generic ENA amplification model of Boore and Joyner (1997) ($V_{s30} = 2880\,\text{m/s}$). The empirical site amplifications and the kappa value used in Atkinson and Boore (2006) for hard-rock sites (NEHRP site class A, $V_{s30} \geq 2000\,\text{m/s}$, κ_0=0..05) are employed in the simulations. This choice is made to be consistent with the use of stress parameters of 250 bars and corresponding path model from the work of Atkinson *et al.* (2009), Boore (2009), and Boore *et al.* (2010), since the same amplification factors and kappa are used in these studies to derive the stress parameter of 250 bars for ENA. The presumed amplifications increase from 1.0 for frequencies less than 0.5 Hz to 1.4 for frequencies greater than 10

Hz as based on Siddiqqi and Atkinson (2002). The amplification factors and the kappa value used for ENA hard-rock sites are provided in Table 4-1.

4.4.3.2 Choice of Site Effects for WNA

Atkinson and Silva (2000) used the amplifications for generic rock sites introduced by Boore and Joyner (1997) for WNA to derive a model for California. Campbell (2003, 2007) and Tavakoli and Pezeshk (2005) also used the generic rock sites of Boore and Joyner (1997) for the stochastic modeling of ground motions in WNA. The WNA generic rock site has an average value of shear velocity in the upper 30 meters of about 620 m/sec. The shear-wave velocity at source depth is 3.5 km/sec at a depth of 8 km. The amplification factors for these sites are calculated using the quarter wavelength method (Boore and Joyner, 1997). In this study, the amplification factors of Boore and Joyner (1997) for generic rock sites in WNA are used.

In the WNA region, the value of κ_0 is in the order of about 0.02-0.04 seconds (Anderson and Hough, 1984). Atkinson and Silva (1997) used an average kappa value of 0.04 in their model. We also used the κ_0 value of 0.04 for the rock site in WNA.

All the seismological parameters for ENA and WNA used for stochastic simulations are summarized in Table 4-1. It should be noted that seismological parameters not mentioned previously, and only presented in Table 4-1 (e.g., duration), are the same as the parameters used in Atkinson and Boore (2006) for ENA and Atkinson and Silva (2000) for WNA.

4.5 Ground-Motion Models in WNA

The ground-motion prediction models developed for the PEER NGA project (Power *et al.,* 2008) are used as the empirical ground-motion models for the host region, WNA. In the NGA project, five sets of ground-motion prediction models are developed for shallow crustal earthquakes in the western United States (WUS) and similarly active tectonic regions. The five models used in this study are the 2008 Abrahamson and Silva (AS08); the 2008 Boore and Atkinson (BA08); the 2008 Campbell and Bozorgnia (CB08); the 2008 Chiou and Youngs (CY08); and the 2008 Idriss (I08). The geometric mean of these five models is used as the WNA empirical ground-motion estimates. The geometric mean of the five modified WNA models are used as the hybrid empirical estimates of the ground-motion for ENA in the regression process.

All NGA models have parameterization such as moment magnitude, distance, and style of faulting. The I08 model is applicable only for rock sites while all other models have the average shear-wave velocity in the upper 30 m, V_{s30}, as well as input rock motion parameters to model nonlinear site response (Abrahamson *et al.,* 2008). The AS08, CB08, and CY08 models have additional terms to account for hanging wall effects, rupture-depth effects, and soil/sediment depth effects (Abrahamson *et al.,* 2008). The ground-motion component used in the NGA models is the new geometric mean, referred to as "GMRotI50" (Boore *et al.,* 2006), which is the geometric mean determined from the 50^{th} percentile values of the geometric means computed for all non-redundant rotation angles and all periods less than the maximum useable period; therefore, it is independent of sensor orientation.

In this study, we used a generic style of faulting to evaluate WNA ground-motion prediction relations. This is done because there is no evidence that differences in the ground motions between faulting styles can be expected in the target and host regions (Campbell 2003, 2007). This generic style of faulting is an average of strike slip and reverse fault mechanisms. For this purpose, we set $F_{RV} = 0.5$ and $F_{NM} = 0$ in the AS08, CB08, and CY08 models, *SS* = 0.5, *RS* = 0.5, *NS* = 0.0, and *U* = 0.0 in the BA08 model, and *F* = 0.5 in the I08 model. We did not include the hanging wall effect for the AS08, CB08, and CY08 models. A depth to the top of rupture of zero is assumed in the AS08, CB08, and CY08 models.

We used R_{rup} as the distance metric. BA08 used R_{JB} as the distance measure, which is the closest horizontal distance to the surface projection of the rupture plane. All other models used the closest distance to the rupture plane, R_{rup}. We used the Scherbaum *et al.* (2004) conversion equations to convert R_{JB} to R_{rup} in the BA08 model.

The NGA relations are evaluated for the Boore and Joyner (1997) generic rock site with $V_{s30} = 620$ m/sec. The soil/sediment depth term is defined using different depth parameters in NGA relations. The AS08 and CY08 models use $Z_{1.0}$, depth to $V_s = 1.0\,\mathrm{km/s}$ at the site, and the CB08 model uses $Z_{2.5}$, depth to $V_s = 2.5\,\mathrm{km/s}$ at the site, to model the soil/sediment depth effects. These models have relations for median $Z_{2.5}$ and $Z_{1.0}$ for a given V_{s30} when no soil profile information is available. In this study, we calculated $Z_{2.5}$ and $Z_{1.0}$ based on the WNA generic rock profile.

4.6 Ground-Motion Prediction Equation Developed for ENA

Median hybrid empirical estimates of ENA ground motion are obtained by scaling the WNA empirical relations using theoretical modification factors. The model is evaluated for moment magnitudes 5.0 to 8.0 in 0.5 magnitude unit increments, and for 25 rupture distances (R_{rup}): 1, 2, 5, 10, 15, 20, 30, 40, 50, 60, 70, 80, 100, 120, 140, 180, 200, 250, 300, 400, 500, 600, 700, 800, and 1000 km.

The NGA models are developed for distances less than 200 km; therefore, using them beyond this range is not appropriate. On the other hand, using the hybrid empirical method for $R_{rup} > 70$ km results in an unrealistic attenuation rate for ENA where ground-motion predictions increase substantially with distance for periods within 0.05-3.0 seconds especially for magnitudes larger than 6.5. The reason is that the rate of attenuation predicted by the stochastic model for WNA is higher than the rate predicted in geometric mean of the NGA models for distances greater than 40 km. The decrease in attenuation rate in ENA from 70 to 140 km reinforces the increase in the hybrid empirical estimations for distances greater than 70 km.

This is one limitation of the hybrid empirical method for ENA, that it only provides reliable estimates out to 70 km. In order to avoid these problems, the hybrid empirical method is applied for $R_{rup} \leq 70$ km and hybrid empirical estimations are supplemented with stochastic ENA predictions for beyond 70 km in order to extend the GMPEs up to 1000 km. This is done using the method proposed by Campbell (2003), which scales the stochastic ENA ground-motion predictions by the factor required to make its estimate at $R_{rup} = 70$ km equal to the hybrid empirical method prediction. These

scaled estimates are then used as estimates for R_{rup} beyond 70 km in regression process (to 1000 km) to develop the GMPEs. The GMPEs are developed for an ENA hard-rock site with $V_{s30} \geq 2000\,\mathrm{m/s}$ (NEHRP site class A). For a different site condition, the predictions must be modified using an appropriate method.

The hybrid empirical estimates of ENA ground motion, for magnitudes 5.0-8.0 and rupture distances up to 1000 km, are used in a nonlinear least-square regression to develop the GMPEs. This regression is used to find coefficients defining a functional form, which fits the hybrid empirical estimates of ground-motion in ENA. Relationships are provided for the PGA and for the 5% damped pseudo-spectral acceleration (PSA) for the spectral periods of 0.01 to 10 seconds consistent with the periods used in NGA models.

The following ground-motion prediction functional form is used in this study

$$\begin{aligned}\log(\bar{Y}) = c_1 + c_2 M_W + c_3 M_W^2 + (c_4 + c_5 M_W) \times \min\{\log(R), \log(70)\} \\ + (c_6 + c_7 M_W) \times \max[\min\{\log(R/70), \log(140/70)\}, 0] \\ + (c_8 + c_9 M_W) \times \max\{\log(R/140), 0\} + c_{10} R\end{aligned} \tag{4-4}$$

where

$$R = \sqrt{R_{rup}^2 + c_{11}^2} \tag{4-5}$$

where $\bar{Y}$ is the median value of PGA or PSA (g), M_W is the moment magnitude, and R_{rup} is the closest distance to fault rupture (km).

The mean aleatory standard deviation of $\log(\bar{Y})$ to be associated with the predictions is defined as a function of earthquake magnitude and is modeled as follows:

$$\sigma_{\log(\bar{Y})} = \begin{cases} c_{12} M_w + c_{13} & M \le 7 \\ -6.95 \times 10^{-3} M_w + c_{14} & M > 7 \end{cases} \quad (4\text{-}6)$$

This aleatory standard deviation is constructed using an equally weighted average of the standard deviations from each of the WNA ground-motion prediction models (Campbell, 2003). Standard deviation in AS08, CB08, and CY08 models is related to the ground motion on the reference rock which varies with respect to distance, magnitude, and site condition (V_{s30}). This is done to model the decrease in the standard deviation caused by a nonlinear site response. We observed that the reduction in the standard deviation is not significant for the assumed generic rock site in WNA with $V_{s30} = 620\,\mathrm{m/s}$. Therefore, in this study we neglected the soil nonlinearity effects in calculation of the standard deviation for NGA relations. After this assumption, the standard deviation in AB08, CY08, and I08 depends only on the magnitude and spectral period. The median aleatory standard deviation of the ground motion in ENA is assumed to equal the average standard deviations of NGA models and therefore depends on magnitude (equation 4-6). The total aleatory standard deviation may be derived by adding the standard deviation of the regression to the aleatory standard deviation from equation (4-6) as follows

$$\sigma^{T}_{\log \bar{Y}} = \sqrt{\sigma^2_{\log \bar{Y}} + \sigma^2_{\mathrm{Reg}}} \quad (4\text{-}7)$$

where σ_{Reg} is the standard deviation of the regression performed to fit the model to ground motion estimates. On the other hand, the model misfit does not represent physical variability and might therefore be neglected for seismic hazard calculation purposes. Regression coefficients c_1 through c_{14} are calculated using a nonlinear least-square method and tabulated in Table 4-2 together with the standard deviation of the fit, σ_{Reg}.

It should be noted that an evaluation of epistemic uncertainty is not included in this study. Based on mathematical framework given by Campbell (2003), the sources of epistemic uncertainty in hybrid empirical method are: (1) the epistemic uncertainty in seismological parameters used in stochastic simulations; and (2) the epistemic uncertainty involved in using different empirical ground-motion models for the host. We did not evaluate epistemic uncertainty in this study because in practice this type of uncertainty can be evaluated by using different models developed for ENA, and the epistemic uncertainty associated with an individual ground-motion model is not generally used (Campbell, 2007).

As mentioned previously, the NGA models are for the GMRotI50 measure of seismic intensity. Therefore, the hybrid empirical model developed in this study predicts the intensity of ground motions for the new geometric mean component, GMRotI50. Boore and Atkinson (2008) suggest using simple conversion factors between GMRotI50 and other measures of seismic intensity given by Beyer and Bommer (2006) and Watson-Lamprey and Boore (2007) as well as by Campbell and Bozorgnia (2008).

Figure 4-2 illustrates a comparison of the result of this study with the update to the 2006 Atkinson and Boore model (Atkinson and Boore, 2011) (hereafter AB06') and the

Tavakoli and Pezeshk (2005) model. The Atkinson and Boore (2006) model is based on a finite-fault stochastic method and is derived for hard rock sites (NEHRP site class A, $V_{s30} \geq 2000\,\mathrm{m/s}$) employing the Atkinson and Boore (2006) empirical site amplification factors; it was recently modified based on new data (Atkinson and Boore, 2011). The new data consist of small-to-moderate ENA events as well as three well-recorded earthquakes with M_w ~5.0. Atkinson and Boore (2011) compared the predictions of the Atkinson and Boore (2006) to the new data and also to the updated version of the Boore and Atkinson (2008) model for WNA to contemplate the magnitude scaling for WNA and ENA, and they inferred that a larger stress parameter should have been used in Atkinson and Boore (2006) for small magnitudes. They defined a magnitude-dependent stress parameter, which decreases as the magnitude increases, to be used in the Atkinson and Boore (2006) model. The modified model (AB06') predicts larger high-frequency amplitudes for $M_w \leq 6$ and lower amplitudes for $M_w \geq 7$ compared to the original Atkinson and Boore (2006) model.

Tavakoli and Pezeshk (2005) used the hybrid empirical method to develop a ground-motion model in ENA for the generic hard-rock site of Boore and Joyner (1997) with $V_{s30} = 2880\,\mathrm{m/s}$ corresponding to the NEHRP A site class. To perform a consistent comparison, the estimations from Tavakoli and Pezeshk (2005) should be adjusted for the site condition in the Atkinson and Boore (2006) model and this study. This adjustment is approximated by multiplying the Tavakoli and Pezeshk (2005) predictions by the ratio of site amplifications in Atkinson and Boore (2006) to the amplification factors of Boore and Joyner (1997). Moreover, the amplification factors of Boore and Joyner (1997) are

Table 4-2

Coefficients of the hybrid empirical model and standard deviation of the regression

T, sec	c_1	c_2	c_3	c_4	c_5	c_6	c_7	c_8	c_9	c_{10}	c_{11}	c_{12}	c_{13}	c_{14}	σ_{Reg}
PGA	1.5828	2.298E-01	-3.847E-02	-3.8325	3.535E-01	3.321E-01	-9.165E-02	-2.5517	1.831E-01	-4.224E-04	6.6521	-2.105E-02	3.778E-01	2.791E-01	0.021
0.010	2.0434	1.987E-01	-3.837E-02	-4.0521	3.688E-01	1.995E-01	-8.918E-02	-2.5948	1.847E-01	-3.965E-04	7.0645	-1.974E-02	3.688E-01	2.792E-01	0.022
0.020	2.3050	1.877E-01	-3.697E-02	-4.0443	3.616E-01	-1.222E-01	-9.157E-02	-2.9998	1.941E-01	-1.707E-04	7.3314	-1.974E-02	3.691E-01	2.796E-01	0.023
0.030	1.9848	2.203E-01	-3.616E-02	-3.8032	3.384E-01	7.814E-02	-1.126E-01	-3.3125	2.017E-01	-5.322E-05	7.1183	-2.094E-02	3.817E-01	2.838E-01	0.022
0.040	1.6854	2.404E-01	-3.578E-02	-3.6129	3.247E-01	2.956E-01	-1.180E-01	-3.3320	1.977E-01	-1.113E-04	6.8113	-2.180E-02	3.914E-01	2.874E-01	0.024
0.050	1.4517	2.414E-01	-3.468E-02	-3.4683	3.177E-01	5.224E-01	-1.296E-01	-3.2109	1.956E-01	-2.669E-04	6.3705	-2.244E-02	3.990E-01	2.905E-01	0.025
0.075	1.0698	2.989E-01	-3.897E-02	-3.3770	3.180E-01	7.422E-01	-1.215E-01	-2.6889	1.723E-01	-6.659E-04	6.0817	-2.312E-02	4.108E-01	2.976E-01	0.025
0.10	0.9314	3.088E-01	-3.844E-02	-3.2926	3.063E-01	7.064E-01	-9.521E-02	-2.2090	1.472E-01	-9.254E-04	6.1621	-2.259E-02	4.102E-01	3.007E-01	0.022
0.15	0.3964	4.317E-01	-4.578E-02	-3.2112	2.937E-01	6.084E-01	-6.727E-02	-1.6121	1.072E-01	-1.077E-03	6.2667	-2.185E-02	4.066E-01	3.023E-01	0.016
0.20	-0.4883	6.278E-01	-5.654E-02	-3.0304	2.673E-01	5.422E-01	-5.347E-02	-1.3516	8.784E-02	-1.045E-03	6.1905	-2.046E-02	3.979E-01	3.033E-01	0.014
0.25	-1.0098	7.401E-01	-6.309E-02	-2.9959	2.623E-01	4.421E-01	-3.625E-02	-1.2309	7.733E-02	-9.648E-04	6.0635	-1.933E-02	3.908E-01	3.041E-01	0.015
0.30	-1.6800	8.860E-01	-7.162E-02	-2.8894	2.481E-01	4.869E-01	-4.324E-02	-1.1490	7.056E-02	-9.049E-04	5.9891	-1.837E-02	3.867E-01	3.068E-01	0.015
0.40	-2.3106	1.022E+00	-7.965E-02	-2.9265	2.515E-01	4.716E-01	-4.039E-02	-1.0923	6.554E-02	-7.853E-04	6.0263	-1.683E-02	3.774E-01	3.082E-01	0.017
0.50	-3.1365	1.201E+00	-9.037E-02	-2.8823	2.456E-01	3.333E-01	-2.105E-02	-1.0022	5.519E-02	-7.069E-04	5.9117	-1.556E-02	3.722E-01	3.119E-01	0.017
0.75	-4.5494	1.508E+00	-1.087E-01	-2.8614	2.424E-01	4.023E-01	-3.092E-02	-0.9750	5.536E-02	-5.685E-04	5.9835	-1.339E-02	3.654E-01	3.203E-01	0.021
1.0	-5.4113	1.690E+00	-1.196E-01	-2.8998	2.465E-01	3.766E-01	-2.928E-02	-0.9470	5.249E-02	-4.563E-04	6.1234	-1.180E-02	3.588E-01	3.249E-01	0.022
1.5	-6.4806	1.867E+00	-1.282E-01	-2.9338	2.525E-01	2.633E-01	-1.442E-02	-0.9007	4.974E-02	-3.540E-04	5.9875	-1.040E-02	3.569E-01	3.327E-01	0.019
2.0	-6.9340	1.907E+00	-1.287E-01	-3.0128	2.639E-01	3.172E-01	-2.150E-02	-0.8749	4.774E-02	-3.025E-04	6.1355	-9.443E-03	3.561E-01	3.387E-01	0.021
3.0	-7.4264	1.881E+00	-1.205E-01	-2.9742	2.576E-01	2.585E-01	-1.520E-02	-0.8821	5.376E-02	-2.641E-04	6.0598	-8.509E-03	3.540E-01	3.431E-01	0.024
4.0	-7.8064	1.895E+00	-1.183E-01	-3.0050	2.588E-01	3.069E-01	-2.545E-02	-0.8808	5.703E-02	-2.423E-04	6.2536	-7.859E-03	3.527E-01	3.463E-01	0.030
5.0	-8.2704	1.938E+00	-1.180E-01	-2.9501	2.503E-01	3.296E-01	-3.023E-02	-1.0125	7.332E-02	-2.002E-04	6.3423	-6.900E-03	3.577E-01	3.580E-01	0.032
7.5	-8.3376	1.806E+00	-1.042E-01	-2.9839	2.542E-01	2.879E-01	-2.252E-02	-1.1817	9.598E-02	-1.624E-04	6.5181	-7.240E-03	3.730E-01	3.710E-01	0.030
10.0	-9.1046	1.899E+00	-1.076E-01	-2.8611	2.395E-01	2.868E-01	-2.290E-02	-1.3786	1.222E-01	-1.268E-04	6.5384	-7.485E-03	3.848E-01	3.810E-01	0.024

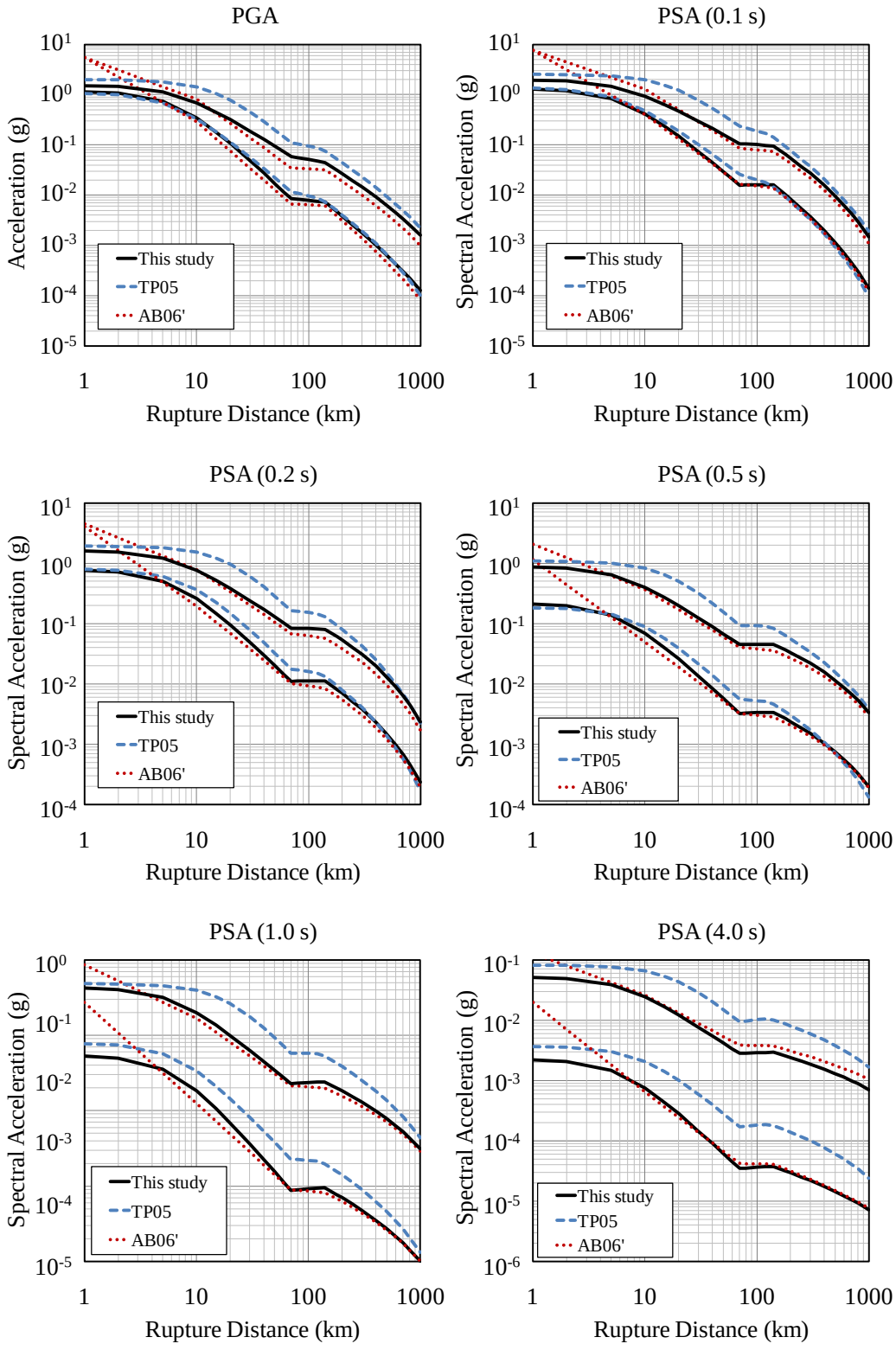

Figure 4-2. Comparison of PGA and PSA developed in this study with the predictions by

two ground-motion models developed for ENA: (lower curve) magnitude 5.0; (upper curve) magnitude 7.0. TP05, empirical hybrid method (Tavakoli and Pezeshk, 2005); AB06', modified version of the 2006 Atkinson and Boore finite-source stochastic model (Atkinson and Boore, 2011). The comparison is for ENA hard-rock sites ($V_{s30} \geq 2000$ m/s) defined in Atkinson and Boore (2006).

evaluated assuming a shear-wave velocity of 3.6 km/s near the source, whereas in the stochastic computations of Atkinson and Boore (2006) and also this study a shear-wave velocity of 3.7 km/s at source is used. Therefore, the amplification ratios of Atkinson and Boore (2006) to Boore and Joyner (1997) are multiplied by $\sqrt{3.7/3.6}$. The modified ratios are used to adjust the Tavakoli and Pezeshk (2005) estimations. The modified amplification ratios are a factor of up to 1.21 at high frequencies.

The ground-motion model comparisons are shown in Figure 4-2 for PGA and PSA at periods of 0.1, 0.2, 0.50, 1.0, and 4.0 seconds for magnitudes 5 and 7 and R_{rup} distances between 1 and 1000 km. It can be observed that the AB06' model has larger values at very close distances in comparison to Tavakoli and Pezeshk (2005) and this study. This may occur because of using a stochastic method, which does not model the saturation effects observed in other active regions (Atkinson, 2008). However, the two models predict similar values for distances greater than 10 km at all magnitudes and frequencies.

Tavakoli and Pezeshk (2005) used a lower median stress parameter compared to this study (150 versus 250 bars) together with the path model of Atkinson and Boore (1995), which consists of a lower near-source attenuation rate than the path model used in this study. Boore *et al.* (2010) evaluated a median stress parameter of about 60 bars for

the Atkinson and Boore (1995) attenuation model. Therefore, it is expected for the Tavakoli and Pezeshk (2005) model (with stress parameter of 150 bars) to predict higher amplitudes than the predictions of this study, especially at higher frequencies. It can be seen in Figure 4-2 that the estimations of Tavakoli and Pezeshk (2005) are similar to the predictions of this study at high frequencies for magnitude 5; however, they are larger for magnitude 7. For larger periods, Tavakoli and Pezeshk (2005) amplitudes are higher for all magnitudes.

4.7 Comparison of Results with Observed Ground-Motion Data for ENA

The predictions of this study are compared to the available ENA ground-motion database used in Assatourians and Atkinson (2010) (see the Data and Resources Section). In Figure 4-3, the 0.2 and 1.0-sec spectral accelerations predicted in this study for M_w 5.0 are compared to the database of Assatourians and Atkinson (2010) for M_w 4.8-5.06 for the NEHRP A site class. It can be seen that the GMPE of this study under-predicts the observations at close distances (60 km). Atkinson and Assatourians (2010) discussed the under-prediction issue of the ENA GMPEs for small magnitudes at close distances for the Val-des-Boise earthquake. They mentioned that applying an average attenuation shape to individual events, despite the event-to-event variation in the attenuation shape, might be the issue. It should be noted that spectral accelerations are shown for both the horizontal components and the vertical component converted to the horizontal component. In general, there is a good agreement between the ground-motion predictions of this study and the ENA database at large distances ($R_{rup} \geq 200\,\text{km}$).

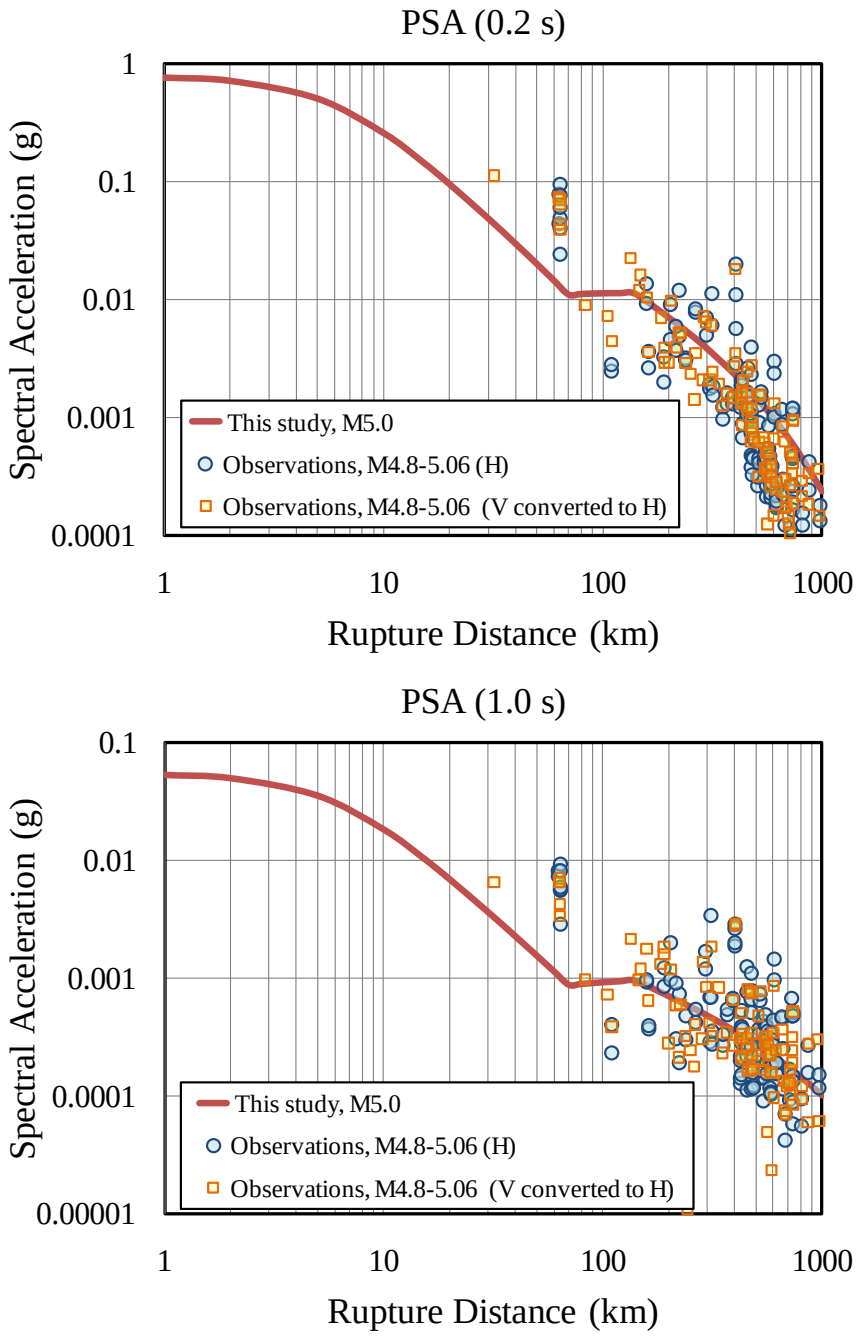

Figure 4-3. Comparison of ground-motion predictions of this study (solid line) for magnitude 5 with the ENA ground-motion observations on the NEHRP A site condition used in Assatourians and Atkinson (2010) for horizontal components (indicated by H) and vertical components (indicated by V) converted to the equivalent horizontal components (a) 5%-damped response spectral acceleration at 0.2-sec period (b) 5%-damped response spectral acceleration at 1.0-sec period.

4.8 Conclusions

A hybrid empirical method is used to develop a ground-motion prediction model (GMPE) for ENA. The hybrid empirical procedure uses WNA empirical ground-motion models from the NGA project (Power *et al.,* 2008) and also, the most recent updated seismological parameters from Boore *et al.* (2010), Boore (2009), Atkinson *et al.* (2009), and Atkinson and Boore (2006) for the ENA stochastic simulations. The major assumption in the hybrid empirical model is that the near-source saturation effects observed in active tectonic regions such as WNA is a general behavior and is the same in other seismic regions. In the hybrid empirical method the empirical models from the host region are scaled by factors accounting for the differences in the source, path, and site effects between the host and the target region. These factors are evaluated using a stochastic method, considering seismological parameters associated to each of the WNA and ENA regions.

For ENA, the stress parameter of 250 bars together with the attenuation model of Atkinson (2004) are used in the stochastic simulation. For WNA, we employed the seismological parameters used in Atkinson and Silva (2000). The effective point-source distance of Atkinson and Silva (2000) is used as the distance measure in stochastic simulations in both regions.

The ground-motion model in this study is developed for M_W 5.0-8.0, $R_{rup} < 1000\,\text{km}$ and the ENA hard-rock site (NEHRP site class A, $V_{s30} \geq 2000\,\text{m/s}$) defined by Atkinson and Boore (2006). The ground-motion estimates for other site conditions can be evaluated using appropriate site amplification factors.

The GMPE developed in this study is an alternative ground-motion model, which can be used along with other preexisting models in ENA regions to provide a better representation of epistemic uncertainty in this region.

4.9 Data and Resources

The ENA observation database used for comparisons are from Assatourians and Atkinson (2010), and is available at http://www.seismotoolbox.ca, last accessed 25 January 2010). The SMSIM programs used for the simulations can be obtained from the online software link on http://www.daveboore.com (last accessed 21 December 2010).

4.10 Acknowledgments

We wish to thank Gail Atkinson, David Boore, Norm Abrahamson, Walter Silva, and Kenneth Campbell for their comments, suggestions, and helpful criticisms which greatly improved the manuscript.

4.11 References

Abrahamson, N., G. Atkinson, D. Boore, Y. Bozorgnia, K. Campbell, B. Chiou, I. M. Idriss, W. Silva, and R. Youngs (2008). Comparisons of the NGA Ground–Motion Relations, *Earthquake Spectra* **24**, 45–66.

Abrahamson, N., and W. Silva (2008). Summary of the Abrahamson & Silva NGA Ground–Motion Relations, *Earthquake Spectra* **24**, 67–97.

Anderson, J. G., and S. E. Hough (1984). A model for the shape of the Fourier amplitude spectrum of acceleration at high frequencies, *Bull. Seism. Soc. Am.* **74**, 1969–1993.

Assatourians, K., and G. M., Atkinson (2010). Database of Processed Time Series and Response Spectra Data for Canada: An Example Application to Study of 2005 M_N 5.4 Riviere du Loup, Quebec, Earthquake, *Seismol. Res. Lett.* **81**, 1013–1031.

Atkinson, G. M. (2004). Empirical attenuation of ground motion spectral amplitudes in southeastern Canada and the northeastern United States, *Bull. Seismol. Soc. Am.* **94**, 1079–1095.

Atkinson, G. (2008). Alternative ground-motion prediction equations for eastern North America from a Referenced Empirical Approach: Implications for epistemic uncertainty. *Bull. Seismol. Soc. Am.*, **98**, 1304–1318.

Atkinson, G. M., and K. Assatourians (2010). Attenuation and Source Characteristics of the 23 June 2010 M 5.0 Val-des-Bois, Quebec, Earthquake, *Seismol. Res. Lett.* **81**, 849–860.

Atkinson, G. M., and D. M. Boore (1995). New ground motion relations for eastern North America, *Bull. Seism. Soc. Am.* **85**, 17–30.

Atkinson, G. M., and D. M. Boore (1998). Evaluation of models for earthquake source spectra in eastern North America, *Bull. Seism. Soc. Am.* **88**, 917–934.

Atkinson, G., and D. Boore (2006). Ground motion prediction equations for earthquakes in eastern North America, *Bull. Seismol. Soc. Am.* **96**, 2181–2205.

Atkinson, G., and D. Boore (2011). Modifications to existing ground-motion prediction equations in light of new data, *Bull. Seismol. Soc. Am*. (in press).

Atkinson, G. M., D. M. Boore, K. Assatourians, K. Campbell, and D. Motazedian (2009). A guide to differences between stochastic point-source and stochastic finite-fault simulations, *Bull. Seism. Soc. Am.* **99**, 3192–3201.

Atkinson, G., and M. Morrison (2009). Regional variability in ground motion amplitudes along the west coast of North America, *Bull. Seism. Soc. Am*. **99**, 2393–2409.

Atkinson, G. M., and W. Silva (1997). An empirical study of earthquake source spectra for California earthquakes, *Bull. Seism. Soc. Am*. **87**, 97–113.

Atkinson, G. M., and W. Silva (2000). Stochastic modeling of California ground motions, *Bull. Seism. Soc. Am.* **90**, 255–274.

Beresnev, I. A., and G. M. Atkinson (1999). Generic finite–fault model for ground motion prediction in eastern North America, *Bull. Seism. Soc. Am*. **89**, 608–625.

Beresnev, I. A., and G. M. Atkinson (2002). Source parameters of earthquakes in eastern and western North America based on finite–fault modeling, *Bull. Seism. Soc. Am*. **92**, 695–710.

Beyer, K., and J. J. Bommer (2006). Relationships between median values and between aleatory variabilities for different definitions of the horizontal component of motion, *Bull. Seism. Soc. Am.* **96**, 1512–1522.

Boore, D. M. (1983). Stochastic simulation of high–frequency ground motion based on seismological models of the radiated spectra, *Bull. Seism. Soc. Am.* **73**, 1865–1893.

Boore, D. M. (2003). Prediction of ground motion using the stochastic method, *Pure Appl. Geophys.* **160**, 635–676.

Boore, D. M. (2005). SMSIM–Fortran programs for simulating ground motions from earthquakes: version 2.3–A Revision of OFR 96–80–A, *U.S. Geol. Surv. Open–File Rept*. 00–509, revised 15 August 2005, 55 pp.

Boore, D. M. (2009). Comparing stochastic point-source and finite-source ground-motion simulations: SMSIM and EXSIM, *Bull. Seism. Soc. Am.* **99**, 3202–3216.

Boore, D. M., and G. M. Atkinson (2008). Ground–Motion Prediction Equations for the Average Horizontal Component of PGA, PGV, and 5%–Damped PSA at Spectral Periods between 0.01 s and 10.0 s, *Earthquake Spectra* **24**, 99–138.

Boore, D. M., K. W. Campbell, and G. M. Atkinson (2010). Determination of Stress Parameters for Eight Well-Recorded Earthquakes in Eastern North America, *Bull. Seism. Soc. Am.* **100**, 1632–1645.

Boore, D. M., and W. B. Joyner (1997). Site amplification for generic rock sites, *Bull. Seism. Soc. Am*. **87**, 327–341.

Boore, D. M., J. Watson-Lamprey, and N. A. Abrahamson (2006). GMRotD and GMRotI: Orientation-independent measures of ground motion, *Bull. Seism. Soc. Am*. **96**, 1502–1511.

Brune, J. (1970). Tectonic stress and the spectra of seismic shear waves, *J. Geophys. Res*. **75**, 4997–5009.

Brune, J. (1971). Correction: Tectonic stress and the spectra of seismic shear waves, *J. Geophys. Res.* **76**, 5002.

Campbell, K. W. (1987). Predicting strong ground motion in Utah, in *Assessment of Regional Earthquake Hazards and Risk Along the Wasatch Front, Utah*, P. L. Gori and W. W. Hays (Editors), *U.S. Geol. Surv, Open-File Rept. 87-585*, Vol. II, L1–L90.

Campbell, K. W. (2000). Predicting strong ground motion in Utah, in *Assessment of Regional Earthquake Hazards and Risk Along the Wasatch Front, Utah*, P. L. Gori and W. W. Hays (Editors), *U.S. Geol. Surv. Profess. Paper 1500-L*, L1–L31.

Campbell, K. W. (2003). Prediction of strong ground motion using the hybrid empirical method and its use in the development of ground–motion (attenuation) relations in eastern North America, *Bull. Seism. Soc. Am.* **93**, 1012–1033.

Campbell, K. W. (2007). Validation and update of hybrid empirical ground motion (attenuation) relations for the CEUS, report to the U.S. Geological Survey, National Earthquake Hazards Reduction External Research Program, Award No. 05HQGR0032.

Campbell, K. (2008). Hybrid empirical ground motion model for PGA and 5% damped linear elastic response spectra from shallow crustal earthquakes in stable continental regions: Example for eastern North America. *Proc. 14th World Conf. Earthq. Eng*., Oct. 12-17, Beijing, China, Paper S03-001.

Campbell, K. W., and Y. Bozorgnia (2008). NGA Ground Motion Model for the Geometric Mean Horizontal Component of PGA, PGV, PGD and 5% Damped Linear Elastic Response Spectra for Periods Ranging from 0.01 to 10 s, *Earthquake Spectra* **24**, 139–171.

Chiou, B. S.–J., and R. R. Youngs (2008). An NGA Model for the Average Horizontal Component of Peak Ground Motion and Response Spectra, *Earthquake Spectra* **24**, 173–215.

Chiou, B., R. Youngs, N. Abrahamson and K. Addo (2010). Ground motion model for small-to-moderate shallow crustal earthquakes in California and its implications for regionalization of ground motion prediction models. *Earthquake Spectra* **26**, 907–926.

Douglas, J., H. Bungum, and F. Scherbaum (2006). Ground-motion prediction equations for southern Spain and southern Norway obtained using the composite model perspective. *Journal of Earthquake Engineering* **10**, 33–72.

Frankel, A., C. Mueller, T. Barnhard, D. Perkins, E. Leyendecker, N. Dickman, S. Hanson, and M. Hopper (1996). National seismic hazard maps: Documentation June 1996, *U.S. Geological Survey Open-File Rept.* 96–532, 110pp.

Hanks, T. C., and R. K. McGuire (1981). The character of high–frequency strong ground motion, *Bull. Seism. Soc. Am.* **71**, 2071–2095.

Idriss, I. M. (2008). An NGA Empirical Model for Estimating the Horizontal Spectral Values Generated By Shallow Crustal Earthquakes, *Earthquake Spectra* **24**, 217–242.

Malagnini, L., K. Mayeda, R. Uhrhammer, A. Akinci, and R. B. Herrmann (2007). A regional ground-motion excitation/attenuation model for the San Francisco region, *Bull. Seism. Soc. Am.* **97**, 843–862.

McGuire, R. K., and T. C. Hanks (1980). RMS accelerations and spectral amplitudes of strong ground motion during the San Fernando, California, earthquake, *Bull. Seism. Soc. Am*. **70**, 1907–1919.

Motazedian, D. and G. M. Atkinson (2005). Stochastic finite-fault modeling based on a dynamic corner frequency, *Bull. Seismol. Soc. Am*. **95**, 995–1010.

Power, M., B. Chiou, N. Abrahamson, Y. Bozorgnia, T. Shantz, and C. Roblee (2008). An overview of the NGA project, *Earthquake Spectra* **24**, 3–21.

Raoof, M., R. Herrmann, and L. Malagnini (1999). Attenuation and excitation of three–component ground motion in southern California, *Bull. Seism. Soc. Am*. **89**, 888–902.

Scherbaum, F., J. Schmedes, and F. Cotton (2004). On the Conversion of Source-to-Site Distance Measures for Extended Earthquake Source Models. *Bull. Seism. Soc. Am*. **94**, 1053–1069.

Scherbaum, F., J. J. Bommer, H. Bungum, F. Cotton, and N. A. Abrahamson (2005). Composite ground-motion models and logic trees: methodology, sensitivities, and uncertainties, *Bull. Seism. Soc. Am.* **95**, 1575–1593.

Siddiqqi, J., and G. Atkinson (2002). Ground motion amplification at rock sites across Canada, as determined from the horizontal-to-vertical component ratio, *Bull. Seism. Soc. Am*. **92**, 877–884.

Tavakoli, B., and S. Pezeshk (2005). Empirical-stochastic ground-motion prediction for eastern North America, *Bull. Seism. Soc. Am*. **95**, 2283–2296.

Toro, G. R., N. A. Abrahamson, and J. F. Schneider (1997). Model of strong ground motions from earthquakes in central and eastern North America: best estimated and uncertainties, *Seismol. Res. Lett.* **68**, 41–57.

Watson–Lamprey, J. A., and D. M. Boore, (2007). Beyond *SaGMRotI*: Conversion to Sa_{Arb}, Sa_{SN}, and Sa_{MaxRot}, *Bull. Seism. Soc. Am.* **97**, 1511–1524.

5 Conclusions

This study consists of three major parts comprising Chapters 2, 3, and 4. First, in Chapter 2, 500 seismograms recorded by CERI's broadband stations for events of magnitude M_w 2.5 to 5.2 are used to determine the path term in the New Madrid seismic zone in the frequency domain. The vertical components of the records are processed over a broad frequency range of 0.2-30 Hz. A regression procedure using GA is used to determine the best values for parameters defining the shape of attenuation caused by path. This attenuation is described by geometrical spreading and quality factor functions. A hinged-trilinear functional form is assumed for geometrical spreading, and the regression indicated that the spectral amplitudes decay as $1/R$ at distances less than 70 km. Between 70 and 140 km, due to the postcritical reflections from the Moho discontinuity, spectral amplitudes increase with distance and the geometrical spreading is defined as $R^{+0.25}$. Beyond 140 km, the geometrical spreading is described as $R^{-0.5}$. The quality factor function is expressed as $Q = 614 f^{0.32}$ for frequencies greater than 1 Hz after the regression analysis. For the broader range of frequency used in this study (0.2 to 30 Hz) the Q function is described by a third-degree polynomial described as $\log Q(f) = 2.898 - 0.464 \log f + 1.238(\log f)^2 - 0.540(\log f)^3$. The Monte Carlo simulation technique is used to derive confidence intervals and standard errors of the estimated path attenuation parameters. The result of this study can be used within the stochastic method to predict ground motions in NMSZ and ENA. It also can be used along with other path models that

already exist in ENA regions to help provide a better representation of epistemic uncertainties caused by the regional variability of path effects in ENA.

In Chapter 3, the Lermo and Chavez-Garcia (1993) *H/V* ratio technique is applied to the shear-wave window for the recorded ground motions in the NMSZ for site effect evaluation. The calculated *H/V* ratios at each station show considerable event-to-event variability; therefore, the mean *H/V* ratio for all events is used as an indicator of the site amplification for the sites. Stations located on Lowlands deposits amplify the weak motions by factors of 2 to 4 at low frequencies and stations located on Uplands deposits show amplification factors between 1.5 and 3 at low-frequencies ($f \leq 5\,\mathrm{Hz}$). The mean *H/V* ratios are compared with the soil amplifications derived by Romero and Rix (2005) for Lowlands and Uplands generic profiles using the one-dimensional equivalent-linear model. The *H/V* ratios are relatively consistent with the Romero and Rix (2005) amplifications for the low frequencies of $f \leq 2\,\mathrm{Hz}$ while for high frequencies the Romero and Rix (2005) amplifications drop off more rapidly than the *H/V* ratios. Romero and Rix (2005) predict a lower amplification for frequencies greater than 1.5 Hz in Lowlands and a higher amplification for frequencies greater than 3 Hz in Uplands.

The observed *H/V* ratios are also compared with the quarter-wavelength method. The *H/V* ratios are in good agreement with the theoretical quarter-wavelength estimates for the Uplands and Lowlands profiles within certain bandwidths (less than 10 Hz for Uplands and outside the range between 2 and 8 Hz for Lowlands) suggesting that the *H/V* ratios could be a first approximation of the site effects. The variability of the *H/V* ratios with distance was also examined and no discernible trends were found; therefore, the path

effect model developed in Chapter 2 for the vertical ground motions in NMSZ is applicable for the horizontal ground motions as well. The path term includes a hinged-trilinear geometrical spreading function and a frequency-dependent quality factor function.

Finally in Chapter 4, the hybrid empirical method is used to develop a ground-motion prediction model (GMPE) for ENA. The hybrid empirical procedure uses WNA empirical ground-motion models from the NGA project by the PEER center and also the most recent updated seismological parameters. The major assumption in the hybrid empirical model is that the near-source saturation effects observed in active tectonic regions such as WNA is a general behavior and is the same in other seismic regions. In the hybrid empirical method the empirical models from the host region are scaled by factors accounting for the differences in the source, path, and site effects between the host and the target region. These factors are evaluated using a stochastic method, considering seismological parameters associated with each of the WNA and ENA regions.

The ground-motion model is developed for M_W 5.0-8.0, $R_{rup} < 1000\,\mathrm{km}$ and the ENA hard-rock site (NEHRP site class A, $V_{s30} \geq 2000\,\mathrm{m/s}$) defined by Atkinson and Boore (2006). The ground-motion estimates for other site conditions can be evaluated using appropriate site amplification factors. The GMPE developed in this study is an alternative ground-motion model, which can be used along with other preexisting models in ENA regions to provide a better representation of epistemic uncertainty in this region.

Appendix A

Table A-1
List of events used in Chapters 2 and 3

Date	Time	latitude	Longitude	Magnitude (Mw)	Depth (km)
1/11/2000	54:55.0	36.03	-89.50	2.70	9.90
1/26/2000	21:49.0	36.22	-89.41	2.80	6.70
6/27/2000	02:57.0	37.13	-88.87	2.90	4.10
7/9/2000	52:36.0	35.27	-90.88	2.60	16.00
7/7/2001	45:43.0	36.27	-89.40	3.10	13.80
7/14/2001	40:28.0	36.26	-89.42	2.70	6.50
2/17/2002	01:41.0	36.54	-89.64	2.90	8.00
4/20/2002	00:00.0	36.13	-89.39	2.80	6.80
7/29/2002	28:07.0	35.92	-90.03	2.80	8.00
10/26/2002	08:39.0	36.47	-89.55	2.90	8.00
1/3/2003	17:07.0	37.83	-88.09	2.90	5.00
4/30/2003	56:22.0	35.92	-89.92	4.00	23.80
5/2/2003	25:03.0	36.73	-89.68	2.70	1.80
5/30/2003	18:24.0	36.13	-89.39	2.80	6.20
6/6/2003	29:34.0	36.87	-88.98	4.00	2.60
7/7/2003	42:18.0	36.40	-89.47	2.60	8.90
7/30/2003	50:19.0	36.52	-89.53	2.80	5.40
8/5/2003	41:06.0	36.49	-89.58	2.60	14.70
9/16/2003	22:45.0	36.10	-89.76	2.70	6.60
12/21/2003	20:06.0	36.29	-89.50	2.70	8.80
5/3/2004	25:48.0	36.28	-89.45	2.70	2.60
6/15/2004	34:21.0	36.73	-89.68	3.40	4.50

6/16/2004	07:21.0	36.73	-89.69	2.80	3.90
7/16/2004	25:17.0	36.86	-89.18	3.60	4.40
7/19/2004	53:38.0	36.28	-89.45	2.60	5.60
2/10/2005	04:54.0	35.76	-90.25	4.10	15.50
5/1/2005	37:32.0	35.83	-90.15	4.10	9.70
5/1/2005	39:16.0	35.83	-90.15	2.60	9.50
6/2/2005	35:11.0	36.15	-89.47	3.90	15.10
6/20/2005	00:32.0	36.93	-88.99	2.70	9.80
6/20/2005	21:42.0	36.92	-89.00	3.60	18.70
6/27/2005	46:52.0	37.63	-89.42	3.00	9.60
7/13/2005	08:13.0	35.81	-90.16	2.80	10.70
8/15/2005	12:57.0	35.87	-90.01	2.90	5.50
12/6/2005	24:14.0	38.42	-89.20	2.70	4.40
12/25/2005	33:45.0	36.53	-89.66	2.80	12.30
1/2/2006	48:57.0	37.84	-88.42	3.60	10.70
3/8/2006	36:20.0	36.60	-89.58	2.60	10.70
3/11/2006	37:20.0	35.20	-88.01	2.70	1.70
9/7/2006	51:13.0	36.27	-89.50	3.30	7.60
10/18/2006	59:21.0	36.54	-89.64	3.40	7.70
1/31/2007	47:43.0	36.91	-89.01	2.90	16.00
4/6/2007	34:37.0	36.09	-89.41	2.70	10.60
9/3/2007	58:30.0	36.38	-89.46	2.60	0.50
11/23/2007	23:06.0	36.77	-90.81	2.80	10.10
12/27/2007	11:31.0	36.12	-89.73	2.80	6.40
4/18/2008	36:59.0	38.45	-87.89	5.20	14.20
4/18/2008	14:17.0	38.46	-87.87	4.60	15.50
4/21/2008	38:30.0	38.45	-87.88	4.00	18.30
4/25/2008	31:00.0	38.45	-87.87	4.20	13.00

5/1/2008	30:38.0	38.45	-87.86	3.30	14.30
5/5/2008	25:44.0	38.49	-90.42	2.70	19.40
5/9/2008	40:03.0	35.88	-89.99	2.80	11.10
5/21/2008	44:29.0	36.30	-89.52	2.70	6.40
6/5/2008	13:15.0	38.45	-87.84	3.60	16.20
7/5/2008	58:02.0	35.85	-90.03	2.70	10.50
8/5/2008	04:33.0	36.33	-89.50	2.60	7.90
8/21/2008	34:05.0	36.00	-89.87	2.70	11.10
8/30/2008	46:00.0	37.27	-89.44	2.60	13.70
10/1/2008	37:02.0	36.55	-89.69	2.60	9.20
11/14/2008	20:56.0	36.40	-89.58	2.60	10.80
1/26/2009	52:32.0	36.08	-90.95	2.90	4.00
2/17/2009	09:49.0	35.92	-89.92	2.60	12.90